DESIGN OF A NUCLEAR QUADRUPOLE RESONANCE SPECTROMETER

BY

T. LAKSHMI VISWANATHAN

DEPARTMENT OF ELECTRICAL ENGINEERING

INDIAN INSTITUTE OF TECHNOLOGY KANPUR

DESIGN OF A NUCLEAR QUADRUPOLE RESONANCE SPECTROMETER

A Thesis Submitted

In Partial Fulfilment of the Requirements

for the Degree of

DOCTOR OF PHILOSOPHY

by

TANDUR LAKSHMI VISWANATHAN

to the

DEPARTMENT OF ELECTRICAL ENGINEERING

INDIAN INSTITUTE OF TECHNOLOGY KANPUR

October 1970

CERTIFICATE

Certified that this work, "DESIGN OF A NUCLEAR QUADRUPOLE RESONANCE SPECTROMETER" by T. Lakshmi Viswanathan has been carried out under my supervision and that this work has not been submitted elsewhere for a degree.

Dr. K.R. Sarma
Assistant Professor
Department of Electrical Engineering
Indian Institute of Technology, Kanpur

October 14, 1970

ACKNOWLEDGEMENTS

The author wishes to thank Professor M.A. Pai and Dr. K.R. Sarma for their guidance and supervision during the various phases of the work. The author is deeply indebted to Professor T.R. Viswanathan, Dr. K.V. Sane and Prof. B.D. Nageswara Rao for their continued interest, stimulating discussions and helpful criticisms during the course of this work. Thanks are due to Professors H.K. Kesavan, C.N.R. Rao and B. Prasada for their encouragement.

The help extended by Mr. Gurudas Singh, Mr. Jagir Singh and Mr. R.S. Tewari in the fabrication of the instrument is gratefully acknowledged. Thanks are due to Mr. M. Natu for doing an excellent job of typing this thesis and Mr. V.K. Khanna for drawing the diagrams.

TABLE OF CONTENTS

LIST OF TABLES

LIST OF FIGURES

SYNOPSIS

TANDUR LAKSHMI VISWANATHAN
Ph.D.
Department of Electrical Engineering
Indian Institute of Technology, Kanpur
October 1970

DESIGN OF A NUCLEAR QUADRUPOLE RESONANCE SPECTROMETER

The study of the phenomenon of nuclear quadrupole resonance (NQR) exhibited by certain solids aids the understanding of their structure. The resonance frequency is characteristic of the substance and can be anywhere in the frequency range of hundreds of kilohertz to hundreds of megahertz. The instrumentation involves the location and display of the absorption line. This is done by placing the sample in the tank coil of an oscillator circuit. When the frequency of the oscillator coincides with the resonance frequency, the substance absorbs a minute amount of energy and this manifests itself as a small change in the tuned circuit impedance. The fractional change in impedance will be of the order of one part in 10^6. This causes a minute change in oscillation amplitude which is detected with the help of an envelope detector. The detector output not only contains the signal due to absorption but also noise from the oscillator circuit. The aim of the present work is to improve the instrumentation from the point of view of

sensitivity and signal to noise ratio.

The lower the frequency of absorption, smaller is the amount of absorption; and hence the instrument used to locate the absorption must be more sensitive. Generally speaking, increasing the sensitivity results in the increase of noise, and the ultimate objective is to obtain higher signal to noise ratio. Spectrometer system based on marginal oscillators is chosen since it is known to reproduce the line shape faithfully.

An experimental approach was first used to study the popular circuit configurations with a view to compare their performance and select a circuit configuration with optimum component values. As a first step towards better performance, low noise field effect transistors were employed in place of vacuum tubes used in the existing circuits. A low frequency analog simulation technique of the oscillator circuits was employed to optimize the circuit components for obtaining maximum sensitivity. Instrumentation with improved signal to noise ratio was evolved for the 30 MHz region based on the oscillator-detector circuit arrangement used by Knight (KNIGHT, 1961; VISWANATHAN ET AL., 1968). Further simulation studies led to a simpler and more sensitive oscillator circuit which was used to detect NQR both at 3 MHz and 30 MHz (VISWANATHAN ET AL., 1970).

An analytical approach to the problem of oscillator behaviour from the point of view of NQR detection was undertaken. The nonlinear differential equations which characterise

practical oscillator circuits are difficult and very often impossible to handle from the standpoint of obtaining closed form solutions. Some workers have attempted to express the nonlinear device characteristic in a polynomial form. But, the results obtained have very little practical value, since it is difficult to synthesise the desired nonlinearity at high frequencies. Either one has to look at the nonlinear terminal behaviour of the existing low noise devices and pick the one which is nearer to the desired characteristic or choose a nonlinearity which can be synthesized.

The analytical approach used in this work is to study the properties of oscillator circuits with piecewise linear characteristic for the active device. The simplest of these which can be easily synthesised is the one with two segments, viz., an amplifying segment and a limiting segment. The differential equation characterising the circuit behaviour is solved using the Kryloff-Bogoliuboff's first approximation. The sensitivity is defined as the ratio of the fractional change in amplitude of oscillation to the fractional change in the tuned circuit resistance. The results show that higher sensitivities are obtained as the nonlinear characteristic becomes softer, i.e., the slope of the limiting segment approaches that of the amplifying segment. But the price paid for obtaining higher sensitivity is in terms of the stringent control required over the loop gain. The analysis has been extended to circuits with a piecewise linear

characteristic with three segments, one amplifying segment and two limiting segments. A similar characteristic has been suggested by Robinson (ROBINSON 1959). The analysis shows that the sensitivity derived by Robinson is the limiting value obtained for large values of loop gain, whereas when the loop gain is in the neighbourhood of unity, higher sensitivities are obtained. The overall sensitivity of the three segment nonlinearity is lower than the two segment one.

The technique used for the detection of absorption generally involves methods of making the absorption periodic by either frequency modulating the oscillator or magnetic field modulation. It is known that the response of the oscillator circuit to periodic absorption varies with sensitivity. Thus, it is important to evaluate the effective detection bandwidth before choosing the modulation frequency. The analysis shows that at higher sensitivity conditions the effective detection bandwidth decreases, so that the sensitivity bandwidth product remains constant. Experiments show that there is an overall improvement of signal to noise ratio at higher sensitivity.

An oscillator detector system has been designed which is based on a piecewise linear characteristic for the active device to operate at the 3 MHz region. Improved performance has been observed. This type of synthesis should be expected to be more effective at lower frequencies.

CHAPTER - I

INTRODUCTION

1.1 NUCLEAR QUADRUPOLE RESONANCE

Many nuclei, in the ground state, have electric quadrupole moment, which is a measure of the departure from spherical symmetry of the nuclear charge distribution. It can be shown rigorously (ABRAGAM, 1961) that nuclei cannot have electric dipole moments. Higher order moments may exist, but they are usually small enough to escape detection. If a nucleus with a quadrupole moment is present in an environment, where the extra-nuclear charge distribution generates electric field gradients, then the interaction between these leads to a set of discrete energy levels and transition between these can be caused by oscillating magnetic fields. The frequency of oscillation ν and the energy gap between the levels (ΔE) are related by the well known Plank-Einstein relation $\Delta E = h\nu$, where h is Plank's constant. This resonant absorption as a function of frequency constitutes Nuclear Quadrupole Resonance (NQR) spectrum.

This phenomenon is restricted to solids, since in liquids and gases molecular motion averages the electric field gradient to zero and hence the quadrupole splittings do not occur. The first NQR signal was observed by Dehmelt and Krüger (DEHMELT AND KRÜGER, 1950).

Macroscopically, the absorption of the radio frequency energy gives rise to a small change in the imaginary component

χ'' of the magnetic susceptibility. χ'' for the solid is essentially zero at all frequencies except for a narrow band around the resonance frequency. It is given by (DEHMELT, 1954)

$$\chi'' = f(I) \frac{N_o \mu^2}{kT} \frac{\nu}{\Delta\nu} \qquad (1.1)$$

where N_o is the number of resonating nuclei per cubic centimetre, ν is the frequency of resonance, $\Delta\nu$ is half the width of the absorption line, μ is the magnetic moment, k is the Boltzmann constant, T is the temperature in degrees Kelvin and f(I) is the spin function which is nearly equal to unity.

The frequency of resonance and the shape of the absorption line give unique information about the electronic structure of atoms and molecules in the solid state, the details of which are available in literature (DAS AND HAHN, 1958; FEDIN AND SEMIN, 1959; RAO AND FERRARO, 1970). The NQR frequencies are found to lie in the range of 1 - 1000 MHz. Over a hundred nuclei have been detected by NQR technique. Out of these, Cl^{35} and N^{14} have been investigated more than others. Cl^{35} has been studied extensively, since the resonances lie in the range of 10 - 70 MHz where the instrumentation is simpler and the signal strength is relatively high compared to N^{14}. The investigation of N^{14} is of interest because of the wide variety of different bonding types that exist in nitrogen containing compounds. As such, there is a need for improved instrumentation in the 1 to 3 MHz region.

1.2 DETECTION OF NQR

In order to observe the resonance, the primary requirement is to subject the solid to a magnetic field oscillating at a frequency in a range where the resonance is expected. Thus, the solid is made the core of an inductance coil, which will show a change in its impedance at resonance.

If the magnetic susceptance of a material is written as

$$\chi = \chi' - j\chi'' \,, \tag{1.2}$$

the inductance of a coil using this material as core is given by

$$L = L_{vac}(1 + 4\pi\xi\chi) \tag{1.3}$$

where L_{vac} is the inductance of the coil without the core in vacuum and ξ is a fraction known as the filling factor which denotes the fraction of energy stored in the core.

If r is the series resistance of the coil, the impedance Z of the coil at the resonance frequency ω_o is given by

$$Z = r + j\omega_o L_{vac}\left[1 + 4\pi\xi(\chi' - j\chi'')\right]$$

$$= r\left(1 + 4\pi\xi\chi''\frac{\omega_o L_{vac}}{r}\right) + j\omega_o L_{vac}(1 + 4\pi\xi\chi') \tag{1.4}$$

χ'' is finite at resonance and is negligible at all other frequencies. χ' is always negligible for the materials of interest. Thus, if Δr is the perturbation of the resistive part of the impedance due to absorption, we can write

$$\frac{\Delta r}{r} = 4\pi \xi \chi'' Q_o \qquad (1.5)$$

where Q_o ($= \frac{\omega_o L_{vac}}{r}$) is the quality factor of the coil without the sample. Theoretically evaluated values of χ'' lead to values of $\frac{\Delta r}{r}$ of the order of 10^{-4} to 10^{-6} for a Q of the order of 100 (FEDIN AND SEMIN, 1960).

From equation (1.1) one can see that χ'' can be enhanced by increasing N_o. This is achieved by increasing the quantity of the sample subjected to the magnetic field. But in practice the limit for this is imposed by the availability of the sample. Another way of increasing χ'' is to reduce the temperature. Thus, more often resonance studies are carried out at liquid nitrogen (77° K) temperatures.

The other factors $f(I)$, μ, and $\nu/\Delta\nu$ are strictly properties of the sample. The spin function $f(I)$ is of the order of unity. The factor $(\nu/\Delta\nu)$ is governed by the shape of the absorption line. In general, a Gaussian shape is assumed for the line (DAN AND HAHN, 1958). $\Delta\nu$ is half the line width. The exact shape of the line is controlled by many factors, such as the neighbouring nuclei, terrestrial magnetic field, defects and stresses in the crystal, thermal oscillations, etc. (FEDIN AND SEMIN, 1960). Observed values of half line width lie in the region of 0.5 KHz to 5 KHz (WANG, 1955). The line width is an independent property of a sample and does not depend on the frequency of resonance. Thus, referring to equation (1.1), on the average, absorption is higher at higher resonance

frequencies.

Oscillator-Detector Systems

Spectrometer systems are based on the methods used for NMR (Nuclear Magnetic Resonance) detection. However, in the case of NMR, there is an additional flexibility, since the frequency of absorption is also a function of the external constant magnetic field applied across the sample. Thus, the resonance frequency can be adjusted to any convenient value with the help of the constant magnetic field. Whereas, in the case of NQR, the resonant frequency is uniquely determined by the sample, which makes it necessary to search for the resonance in the frequency domain.

In order to measure the impedance of a coil as a function of frequency, bridge methods are usually adopted. In this case, as we are interested only in a minute variation of the real part, it would be convenient to neutralise the imaginary part by connecting a variable capacitor in parallel. This method has been used for NMR detection (BLOEMBERGEN ET AL., 1948). But it cannot be used for NQR detection as this involves varying the frequency of operation while maintaining perfect tracking of the three tuned circuits employed in the excitation source and the arms of the bridge. Thus, methods which involve only one resonant circuit have been adopted for NQR. The sample coil is made part of the frequency determining network of an oscillator circuit which has facility for varying the frequency

over a wide range. The oscillator configuration is designed to make the amplitude of oscillation sensitive to changes in the tank circuit resistance. Thus, when the frequency of the oscillator coincides with the NQR frequency, the amplitude of oscillation shows a minute change. This change due to absorption is detected with the help of a suitable detector. In order to distinguish the signal due to absorption from noise present in the oscillator-detector system, the detected output is made periodic at a known audio frequency by frequency modulating the oscillator over a small region around the resonance frequency. Alternately, field modulation can be employed by applying a periodic magnetic field across the sample. The magnetic field is adjusted to completely blurr the absorption signal over half the period of the modulating cycle. The modulation frequency used by different workers is in the range of 20 to 300 Hz. The criterion for choosing the value of the modulating frequency is that it should be smaller than the half line width (MYERS ET AL., 1959). An improvement over the signal to noise ratio available at the output of the detector is achieved with the help of phase sensitive detection. In many spectrometer circuits, the same active device is used for oscillation and detection. These circuits are referred to as oscillator-detector circuits.

There are basically two types of oscillator circuits used for the detection of NQR, viz., the super-regenerative type and the regenerative type.

In the super-regenerative oscillator (DEAN AND POLLAK, 1958), oscillations are quenched periodically at a frequency which is large compared to the modulating frequency but small compared to the frequency of absorption. The advantage of quenching is said to be that the oscillator goes periodically through the most sensitive condition, namely, of unity loop gain. However, since absorption might take place at the centre frequency or at any sideband frequency, it becomes difficult to determine the exact NQR frequency though this can be achieved by varying the quench frequency. Recovery of the signal after detection involves several stages of filtering. The main advantage of super-regenerative oscillators is that they are more sensitive than the regenerative type. Hence they are employed to detect unknown resonances. The disadvantage of this method is that no line shape information can be obtained as the detection is performed under highly nonlinear conditions.

The regenerative type of oscillator-detector, though not so sensitive, reproduces the line shape faithfully. This thesis is concerned only with the design of this type of oscillator-detector systems which will now be described in detail.

1.3 SPECTROMETER BASED ON REGENERATIVE TYPE OF OSCILLATOR-DETECTOR

The block diagram of a complete spectrometer system employing frequency modulation is shown in Figure 1. The frequency of the oscillator is coarsely controllable over a

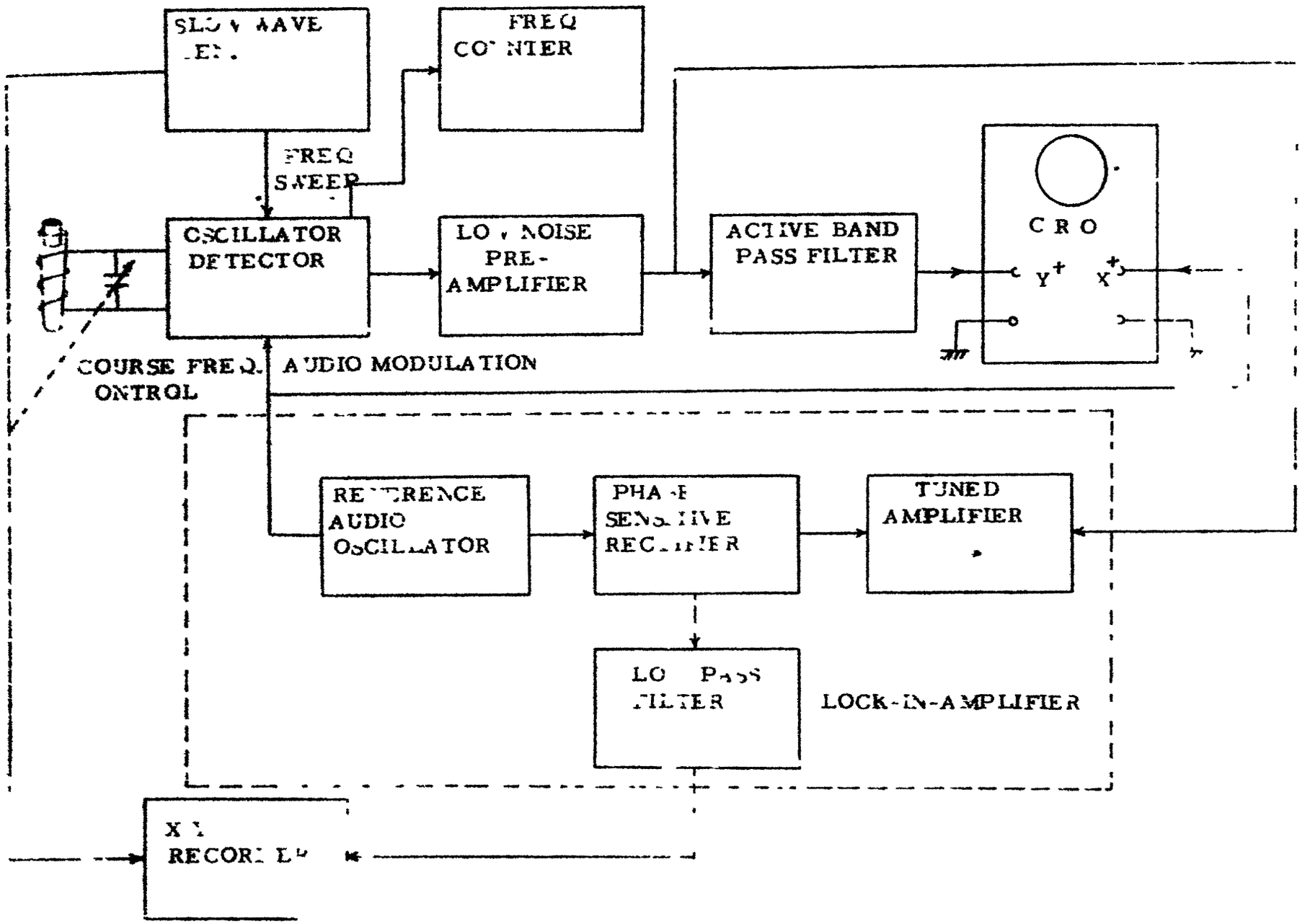

FIG. 1 NQR SPECTROMETER SYSTEM EMPLOYING A FREQUENCY
REFERENCED OSCILLATOR DETECTOR

wide range with the help of the variable capacitor. Fine frequency control as well as frequency modulation are achieved using a variable capacitance diode (Varicap). There are two methods of displaying the absorption line. If the signal strength due to absorption is known to be sufficiently high, a cathode ray oscilloscope is used to first locate and display the line. This type of display is referred to as a wide band display and the frequency deviation is arranged to be four or five times the line width. After preamplification with the help of a low noise preamplifier, the signal is passed through a bandpass filter, the output of which is fed to the cathode ray oscilloscope. The bandwidth of the filter is adjusted to allow the modulating frequency as well as the significant harmonics to pass through so that a good picture of the line is obtained.

In cases where the signal to noise ratio is less than one, the oscilloscope display cannot be used to detect the line. Under these circumstances, an improvement in signal to noise ratio is obtained by arranging the deviation to be a fraction of the line width. Now, the frequency of the oscillator is swept slowly so that it passes through the absorption band. Thus, the output of the oscillator-detector will be proportional to the derivative of the absorption line. In this case, the output is at the modulating frequency itself. Thus, the signal after preamplification is fed to an amplifier tuned to the modulating frequency. The output of the tuned

amplifier is fed to the phase sensitive detector whose reference signal is derived from the audio oscillator. The output of the phase sensitive rectifier is fed to a low pass filter whose time constant can be adjusted to several seconds. The time constant of the low pass filter essentially controls the effective bandwidth of the system. The larger the filtering time constant, the smaller is the effective bandwidth, and this gives rise to a higher signal to noise ratio at the output of the filter. Correspondingly, the rate at which the oscillator frequency is swept has to be reduced. Thus, the improvement in signal to noise ratio is achieved at the cost of speed of passage through the line. The derivative of the absorption line is finally obtained by feeding the output of the low pass filter to the y input of the x-y recorder and feeding the output of the sweep generator to the x input.

1.4 OUTLINE OF THE WORK

The investigations are directed towards the design of an NQR spectrometer system to obtain a display of the absorption line with the maximum possible signal to noise ratio. The performance of the system is primarily controlled by the oscillator-detector circuit, which must have a high sensitivity so that subsequent signal processing will not unduly deteriorate the signal to noise ratio.

In order to obtain an improvement in signal to noise ratio, low noise field effect transistors were employed in the

oscillator circuit. These circuits can be battery operated, thus obviating the need for high voltage power supplies with the associated filtering problems in reducing hum or pick up.

Sensitivity of the oscillator-detector is also a function of both the active device characteristics and the circuit configuration. An experimental approach was used to study the popular circuit configurations with a view to compare their performance in terms of sensitivity. As a result of such a study, a configuration due to Knight (KNIGHT, 1961) was chosen. Using field effect transistors for the active device, the analog simulation technique was used to optimise the values of circuit components for obtaining maximum sensitivity. The oscillator-detector configuration evolved in this manner was used to detect NQR in the 30 MHz (VISWANATHAN ET AL., 1968) region with improved signal to noise ratio. Further modification and simulation studies led to a simpler and more sensitive circuit which was used to detect NQR both at 30 MHz and 3 MHz (VISWANATHAN ET AL., 1970).

An analytical approach to the problem of oscillator behaviour from the point of view of NQR detection was undertaken. Properties of oscillators, with a piecewise linear characteristic for the active device, have been studied. The simplest of the piecewise linear characteristics is one with two segments, an amplifying segment and a limiting segment. The nonlinear differential equations characterising the behaviour of the

oscillator were solved using Kryloff-Bogoliuboff's first approximation. The results show that higher sensitivities are obtained as the nonlinearity becomes softer. It has been shown that, in order to exploit higher sensitivity conditions, the loop gain has to be controlled to a high degree of stability.

The analysis has been extended to the case of a piecewise linear characteristic with one amplifying segment and two limiting segments, a configuration suggested by Robinson (ROBINSON, 1959). The analysis shows that the sensitivity of unity derived by Robinson is the limiting value when the loop gain is large; whereas when the loop gain is in the neighbourhood of unity, the sensitivity tends to infinity. The overall sensitivity of the three segment nonlinearity is less than that with two segments.

Since frequency modulation or field modulation, at a low frequency, is employed in the detection of NQR, it is important to know the response of the oscillator to periodic absorption. It is known that the response is a function of sensitivity (WATKINS, 1952). An analysis was carried out to determine the effective bandwidth of the oscillator. The results show that at higher sensitivity conditions the effective bandwidth decreases, but the sensitivity-bandwidth product remains constant.

Experiments with an oscillator circuit employing a two segment piecewise linear characteristic show that there is an overall improvement of signal to noise ratio at higher sensitivity

conditions.

An oscillator-detector circuit based on piecewise linear characteristic has been designed to operate in the 3 MHz region. Improved performance has been observed. This type of synthesis should be expected to be even more effective at lower frequencies.

CHAPTER - II

EXPERIMENTAL APPROACH

2.1 FIELD EFFECT TRANSISTOR (FET)

The oscillation voltages required across the tank coil in an NQR oscillator are of the order of ten volts RMS or less (WANG, 1955). Higher voltages saturate the sample. A level of ten volts or less can be easily achieved with the help of semiconductor devices. The use of a semiconductor device eliminates the need for high voltage and heater power supplies and the circuit can be battery operated. Thus extensive filtering circuits to eliminate hum and pick-up can be avoided.

The FET, by virtue of its low noise property, high input impedance and thermal stability, makes an ideal choice for the active device in oscillator-detector circuits. While both the junction type and the insulated gate type of FETs have these advantages, we will restrict our discussion to the use of junction FETs in oscillator circuits.

The symbol for a junction FET with the reference directions for currents and voltages is shown in Figure 2. The output characteristics (Figure 2) of FETs are very similar to those of pentodes. The transfer characteristic in the pentode region is very nearly parabolic and is given by

$$I_D = I_{DSS} \left[1 - \frac{V_{GS}}{V_P} \right]^2 \qquad (2.1)$$

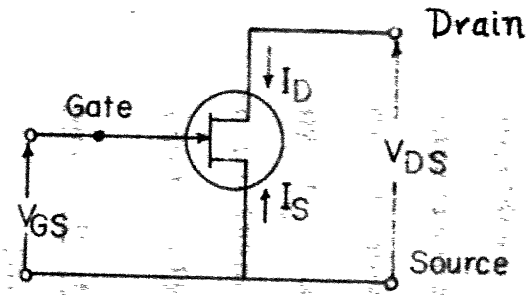

FIG. 2 SYMBOL OF n-CHANNEL FET, AND ITS OUTPUT CHARACTERISTICS

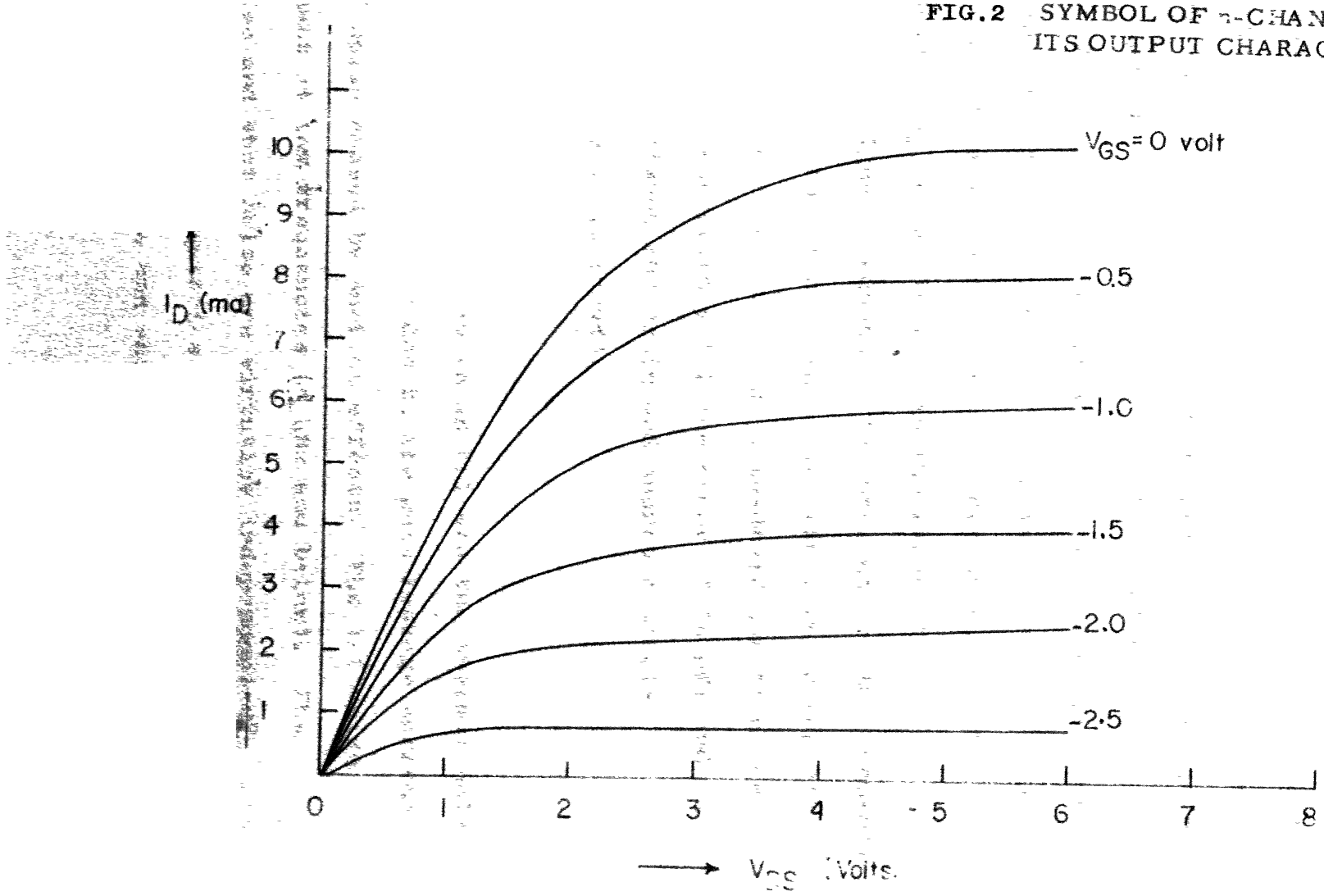

where I_{DSS} is the drain current when $V_{GS} = 0$, and V_P is the pinch-off voltage.

Small Signal Parameters

The small signal equivalent circuit is shown in Figure 3a Because of the reverse biased junction between the input terminals, viz., the gate and the source, the FET is characterised by a very high input impedance of the order of 10^9 ohms, which is very large compared to the source resistance usually encountered in practice. The output resistance r_d is given by the slope of the output characteristic and is of the order of MΩ. The transconductance g_m normally lies in the range of 100 to 10,000 $\mu\mho$. At higher frequencies the presence of the terminal capacitances becomes important. These are the barrier capacitances of the reverse biased gate-source and gate-drain junctions denoted by C_{gs} and C_{gd} respectively (of the order of 10 pF) and the capacitance C_{ds} between the drain and source contacts (generally less than a picofarad).

Noise Performance of FETs

The main sources of noise in an FET are the thermal noise in the channel, the shot noise due to the gate leakage current and the 1/f noise caused by surface effects. The 1/f noise is predominant at low frequencies (1 KHz and below). The thermal noise and shot noise are virtually independent of frequency. At higher frequencies where the power gain of the FET reduces, thermal noise and shot noise become predominant.

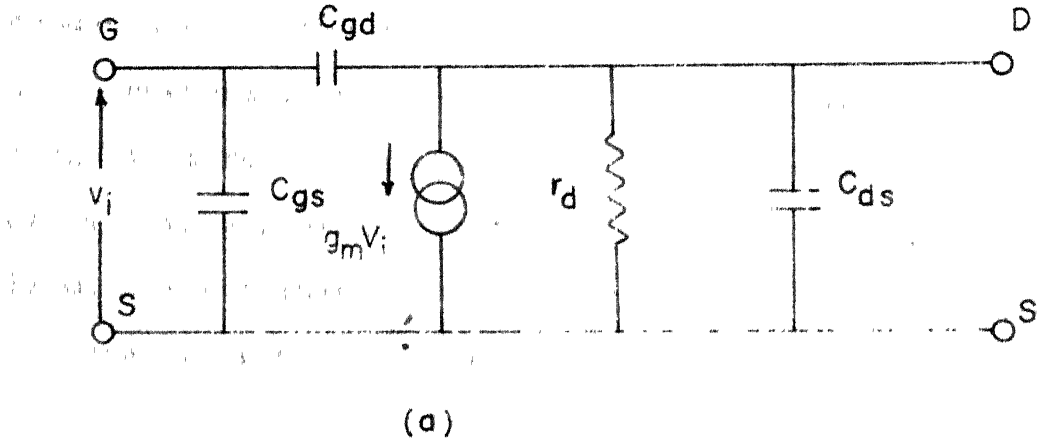

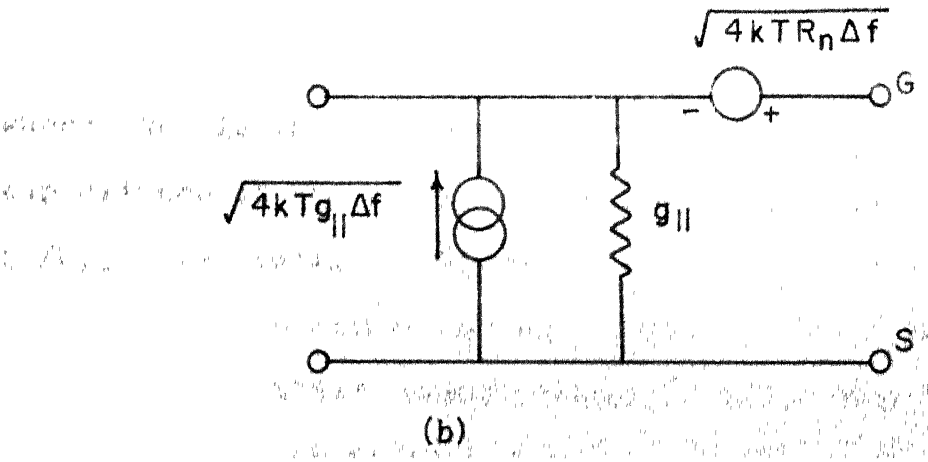

FIG. 3 (a) SMALL SIGNAL EQUIVALENT CIRCUIT
(b) NOISE EQUIVALENT CIRCUIT REFERRED TO THE INPUT

The noise equivalent circuit (Van DER ZIEL, 1962, 1966) referred to the input of an FET is shown in Figure 3b. The noise current source $\overline{ig}^2 = 4KTg_{11} \Delta f$ takes care of the shot noise component in the gate circuit. Here g_{11} is the input conductance of the device. The thermal noise component of the drain current is expressed by a noise voltage source at the input in terms of an equivalent noise resistance R_n. The value of R_n is approximately $(1/g_m)$. This equivalent noise resistance is much lower than that of a vacuum tube ($R_n = 2.5/g_m$) with comparable transconductance.

A figure of merit η, is proposed for the selection of FETs to be employed in the oscillator-detector circuit. This is given by

$$\eta = \frac{g_m}{C_{iss}\,(NF)} \qquad (2.2)$$

where NF is the spot noise figure and C_{iss} is the input capacitance of the common-source configuration. The ratio g_m/C_{iss} is usually referred to as the high frequency figure of merit by the manufacturers. Based on these considerations the FET type 2N3823 manufactured by Texas Instruments was chosen for use in the oscillator-detector circuit. The important specifications of the FET are shown in Table 1.

2.2 ANALOG SIMULATION

In attempting to build a spectrometer, the first step

TABLE 1

IMPORTANT SPECIFICATICNS OF THE N-CHANNEL EPITAXIAL PLANAR SILICON FET,

TYPE 2N3823 (TEXAS INSTRUMENTS)

PARAMETER	TEST CONDITIONS	MIN	MAX	UNIT
Gate-Source Breakdown Voltage	I_G=-1 μa, V_{DS}=0	-30		v
Gate Cutoff Current	V_{GS}=-20v, V_{DS}=0		-0.5	na
	V_{GS}=-20v, V_{DS}=0, T_A=150°C		-0.5	μa
Zero-Gate-Voltage Drain Current	V_{DS}=15v, V_{GS}=0	4	20	ma
Gate-Source Voltage	V_{DS}=15v, I_D=400 μa	-1	-7.5	v
Gate-Source Cutoff Voltage	V_{DS}=15v, I_D=0.5 na		-8	v
Small-Signal Common-Source Forward Transfer Admittance	V_{DS}=15v, V_{GS}=0, f=1 kc	3500	6500	μ mho
Small-Signal Common-Source Output Admittance	V_{DS}=15v, V_{GS}=0, f=1 kc		35	μ mho
Common-Source Short-Circuit Input Capacitance	V_{DS}=15v, V_{GS}=0, f=1 Mc		6	pf
Common-Source Short-Circuit Reverse Transfer Capacitance			2	pf
Small-Signal Common-Source Forward Transfer Admittance	V_{DS}=15v, V_{GS}=0, f=200 Mc	3200		μ mho
Small-Signal Common-Source Input Conductance			800	μ mho
Small-Signal Common-Source Output Conductance			200	μ mho
Common-Source Spot Noise Figure	V_{DS}=15v, V_{GS}=0, f=100 Mc, R_G=1K Ω		2.5	db

is to choose an oscillator configuration. The configuration is chosen with a view to obtain highest sensitivity. The nonlinear nature of the differential equation governing the circuit behaviour makes an analytical approach towards determining the sensitivity complex. The nonlinear differential equation can be solved with the aid of a digital computer. However, a quick and direct approach is by a comparative evaluation using a low frequency analog simulation technique.

The low frequency analog simulation of the RF oscillator is carried out by using the same devices in the given configuration, but scaling the inductances and capacitances up by a factor (e.g. 1000) and consequently bringing the oscillator frequency down by the same factor. The low frequency technique has the advantage that more accurate measurements can be carried out without disturbing the circuit conditions. The effect of parasitic elements like interelectrode capacitances and lead inductances can be also taken into account by appending their scaled versions to the simulation circuit. Simulation of periodic absorption is achieved in the following manner. A relay contact is used to periodically shunt the tank coil by means of a large resistance (100 KΩ to 1 MΩ), thus producing a periodic perturbation of the parallel resistance of the tuned circuit. This will not be possible at high frequencies like 30 MHz, as the capacitance across the relay contacts would present a low impedance. Another important feature of the simulation is that it lends itself to the optimization of

circuit components from the point of view of obtaining the highest possible sensitivity. This becomes possible with the help of variable inductor (GR type 107) and capacitor (Heathkit type IN-21) boxes. This procedure cannot be adopted at high frequencies. Thus, the simulation provides a direct method of obtaining a comparative estimate of different circuits from the point of view of sensitivity and also for optimization of circuit components.

In practice, the amount of energy absorbed by the substance due to NQR is a function of the amplitude of oscillation. The sample saturates when the amplitude of oscillation of the voltage across the coil is increased beyond a certain limit (WANG, 1955) and the energy absorbed reduces. This voltage dependence of absorption is not simulated.

Detection Procedure

The perturbation of the resistance of the tank coil results in a modulation of voltage and current oscillations everywhere in the circuit. This also produces, generally, a periodic change in the d.c. levels in the circuit, which depends on the nature of the overall nonlinearity causing the limit cycle.

There are two very well known techniques of detection. The first one consists of detecting the modulation envelope of the oscillation voltages in the circuit, while the other involves the detection of the changes in the d.c. levels

themselves. The detection of the periodic change in d.c. levels is brought about due to the nonlinear nature of the device characteristics. Thus the oscillator circuit itself acts as the detector. Whereas if the modulation of the oscillation voltage has to be recovered, a separate detector has to be employed.

Results of Simulation

The results obtained from simulation studies of two well known circuits are presented. The circuit of Figure 4 is due to Wang and is referred to as the autodyne type of circuit, which consists of an oscillator-detector and an additional positive feedback loop to enhance the sensitivity (not shown in the Figure). The increase in sensitivity obtained from the positive feedback is reported to cause considerable distortion of the line shape (FEDIN AND SEMIN, 1960). The oscillator-detector part of the circuit was simulated at 30 KHz and absorption was simulated by switching a 100 KΩ resistor across the tuned circuit. In this circuit, the output is obtained by detecting the variations in the d.c. plate current. Thus, the voltage change across the 43 KΩ resistor was measured, the maximum value of which was about 2 volts after optimizing all the components including the potentiometer which controls the regeneration. This corresponds to a variation in the plate current of approximately 50 microamperes.

A similar procedure was adopted for evaluating the sensitivity of the cathode coupled circuit due to Knight, shown

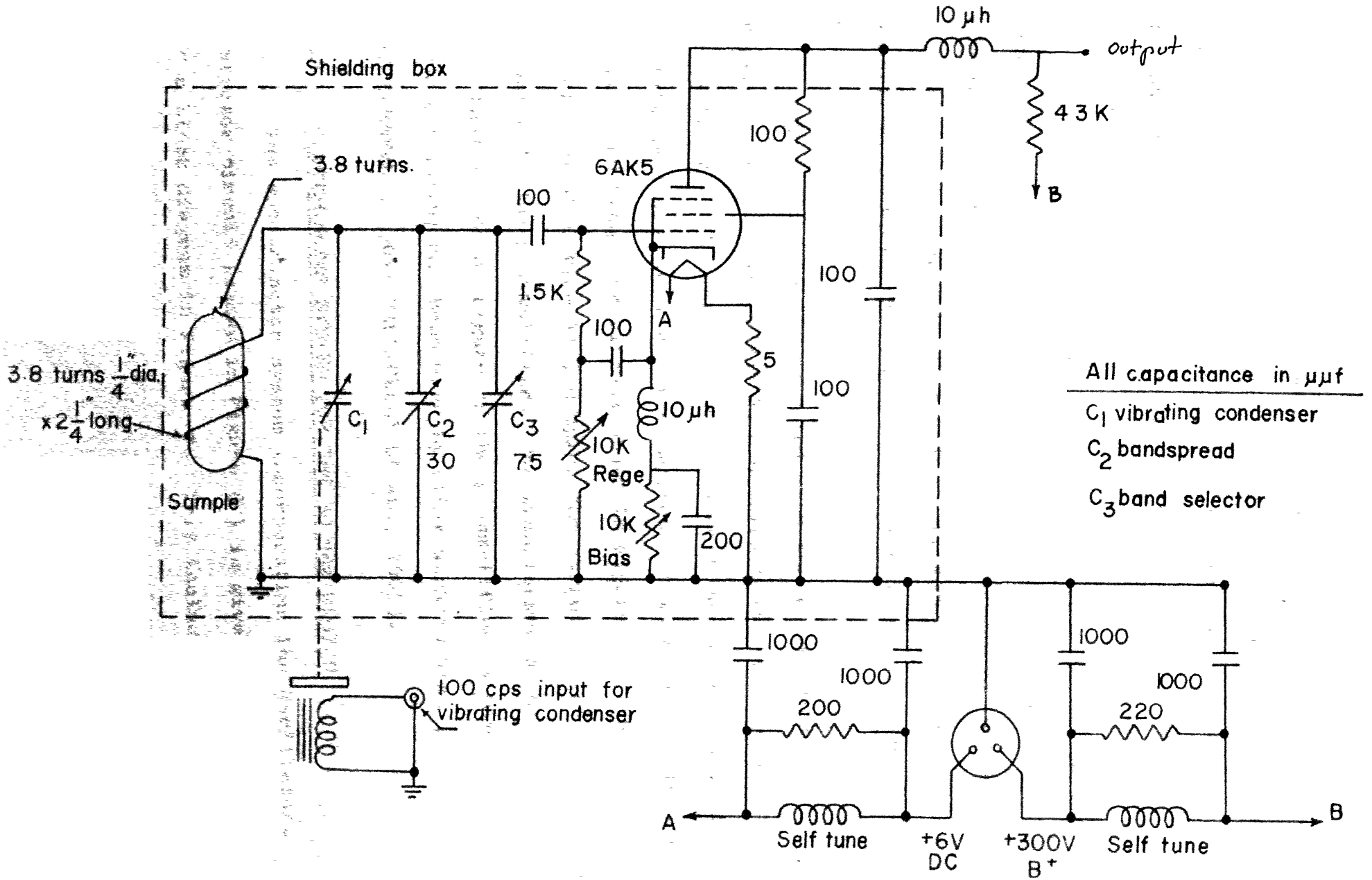

FIG. 4 WANG'S OSCILLATOR-DETECTOR CIRCUIT

in Figure 5. In order to make the comparison meaningful, the same coil used in Wang's circuit was employed in this circuit also. Here the change of current in the 10 KΩ resistor in the grid circuit was measured, the maximum magnitude of which was 25 microamperes.

A much higher current variation was anticipated in the cathode circuit, which when measured after optimizing the circuit components, was found to be of the order of 100 microamperes. Thus, the cathode coupled configuration is more sensitive, provided the cathode current changes are sensed to form the output.

The procedure was repeated with the vacuum tubes replaced by FETs (Type 2N3822) and using a low voltage supply (9V battery). The maximum source current variation obtained in this case was about 80 microamperes. This study led to the actual high frequency circuit shown in Figure 6. The audio transformer (UTC type A11) couples the output of the oscillator-detector to the preamplifier. The transformer turns ratio is such that the noise figure of the preamplifier is minimised. Such a coupling has been used by other workers also (VERDIECK AND CORNWELL, 1961; VALPICELLI ET AL., 1965).

2.3 SPECTROMETER SYSTEM FOR THE 30 MHz REGION

The spectrometer system incorporating the oscillator-detector circuit (shown in Figure 6) is given in the form of a block diagram in Figure 7. This includes arrangements

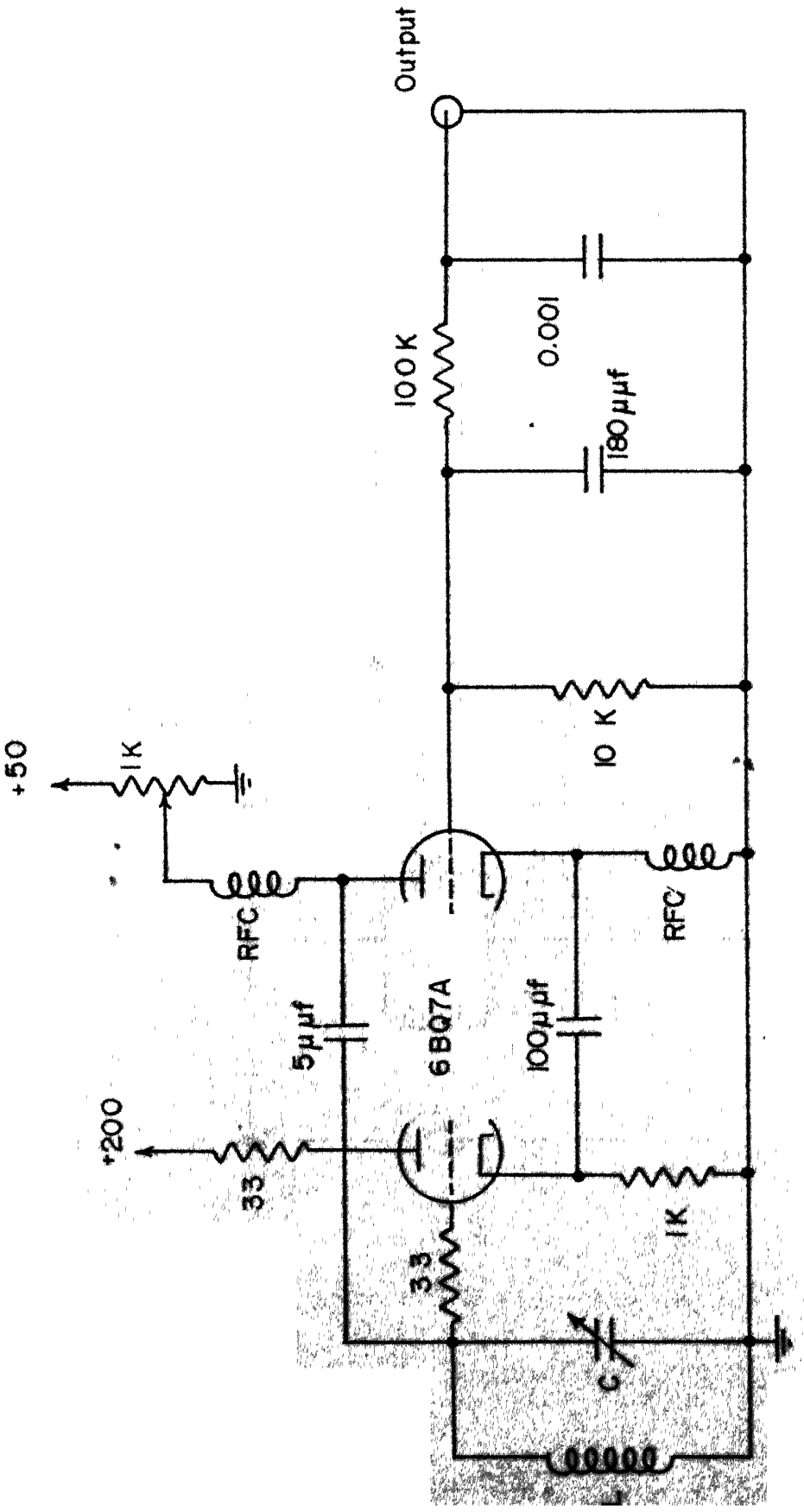

FIG. 5 KNIGHT'S OSCILLATOR-DETECTOR CIRCUIT

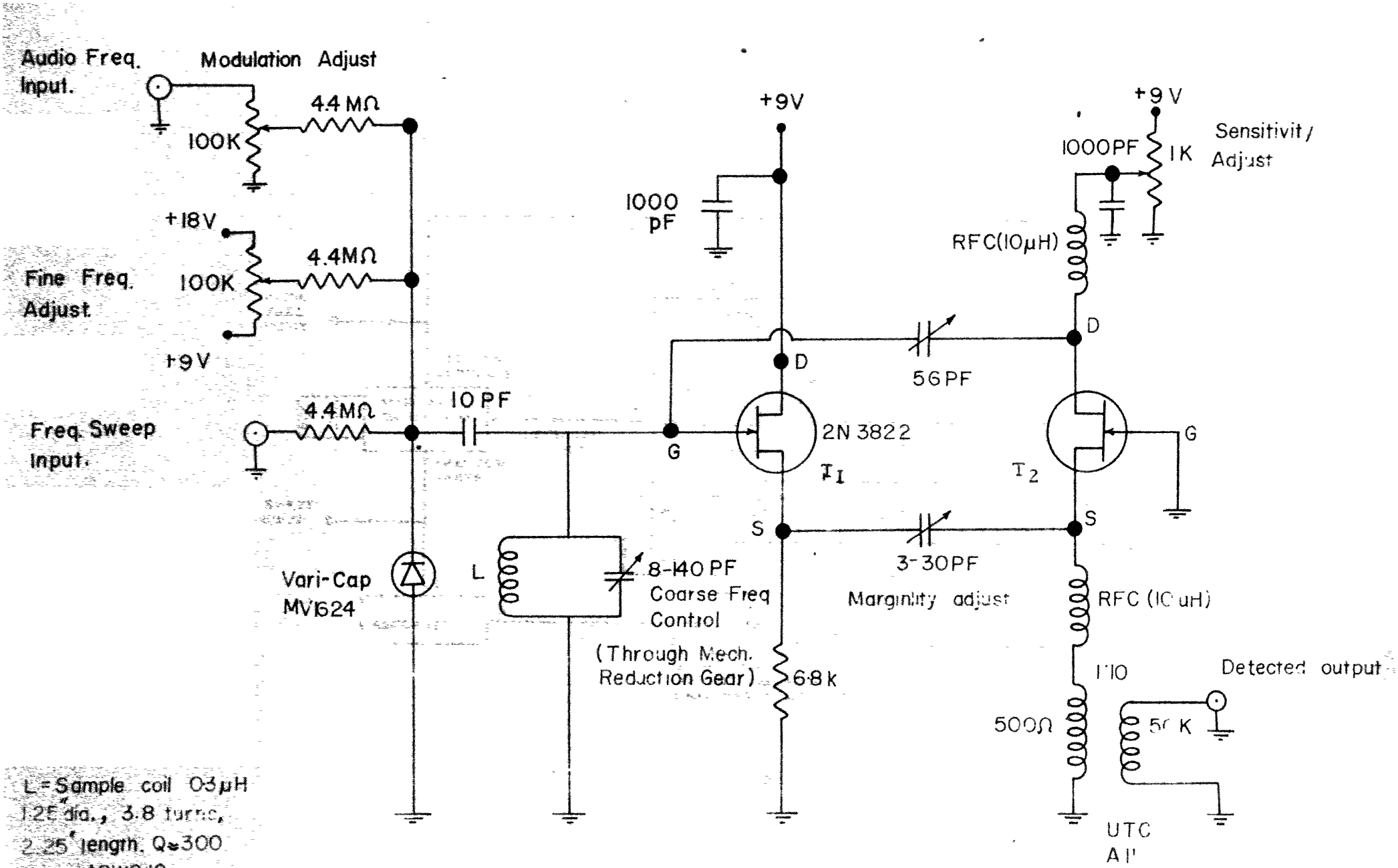

FIG.6 OSCILLATOR-DETECTOR CIRCUIT FOR THE 5 MHz REGION USING FET.

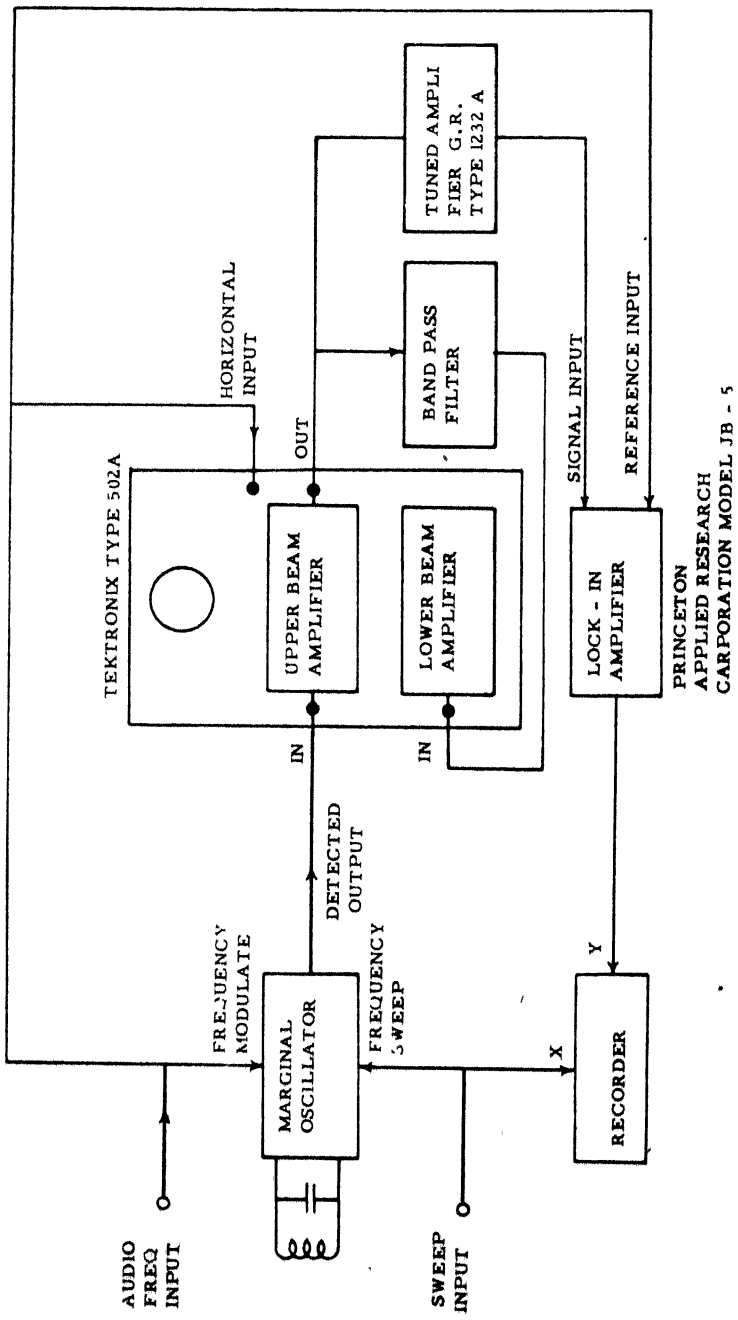

FIG. 7 THE SPECTROMETER SYSTEM

for obtaining an oscilloscope display as well as the derivative plot on an x-y recorder. This system employs frequency modulation of the oscillator for obtaining the periodic output. This is achieved with the help of a variable capacitance diode (Varicap) across the tank coil.

Selection of the Varicap

With reference to Figure 6, the modulating signal is derived from the reference oscillator of the lock-in amplifier (Princeton Applied Research type JB4). The varicap is chosen such that it gives the necessary capacitance variation for a maximum frequency deviation of 10 KHz. The frequency deviation should be about 10 times the line width. Another important criterion for choosing the varicap is the quality factor $(1/\omega\, Cr_s)$ where ω is the angular frequency, C the capacitance and r_s the equivalent series resistance of the diode.

The fractional change in the tuning capacitor needed for a given fractional change in frequency of resonance is given by

$$\frac{\Delta C}{C} = -2\,\frac{\Delta f}{f} \qquad (2.3)$$

For a 10 KHz change centred around 30 MHz,

$$\frac{\Delta f}{f} = \left(\frac{1}{30}\right) \times 10^{-2}$$

For an inductance of 0.37 μ h (coil used by Wang), the capacitance C needed to tune the coil to 30 MHz is 75 pf.

Therefore

$$C = 0.05 \text{ pF}.$$

This change in capacitance can be easily brought about since a voltage of 5 volts peak to peak is available at the output of the reference oscillator.

Referring to Figure 8 , the varicap is reverse biased by a d.c. voltage which can be varied from 9 to 18 volts. This provides a "fine frequency tuning" control. The varicap Motorola type MV1624 is used and its capacitance as a function of reverse bias voltage is shown in Figure 8 . It has a quality factor of 300 at 50 MHz. Around a reverse bias voltage of 12 volts, the capacitance is 12 pF and the slope dc/dv is 0.5 pF/volt. Since this variation is too large, in order to get a finer control of frequency, a capacitance of 10 pF is connected in series with the varicap. This reduces the variation to about 0.1 pF/volt.

The "modulation adjust" potentiometer is calibrated in terms of frequency deviation by applying a known d.c. voltage change into the modulation input and counting the corresponding frequency difference using HP type 524C frequency counter.

Preamplifier

The output of the oscillator-detector is fed to a low noise preamplifier. If the signal voltage output is of the order of a few hundred microvolts, Tektronix type 502A

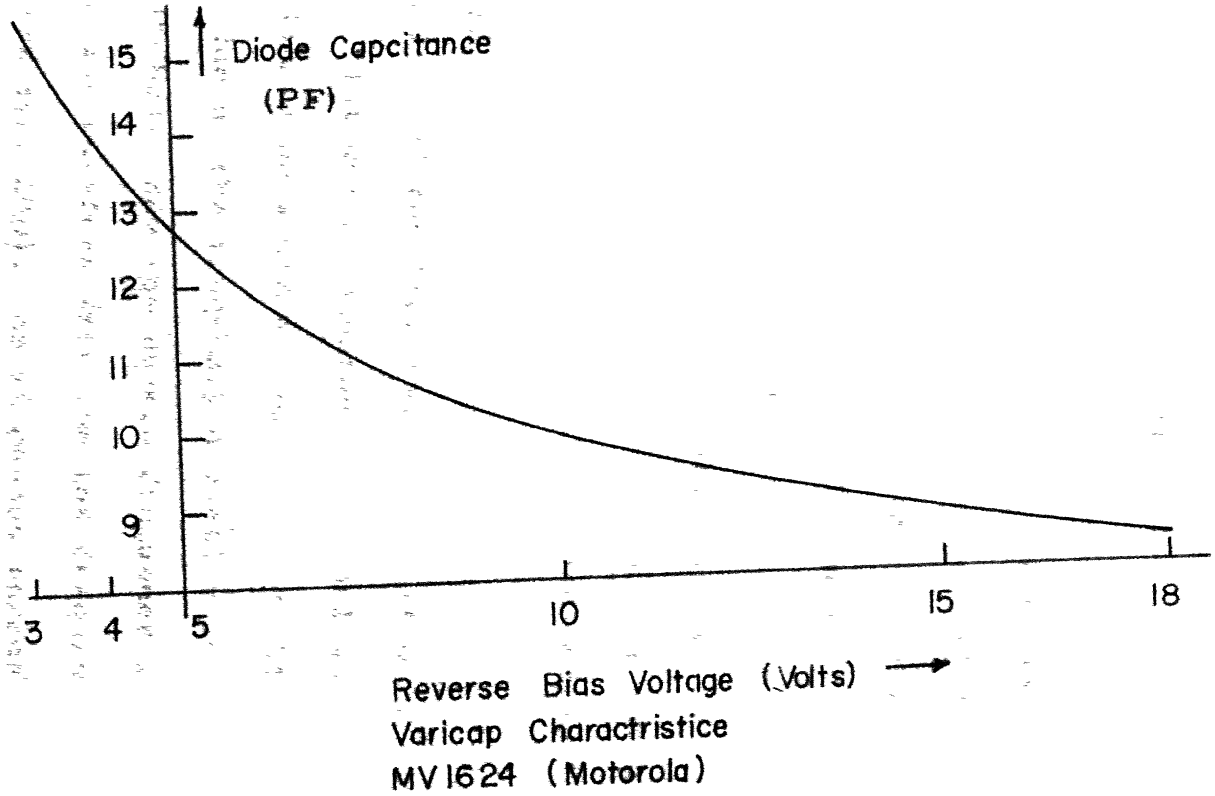

FIG. 8 CAPACITANCE AS A FUNCTION OF THE REVERSE BIAS VOLTAGE OF THE VARICAP MV1624

oscilloscope can be used for this purpose as it has a low noise preamplifier with 100 microvolts per centimetre sensitivity. Further improvement in signal to noise ratio is obtained by feeding the output of the preamplifier to an active bandpass filter (Appendix 1).

Alternatively, the plug-in unit Tektronix type 1A7A (in conjunction with any 530, 540 or 550 series Tektronix oscilloscope) which has a low noise FET input stage and 10 microvolts per centimetre sensitivity can be used. Furthermore, it has the facility for controlling the bandwidth thus eliminating the need for the bandpass filter. The bandwidth to be used depends on the ratio of the line width to the frequency deviation employed. The details of this will be discussed in Chapter IV.

Derivative Plot

Having located the line and centred it on the oscilloscope, the derivative plot which enhances the signal to noise ratio (thereby enabling line width measurement) is obtained. This is achieved by reducing the frequency deviation to a fraction of a line width (100 Hz). Now the centre frequency is swept slowly using a triangular waveform from the low frequency function generator (Exact type 240). As it passes through the resonance frequency, the output is obtained using the tuned amplifier phase sensitive detector system (Lock-in amplifier).

The sweep rate is related to the time constant of the low pass filter at the output of the lock-in amplifier which

effectively controls the bandwidth of this narrow band filtering system. The sweep rate should be adjusted such that the time taken for traversing the region of absorption is large compared to the time constant of the filter (BROWER LABORATORY, INC., 1968). The maximum time constant that can be employed is limited by the frequency stability of the oscillator. The values of the filter time constant and sweep rate are arrived at by trial and error to obtain a plot with maximum signal to noise ratio. The derivative plot of a polycrystalline sample (30 cc) of sodium chlorate at room temperature is shown in Figure 9.

2.4 MODIFIED OSCILLATOR-DETECTOR CONFIGURATION

In the oscillator-detector circuit of Figure 6, the source follower transistor T_1 provides the impedance transformation necessary to drive the transistor T_2. Alternatively, this impedance transformation can be achieved by a capacitive voltage divider. By doing this one of the active devices can be eliminated which, in turn, reduces the noise in the circuit. Figure 10 shows the circuit with these modifications. It may be mentioned that the input capacitance of the device becomes part of the capacitive voltage divider. The impedance matching provided by the voltage divider also helps to operate the transistor under minimum noise conditions (ROBINSON, 1967). An interesting feature of the circuit is that there are no resistors in the circuit. The circuit components are again optimized with the help of a low frequency

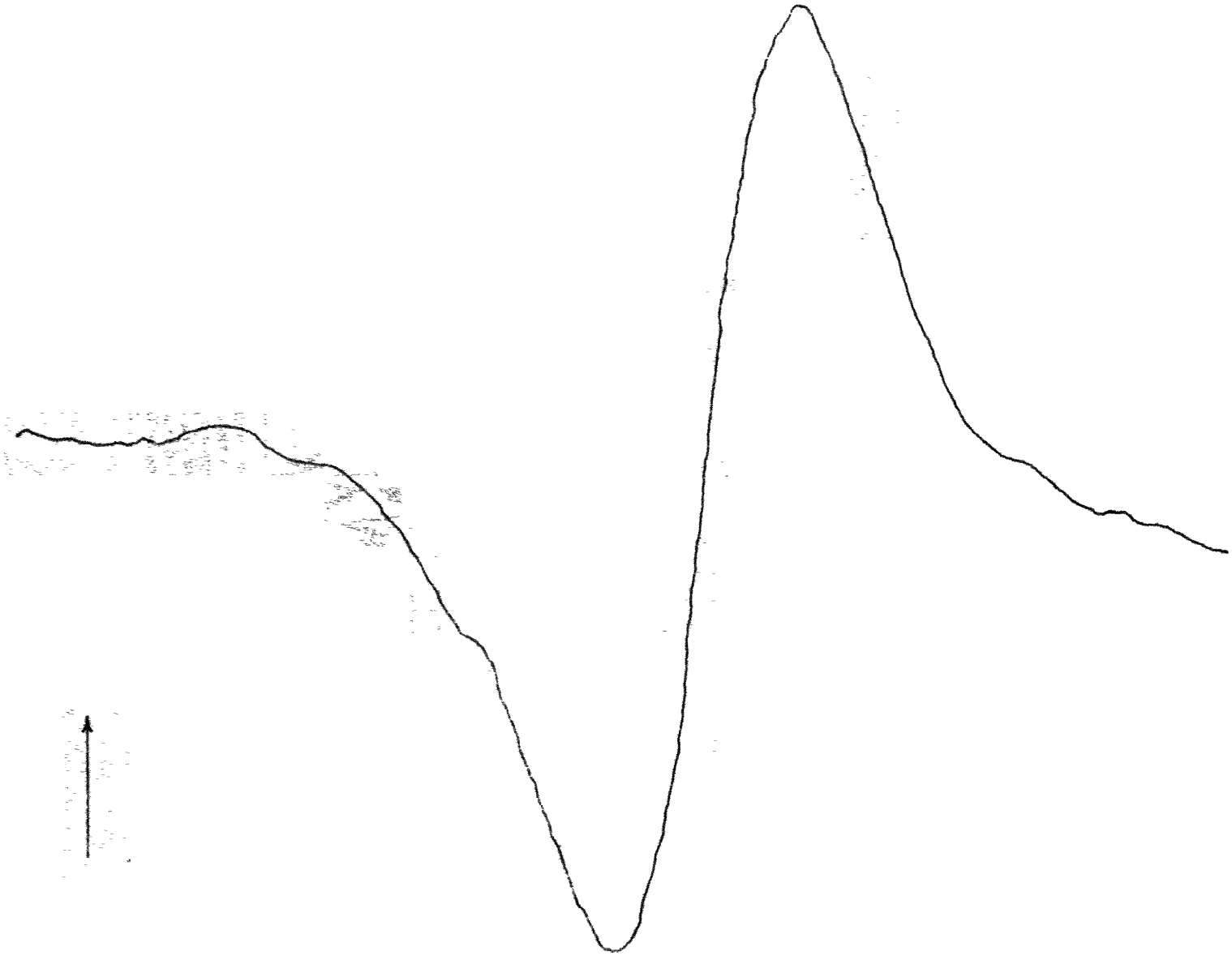

FIG. 9 DERIVATIVE OF THE ABSORPTION LINE OF SODIUM CHLORATE

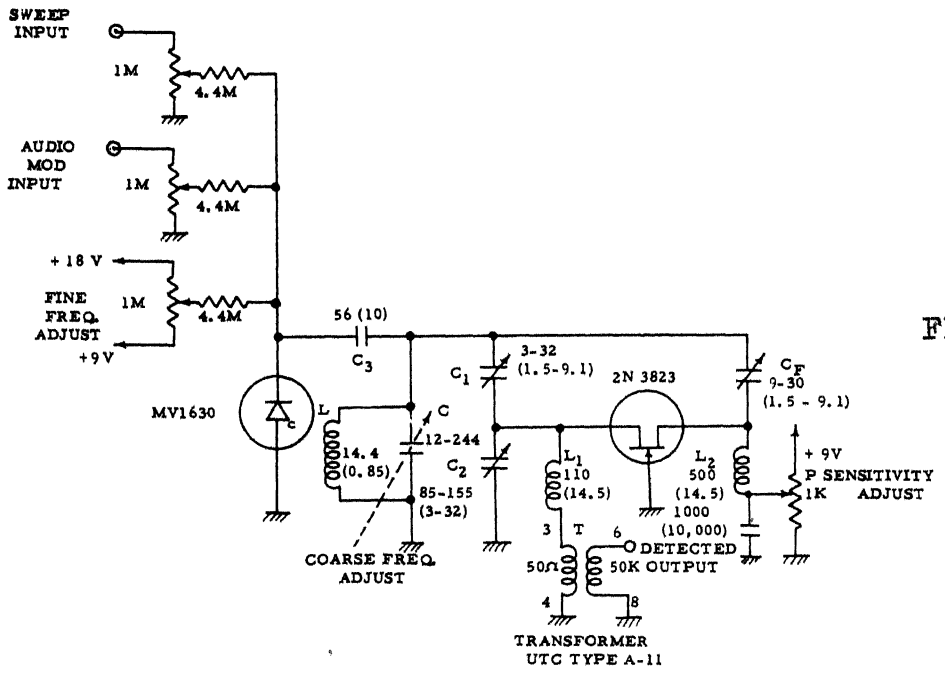

FIG.10 Circuit diagram of the oscillator–detector.

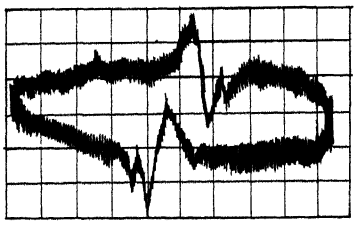

FIG.11 The spectrum of sodium chlorate at room temperature. (The output of the transformer T is connected directly to the vertical input of the oscilloscope using a Tektronix type 1A7 plug-in unit. Vertical sensitivity 200 μV/div.) Sample coil (L) diameter 2.54 cm (3.5 cm), length 7.62 cm (3.5 cm), No. of turns 32(6), ASWG 18(19), Q 240 (330). All inductors and capacitors are in microhenries and picofarads, respectively.

simulation and the final circuit obtained is shown in Figure 10.

The spectrometer for the 30 MHz region is tunable over a range of 10 MHz and has been also used for obtaining several NQR spectra (22 MHz - 30 MHz, (KUMAR, 1970)). The wide-band display obtained for a polycrystalline sample (30 cc) of sodium chlorate at room temperature is shown in Figure 11.

In the 3 MHz region, the derivative plot obtained for a polycrystalline sample of Hexamethylene-tetramine (35 cc) at room temperature is shown in Figure 12.

2.5 CONSTRUCTIONAL DETAILS

The success of being able to detect NQR absorption signals lies in observing a few practical details. Although these are well established principles known to electrical engineers and physicists who have dealt with high frequency circuits, even the spectrometers based on tried out circuits cannot be made to work without proper adherence to these fabrication details which will now be briefly outlined.

It has been shown in Chapter I that the percentage change in the conductance of the tank coil due to absorption is directly proportional to the quality factor Q of the coil. Thus, in order to achieve a high quality factor, the coil must be well designed. With the use of a few turns of silver plated copper wire (ASWG 18) wound directly on the sample holder (made of perspex*) one can easily obtain a quality factor of 300 in

---

*Methyl methacrylate

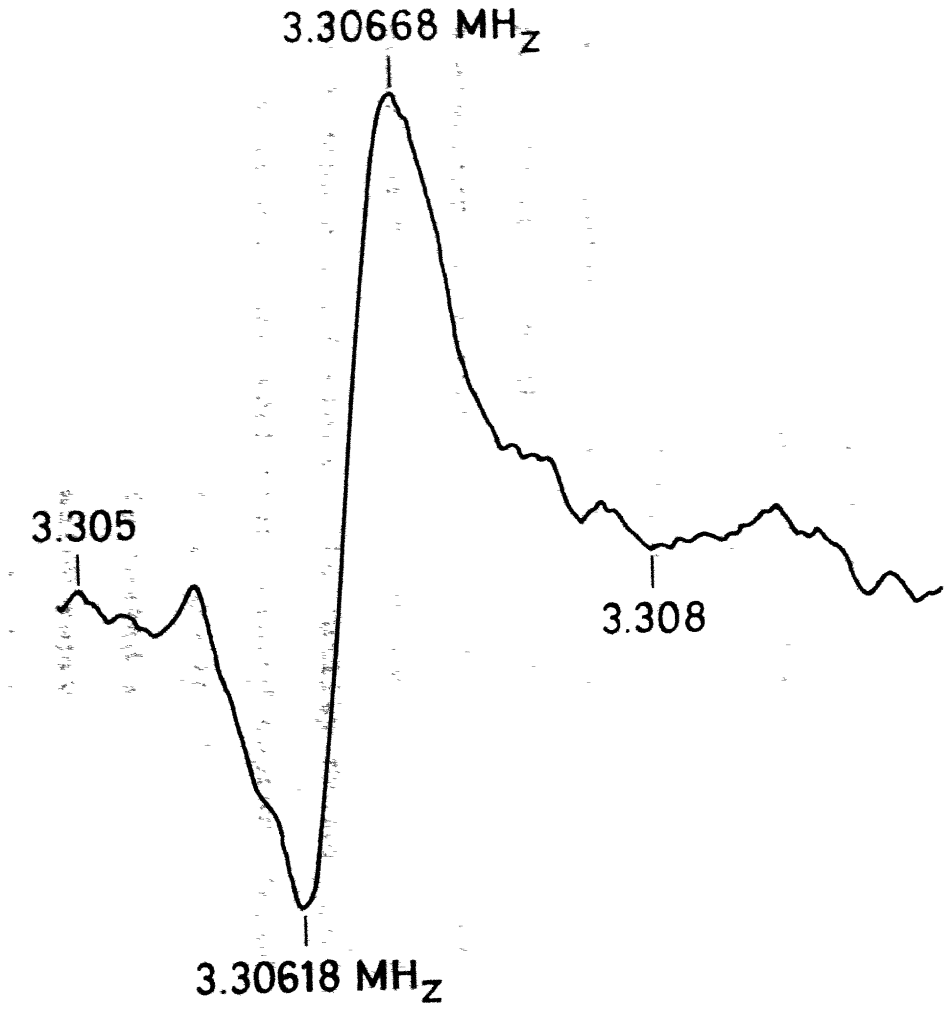

Fig. 12 Derivative of the absorption line of Hexamethylene - tetramine.

the region of 30 MHz. It may be mentioned that the ratio of length to diameter of the coil should be approximately unity (3.5 cm : 3.5 cm). For the 3 MHz region, since the inductance of the coil is much higher, larger number of turns (= 32) of thinner wire will have to be employed in order to see that the coil does not become unduly large. An effective way of imparting rigidity to the coil is to wind it tightly on a hollow perspex former on which grooves are cut using a lathe. Further, the coil is held in position by potting it in epoxy resin.

The coil must be preferably mounted directly on the tuning capacitor itself using high conductivity silver solder, or any mechanical connection employed should be designed carefully to preserve the Q of the tank circuit. If low temperature operation is required, once again care should be exercised to see that the extension from the capacitor to the coil does not deteriorate the quality factor appreciably. An extender with one inch wide printed copper strips (tinned) has been successfully used to enable the immersion of the coil in the coolant. The strip is coated with epoxy resin to prevent reduction of Q due to water vapour condensing on it. The vacuum flask to hold the coolant should preferably have no silver coating. Alternately, if a silver coated flask is used, it should have a diameter greater than twice the diameter of the coil.

The printed oscillator-detector circuit is mounted directly on the tuning capacitor as shown in the photograph.

Reduction gear is provided for the tuning capacitor (E.F. Johnson type 154-1) so that its range (12 - 244 pF) is covered in 25 rotations of the tuning knobs. Grade 1 metal film resistors and silvered mica capacitors are used in the oscillator-detector circuit. The assembly including the batteries is enclosed in a metal box to shield it from electrostatic disturbances and nearby radio stations which give rise to spurious signals. The audio transformer used in the circuit must have both electrostatic and magnetic shielding since the signal level can be as low as 10 to 20 μ v. This low level output is coupled to the preamplifier using a shielded cable (Figures 13, 14).

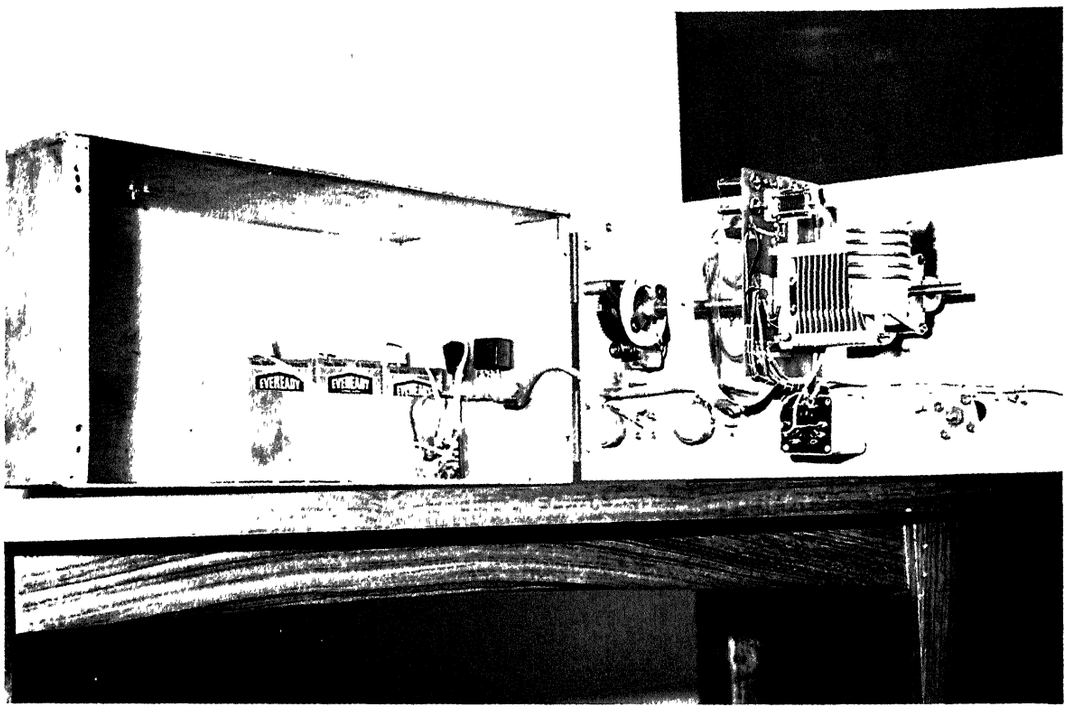
EVEREADY
EVEREADY

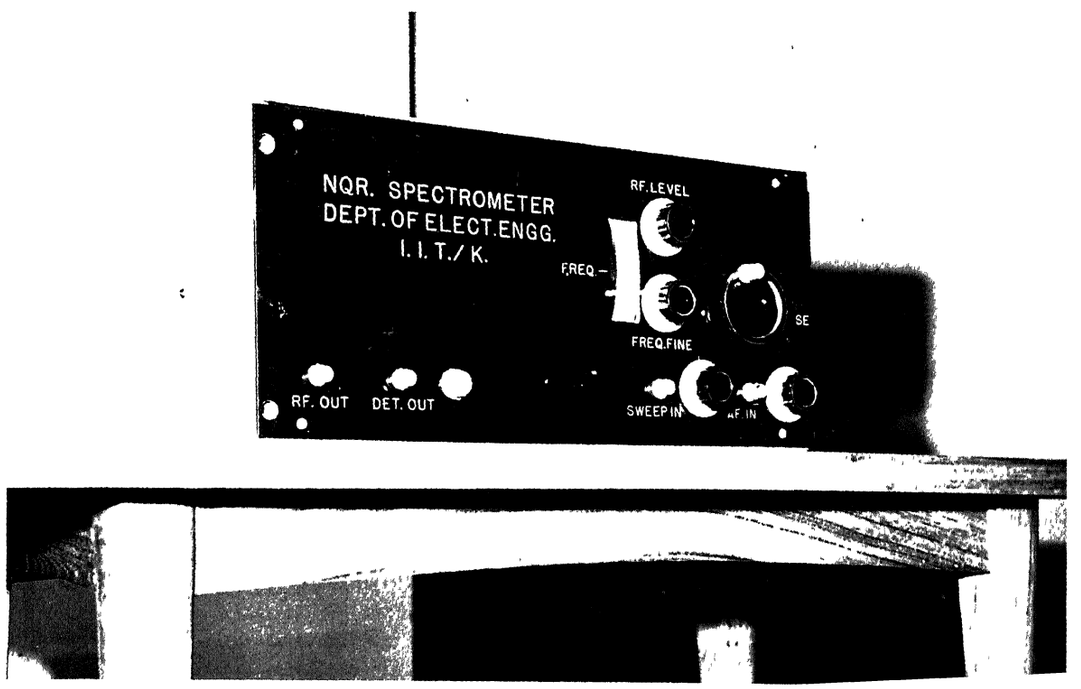
NQR. SPECTROMETER
DEPT. OF ELECT. ENGG.
I. I. T./ K.
RF. LEVEL
FREQ.-
FREQ.FINE
SE
RF. OUT
DET. OUT
SWEEP IN
AF. IN

CHAPTER - III

ANALYTICAL APPROACH

3.1 INTRODUCTION

It is well known that the output of a regenerative oscillator-detector is a function of the circuit configuration and the loop gain. In general, the output tends to be maximum when the circuit conditions are such that the loop gain is just sufficient to maintain oscillations. It is of interest to obtain a quantitative relationship between detected output and the circuit conditions. In order to do so, a generalised representation shown in Figure 15 is used for the oscillator. It consists of a parallel resonant circuit and an active device connected in a positive feedback configuration. The active device is characterised by a transfer characteristic given by

$$i = g(v) \qquad (3.1)$$

This relationship is, in general, nonlinear, which is essential to obtain a stable limit cycle.

3.2 THE PIECEWISE LINEAR (PWL) MODEL

A simple PWL model forms a good approximation for the nonlinear device in most of the situations encountered in practice. Generally, the PWL characteristic will consist of an amplifying segment and two limiting segments. For example, in the case of the bipolar transistor, the limiting segments arise from the saturation and cut-off regions. The active

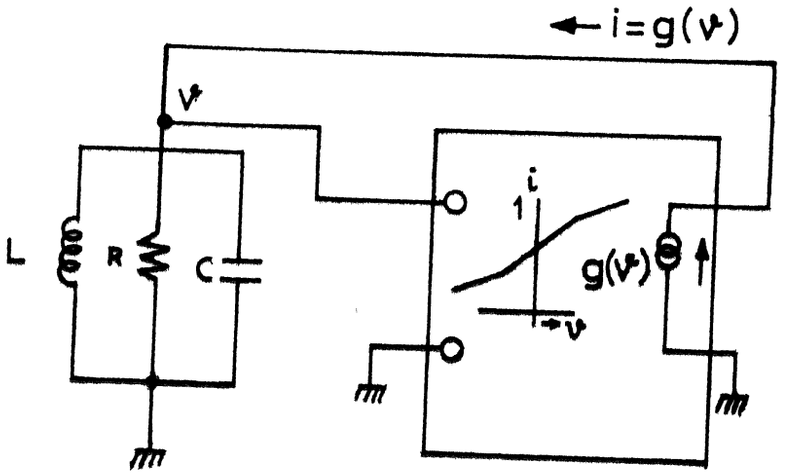

FIG.15 SCHEMATIC DIAGRAM OF AN OSCILLATOR

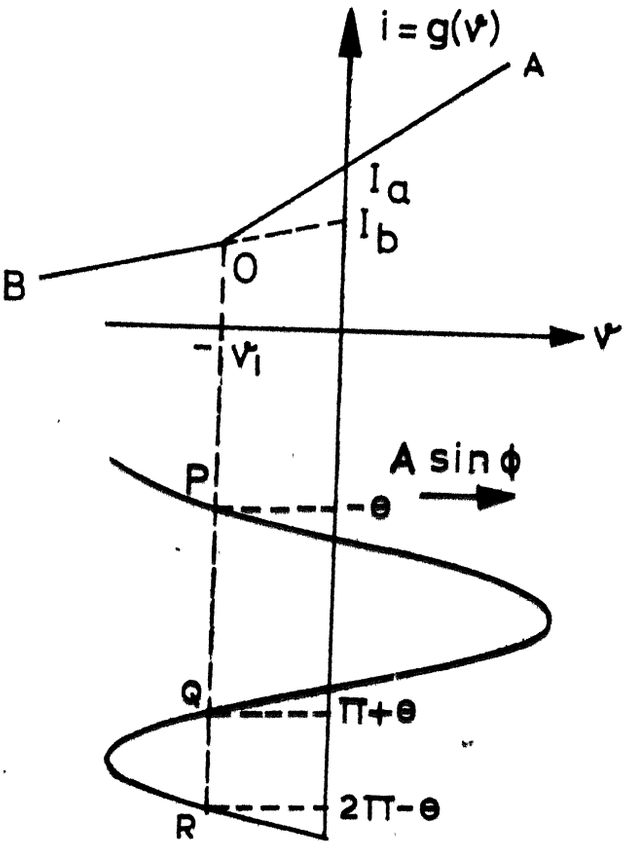

FIG.16 PIECEWISE LINEAR CHARACTERISTIC WITH TWO SEGMENTS

device is always biased in the amplifying region so that oscillations start when the loop gain exceeds unity. The oscillations grow until one or the other or both the limiting regions come into the picture. If the biasing is symmetrical with respect to the break points, the limiting takes place due to both the regions. Whereas, if it is asymmetrical, only one of the two limiting regions will play a part in giving rise to the limit cycle. Once again, the influence of both the limiting regions will be felt when the amplitude of oscillation becomes large.

With this picture in mind, in the following sections, analysis of the sensitivity of oscillators has been carried out for two different cases, namely, one with a single limiting region and one with two limiting regions.

3.3 PWL CHARACTERISTIC WITH ONE LIMITING SEGMENT

Figure 16 shows the characteristic, where the segment OA forms the amplifying part and OB forms the limiting part. As the slope of OB varies from zero to the slope of OA, the change in the nature of the nonlinearity will be referred to as changing from "hard" to "soft".

The characteristic $i=g(v)$ is expressed as

$$i = I_a + g_a v \quad \text{for} \quad v \geq -v_1$$

and

$$i = I_b + g_b v \quad \text{for} \quad v < -v_1 \qquad (3.2)$$

where I_a and I_b are intercepts on the current axis as

shown in Figure 16. Conductances g_a and g_b are slopes of the segments OA and OB respectively. The bias point is given by $(0, I_a)$.

The differential equation governing the behaviour of the circuit is given by

$$\frac{d^2v}{dt^2} + \omega_o^2 v + \omega_o^2 L \frac{dv}{dt} \left[\frac{1}{R} - g'(v) \right] = 0 \qquad (3.3)$$

In the absence of the third term, equation (3.3) has a sinusoidal solution. The condition for obtaining nearly sinusoidal solution is evaluated by substituting the sinusoidal solution itself in each of the terms on the left hand side of equation (3.3) and comparing their coefficients. Thus we get

$$\omega_o L \left[\frac{1}{R} - g'(v) \right] << 1$$

$$\text{i.e. } \frac{1}{Q} \left[1 - g'(v)R \right] << 1$$

$$\text{where } Q = R \omega_o C = \frac{R}{\omega_o L}$$

The product $g'(v)R$ represents the loop gain which is arranged to be very nearly equal to unity for marginal oscillators. The quality factor Q should be of the order of hundred so that the above condition is satisfied. The higher the value of Q the better is the approximation. Q of the order of 300 is practically achievable at the frequencies of interest.

The Kryloff-Bogoliuboff First Approximation

The equation (3.3) can be written in the form

$$\frac{d^2v}{dt^2} + \omega_o^2 v + \epsilon \cdot f(v, \frac{dv}{dt}) = 0 \qquad (3.4)$$

where $\epsilon f(v, \frac{dv}{dt}) = \omega_o^2 L \left(\frac{1}{R} - g'(v) \right) \frac{dv}{dt}$ and ϵ is a number very much smaller than unity.

The form of equation (3.4) suggests that it is amenable to the mode of analysis suggested by Kryloff and Bogoliuboff (KRYLOFF AND BOGOLIUBOFF, 1947) for nearly simusoidal solution. According to their first approximation method, we assume a solution of the form

$$v = A \operatorname{Sin} (\omega_o t + \phi)$$
$$\text{and} \quad \frac{dv}{dt} = A \omega_o \operatorname{Cos} (\omega_o t + \phi). \qquad (3.5)$$

Here A and ϕ are slowly varying functions of time. Within one period corresponding tc the frequency ω_o, A and ϕ are assumed to be constant. Using equations (3.4) and (3.5) it can be easily shown that

$$\frac{dA}{dt} = - \frac{\epsilon}{\omega_o} f \left[A \operatorname{Sin}(\omega_o t + \phi), A \omega_o \operatorname{Cos}(\omega_o t + \phi) \right] \operatorname{Cos}(\omega_o t + \phi)$$

$$\frac{d\phi}{dt} = \frac{\epsilon}{A \omega_o} f \left[A \operatorname{Sin}(\omega_o t + \phi), A \omega_o \operatorname{Cos}(\omega_o t + \phi) \right] \operatorname{Sin}(\omega_o t + \phi).$$

If ϵ is small, dA/dt and $d\phi/dt$ are also small and A and ϕ are thus slowly varying functions of time, to a

first approximation. Therefore, dA/dt and dØ/dt can be considered to be constant at their average value over a single cycle. Thus,

$$\frac{dA}{dt} = -\frac{\epsilon}{2\pi\omega_o}\int_0^{2\pi} f(A\,\mathrm{Sin}\,\phi,\ A\omega_o\,\mathrm{Cos}\,\phi)\,\mathrm{Cos}\,\phi\,d\phi$$

The detected output tracks only the variations of amplitude of oscillation, thus we are interested in only the expression for dA/dt

$$\text{i.e.}\quad \frac{dA}{dt} = -\frac{A\omega_o^2 L}{2\pi}\int_0^{2\pi}\left[\frac{1}{R} - g'(A\,\mathrm{Sin}\,\phi)\right]\mathrm{Cos}^2\phi\,d\phi \qquad (3.6)$$

From Figure 16 , we have

$$v_1 = A\,\mathrm{Sin}\,\theta \qquad (3.7)$$

and $\quad g'(v) = g_a \quad \text{for} \quad -\theta \leq \phi \leq (\pi + \theta)$

and $\quad g'(v) = g_b \quad \text{for} \quad \pi + \theta < \phi < (2\pi - \theta)$

Substituting for g'(v) in equation (3.6),

$$\frac{dA}{dt} = -\frac{L\omega_o^2 A}{2\pi}\left[\left(\frac{1}{R}-g_a\right)\int_{-\theta}^{\pi+\theta}\mathrm{Cos}^2\phi\,d\phi + \left(\frac{1}{R}-g_b\right)\int_{\pi+\theta}^{2\pi-\theta}\mathrm{Cos}^2\phi\,d\phi\right]$$

$$= -\frac{L\omega_o^2 A}{4\pi}\left[\left(\frac{1}{R}-g_a\right)(\mathrm{Sin}\,2\theta + 2\theta + \pi) + \left(\frac{1}{R}-g_b\right)(-\mathrm{Sin}\,2\theta - 2\theta + \pi)\right] \qquad (3.8)$$

Equation (3.8) gives the condition for stability of oscillations. For values of A less than v_1, the entire

voltage excursion will be in the region OA of Figure 16. Thus

$$\frac{dA}{dt} = -\frac{L\omega_o^2 A}{2\pi}\int_0^{2\pi}\left(\frac{1}{R} - g_a\right)\cos^2\phi\, d\phi = -\frac{L\omega_o^2 A}{2}\left(\frac{1}{R} - g_a\right) \quad (3.9)$$

We see that dA/dt is positive, as long as g_a is greater than $\frac{1}{R}$, representing growing oscillations. Thus $g_a R > 1$, gives the starting condition for oseillations.

Amplitude of Oscillation

The steady state amplitude of oscillation is obtained by setting $\frac{dA}{dt}$ equal to zero. Thus from equation (3.8) we get

$$\sin 2\theta + 2\theta = \frac{\pi}{(g_a - g_b)}\left[\frac{2}{R} - (g_a + g_b)\right] \quad (3.10)$$

Given a set of values of g_a, g_b and R, θ is first calculated using equation (3.10), and then A is obtained as a function of v_1 from equation (3.7).

Equation (3.10) can be rewritten as follows

$$\sin 2\theta + 2\theta = \frac{\pi}{g_a R - g_b R}\left[2 - (g_a R + g_b R)\right] \quad (3.11)$$

$$\text{or} \quad \sin 2\theta + 2\theta = \frac{\pi}{(1 - g_b/g_a)}\left[\frac{2}{g_a R} - (1 + g_b/g_a)\right] \quad (3.12)$$

Equation (3.11) is useful when g_a and g_b are chosen independently to obtain a certain amplitude. The form of the equation (3.12) is advantageous, when the nonlinearity is fixed,

i.e., g_a and g_b are chosen in such a way that g_b/g_a is maintained constant.

From Figure 16 we can find out the range of θ which is relevant to this discussion. The maximum value happens to be $\pi/2$ when $A = v_1$. The minimum value of θ is zero when A tends to infinity.

Equation (3.11) has been solved (for the of values of θ extending from 0 to $\pi/2$) numerically using a digital computer* and Figure 17 shows the variation of A (normalised with respect to v_1) with g_aR for different values of g_bR. For each value of g_bR the value of g_aR at which the amplitude tends to infinity is given by

$$g_aR = 2 - g_bR \qquad (3.13)$$

Equation (3.13) gives the maximum permitted values of g_aR for given values of g_bR. The maximum range of variation for g_aR is from one to two which is obtained when $g_bR = 0$.

Sensitivity

Having obtained the amplitude of oscillation A as a function of the resistance R and the transconductances g_a and g_b, we are in a position to determine the sensitivity of A with respect to changes in R. We define the sensitivity S as the ratio of the fractional change in amplitude of oscillation to the fractional change in R,

$$\text{i.e.} \qquad S = \frac{\partial A/A}{\partial R/R}$$

*Refer to Appendix III.

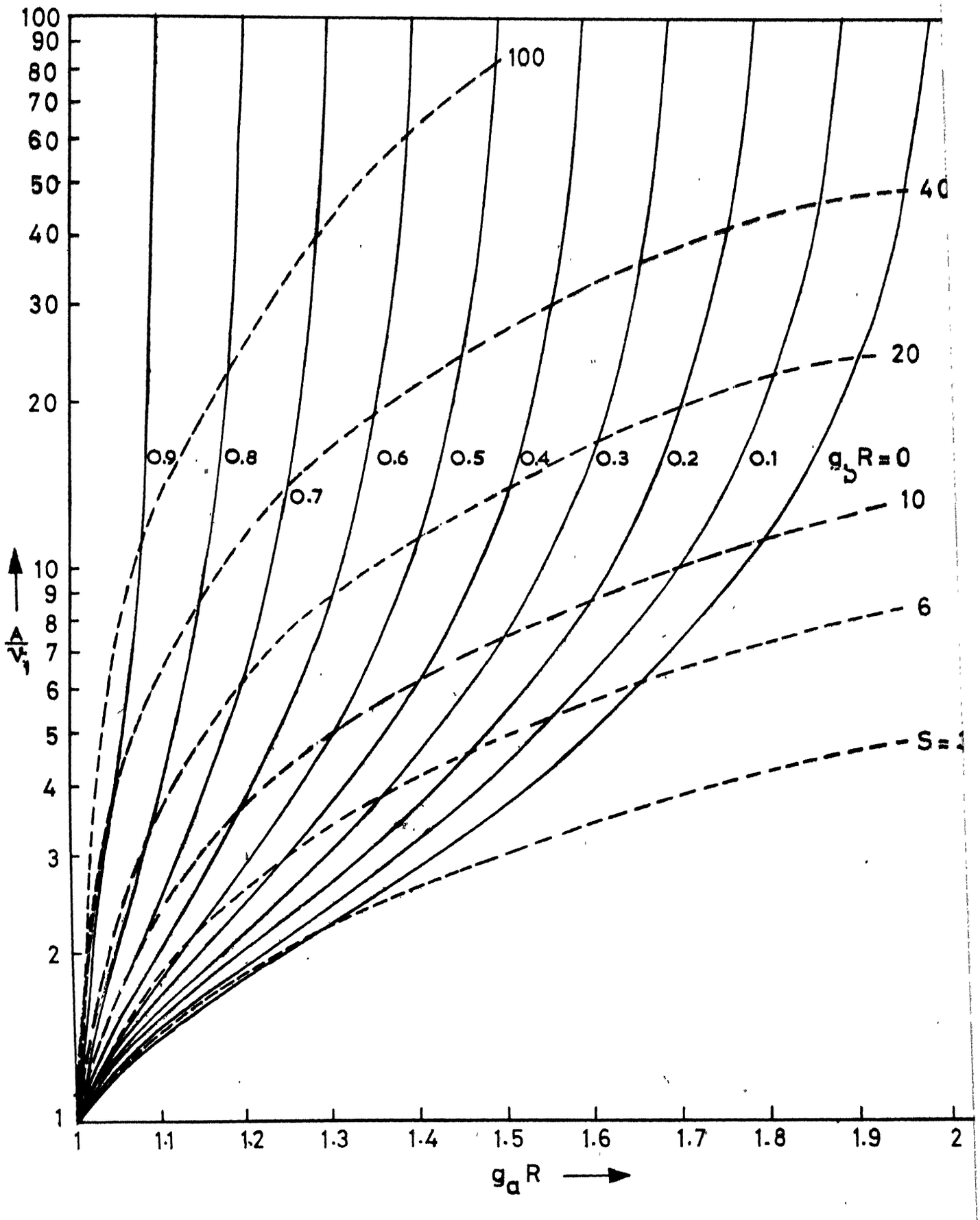

FIG.17 AMPLITUDE OF OSCILLATION (NORMALISED WITH RESPECT TO v_1) AS A FUNCTION OF g_aR AND g_bR. DOTTED LINES INDICATE CONSTANT SENSITIVITY LOCI.

which can be rewritten as

$$S = \frac{\partial A}{\partial \theta} \quad \frac{\partial \theta}{\partial R} \quad \frac{R}{A}$$

Differentiating equation (3.11), we get

$$\frac{\partial \theta}{\partial R} = \frac{-\pi}{(g_a R - g_b R)\, R(1 + \text{Cos } 2\theta)}$$

Differentiating equation (3.7), we have

$$\frac{\partial A}{\partial \theta} = - \frac{v_1}{\text{Sin}^2 \theta} \text{ Cos } \theta$$

Thus

$$S = \frac{\pi}{(g_a R - g_b R) \text{ Sin } 2\theta} \qquad (3.14)$$

Given a set of values of g_a, g_b and R, θ is first evaluated using equation (3.11) and then S is evaluated by substituting for θ in equation (3.14). Figure 18 shows S as a function of $g_a R$ and $g_b R$. The same Figure also shows constant amplitude loci (dotted lines). The utility of these loci will be evident later. From Figure 18, we can conclude that for a given value of $g_a R$, higher sensitivity is obtained at higher values of $g_b R$. Further, S tends to infinity when $g_a R$ tends to unity and at the upper limit of $g_a R$ given by equation (3.13). $g_a R$ tending to unity indicates the condition when the loop gain is just enough to sustain oscillations. This is what is usually referred to as the marginal state.

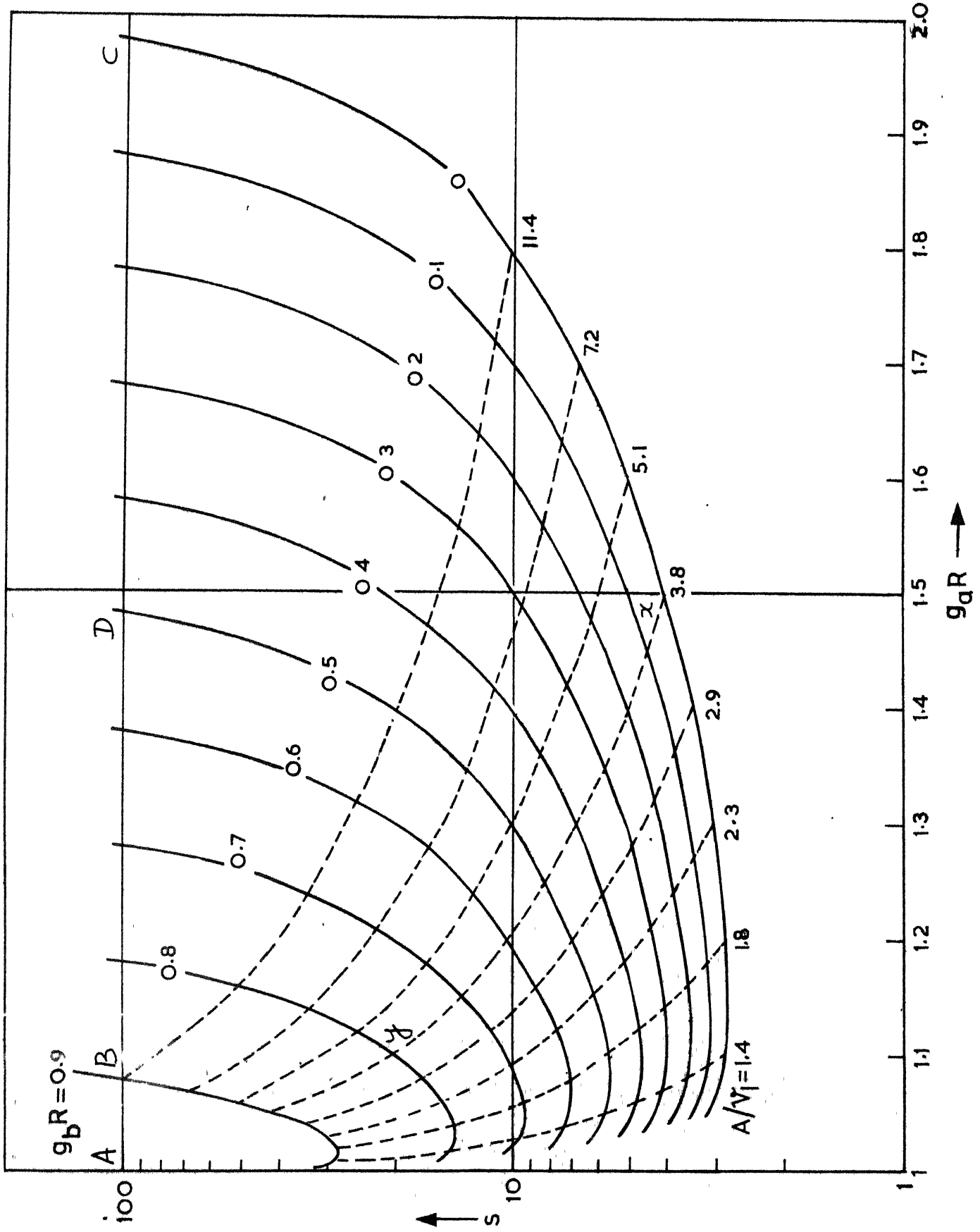
A
B
C
D
$g_b R = 0.9$
0.8
0.7
0.6
0.5
0.4
0.3
0.2
0.1
0
11.4
7.2
5.1
3.8
2.9
2.3
1.8
$A/V_j = 1.4$
γ
α
100
10
1
S
1.1
1.2
1.3
1.4
1.5
1.6
1.7
1.8
1.9
2.0
$g_a R$

Stability Requirements of g_a, g_b and v_1

From equation (3.10) it is evident that any fluctuation in g_a and g_b will cause variation in the amplitude of oscillation. We will now evaluate the sensitivity of the amplitude of oscillation with respect to g_a and g_b in order to obtain a quantitative idea of the degree of stability required for g_a and g_b. Defining N_1 as the sensitivity of the amplitude with respect to g_a, we have

$$N_1 = \frac{\partial A/A}{\partial g_a/g_a}$$

which can be rewritten as

$$N_1 = \frac{\partial A}{\partial \theta} \cdot \frac{\partial \theta}{\partial g_a} \cdot \frac{g_a}{A}$$

Using equations (3.7) and (3.10) we can evaluate $\frac{\partial A}{\partial \theta}$ and $\frac{\partial \theta}{\partial g_a}$. Thus

$$N_1 = \frac{\pi g_a R\ (1 - g_b R)}{(g_a R - g_b R)^2 \sin 2\theta} \qquad (3.15)$$

Similarly we have

$$N_2 = \frac{\partial A/A}{\partial g_b/g_b} = \frac{\pi g_b R\ (g_a R - 1)}{(g_a R - g_b R)^2 \sin 2\theta} \qquad (3.16)$$

In order to facilitate comparison of S and N_1 and N_2, it is useful to evaluate the ratios S/N_1 and S/N_2. These

are given by

$$\frac{S}{N_1} = \frac{g_aR - g_bR}{g_aR(1-g_bR)} \tag{3.17}$$

$$\frac{S}{N_2} = \frac{g_aR - g_bR}{g_bR(g_aR-1)} \tag{3.18}$$

The Table 2 gives the limits of S/N_1 and S/N_2 at the extreme values of g_aR and g_bR. With reference to Table we conclude that when the nonlinearity is hard ($g_bR \rightarrow 0$), the stability demanded for g_bR is not high ($S/N_2 \rightarrow \infty$). In any case, the stability required for the loop gain g_aR is always stringent (maximum value of S/N_1 is 2). When the nonlinearity becomes soft ($g_bR \rightarrow 1$ and $g_aR \rightarrow 1$) the sensitivity becomes high, but both the slopes in the PWL characteristic have to be controlled to a high degree of stability (S/N_1 and $S/N_2 \rightarrow 2$).

If we have to obtain a sensitivity of 100, by referring to Figure 18(S vs. g_aR), we can see that there are several possible combinations of g_aR and g_bR which will permit this. A choice of g_bR tending to zero (an operating point like C) will require a value of g_aR tending towards 2. This results in A/v_1 tending to infinity (Figure 17). In such a situation, to keep the amplitude within reasonable limits, v_1 will have to be very small. Further, the stability demanded of v_1 will become too stringent for this choice to have any practical value.

TABLE 2

LIMITS OF S/N_1 AND S/N_2

	$g_aR \rightarrow 1$	$g_aR \rightarrow (2 - g_bR)$
$g_bR \rightarrow 0$	$\frac{S}{N_1} \rightarrow 1$; $\frac{S}{N_2} \rightarrow \infty$	$\frac{S}{N_1} \rightarrow 1$, $\frac{S}{N_2} \rightarrow \infty$
$g_bR \rightarrow 1$	$\frac{S}{N_1} \rightarrow 1$, $\frac{S}{N_2} \rightarrow \infty$	$\frac{S}{N_1} \rightarrow 2$, $\frac{S}{N_2} \rightarrow 2$

Considering the choice of g_bR around unity, there are two possible values of g_aR which result in the given sensitivity (operating points like A and B). One of these values of g_aR is very close to unity to be practicable. Further, if the oscillator is operated at this point, a small increase in g_aR will result in a large decrease in sensitivity. That leaves us with the operating point B, where one can strike a compromise. A/v_1 value for this operating condition is of the order of 10 which is reasonable. From Table 2 we see that the stability requirements for g_aR and g_bR are compatible, though stringent. Thus, the success of obtaining high sensitivity at reasonable values of A/v_1 lies in controlling the gains g_aR and g_bR precisely.

As the operating point is moved from B to D, A/v_1 increases. But the pay-off is in terms of an increased magnitude for S/N_2. However, the value of S/N_1 falls below two. In many practical situations, the degree of nonlinearity of the PWL characteristic is fixed by keeping g_b/g_a constant. One controls the overall gain of the circuit to fix g_aR and g_bR. Thus, once the overall gain is controlled to a given degree of stability, both g_a and g_b have the same stability. Under these circumstances, nothing much is achieved by moving from B to D.

Response of the Oscillator to a Step Change in R

Equation (3.8) will now be used to determine the

behaviour of the amplitude of oscillation when a step perturbation ΔR is introduced in the resistance R. It is important to know the response time as it is inversely related to the effective bandwidth of the oscillator. The effective bandwidth, in turn, controls the signal to noise ratio and also gives information regarding the frequency of modulation to be used.

Equation (3.8) can be rewritten in the following fashion.

$$\frac{dA}{dt} = \frac{-A}{2QT}\left[\pi\{2 - (g_aR + g_bR)\} - (\text{Sin } 2\theta + 2\theta)(g_aR - g_bR)\right] \quad (3.19)$$

Different values of g_aR and g_bR were chosen subject to the condition that the initial amplitude is the same in all cases. The change ΔR was determined using the equation (3.14) such that a 10 per cent change in amplitude is obtained. The final value of g_aR and g_bR evaluated by taking into account the corresponding change ΔR, were used to determine the final amplitude using equation (3.11). The equation (3.19) was used to numerically evaluate on the digital computer, the time taken by the amplitude to go from the initial value to 95 per cent of the difference between the final and initial values.* An iterative method was adopted for this evaluation. The variation of the amplitude of oscillation as a function time is given in Figure 19. We see that the larger the value of g_bR, longer is the time taken to attain the final value. The response is very nearly exponential. The time constant τ

*Refer to Appendix III.

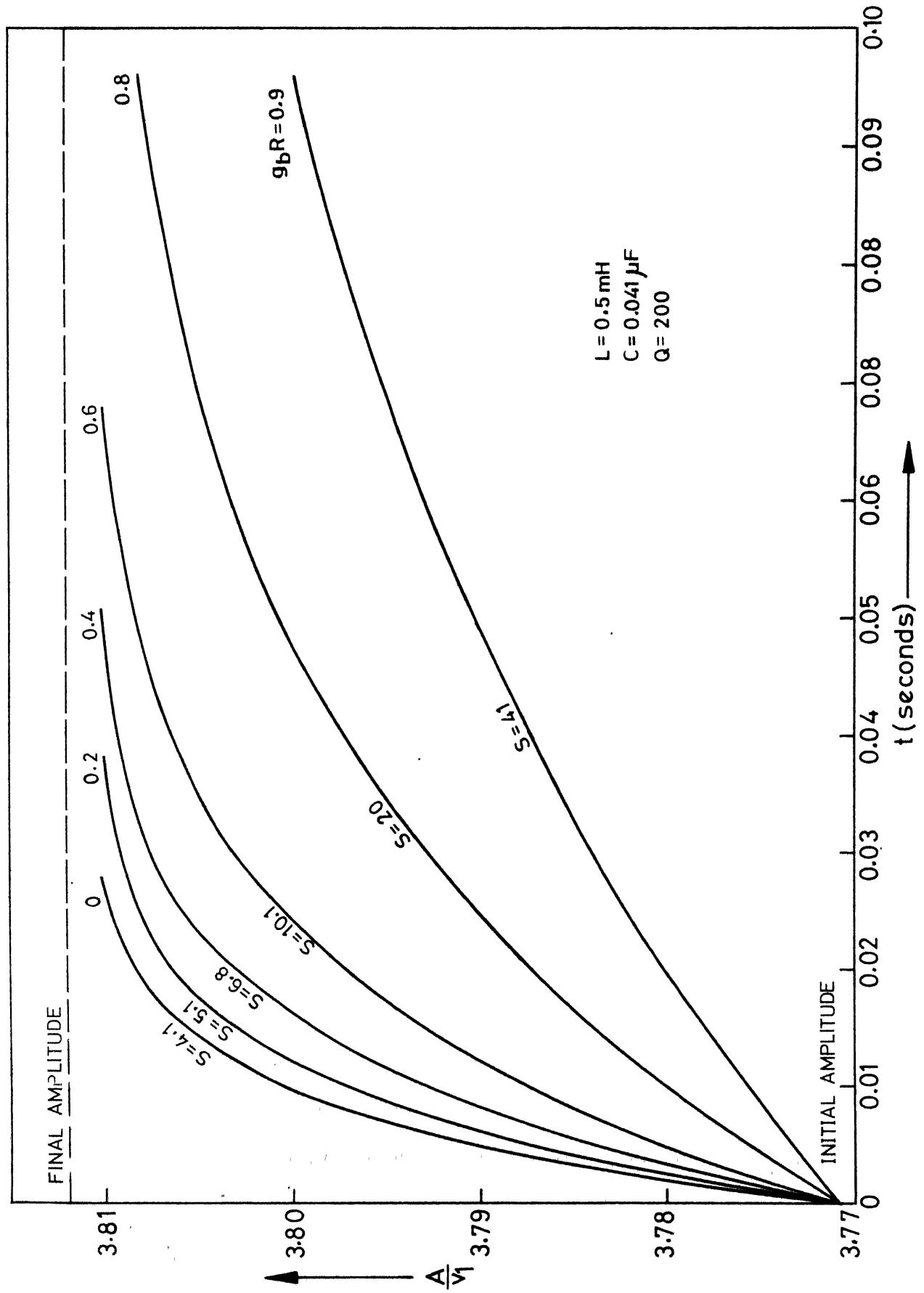

FIG. 19 RESPONSE OF THE AMPLITUDE OF OSCILLATION FOR A STEP CHANGE ΔR IN R. ΔR IS CHOSEN TO PRODUCE 10% CHANGE IN AMPLITUDE.

was evaluated by finding the time taken by the amplitude to rise by $1/e$ of the difference between initial and final values. The Table 3 gives the different values of $g_b R$ and the corresponding values of τ, S and S/τ.

The object of evaluating S/τ is to bring into focus the fact that its value remains very nearly constant and is equal to $1/2RC$.

3.4 THREE SEGMENT NONLINEAR CHARACTERISTIC

Figure 20 shows the nonlinear characteristic with two limiting segments of identical slope. A similar characteristic was suggested by Robinson for a nuclear resonance oscillator circuit. The following analysis has been carried out for the case of the symmetric biasing. The i-v characteristic of the active device is given by

$$\begin{aligned} i &= I_a + g_a v \quad \text{for} \quad -v_1 \leq v \leq +v_1, \\ i &= I_b + g_b v \quad \text{for} \quad v < -v_1, \\ \text{and} \quad i &= I_b' + g_b v \quad \text{for} \quad v > +v_1 \end{aligned} \tag{3.20}$$

The differential equation governing the circuit behaviour is same as (3.3). As in the two segment case, if we assume that a nearly sinusoidal solution exists, we can adopt Kryloff-Bogoliuboff's first approximation technique. Assuming v and $\frac{dv}{dt}$ as given by equation (3.5), we can write the stability equation for the amplitude of oscillation A, as

TABLE 3

SENSITIVITY AND TIME CONSTANT AS FUNCTIONS OF g_{bR} (AT CONSTANT AMPLITUDE)

g_{aR}	S	τ-sec	S/τ
0	4.10	0.008	512
0.2	5.1	0.01	510
0.4	6.8	0.0136	500
0.6	10.1	0.0196	515
0.8	20.0	0.0392	510
0.9	41	0.0796	515

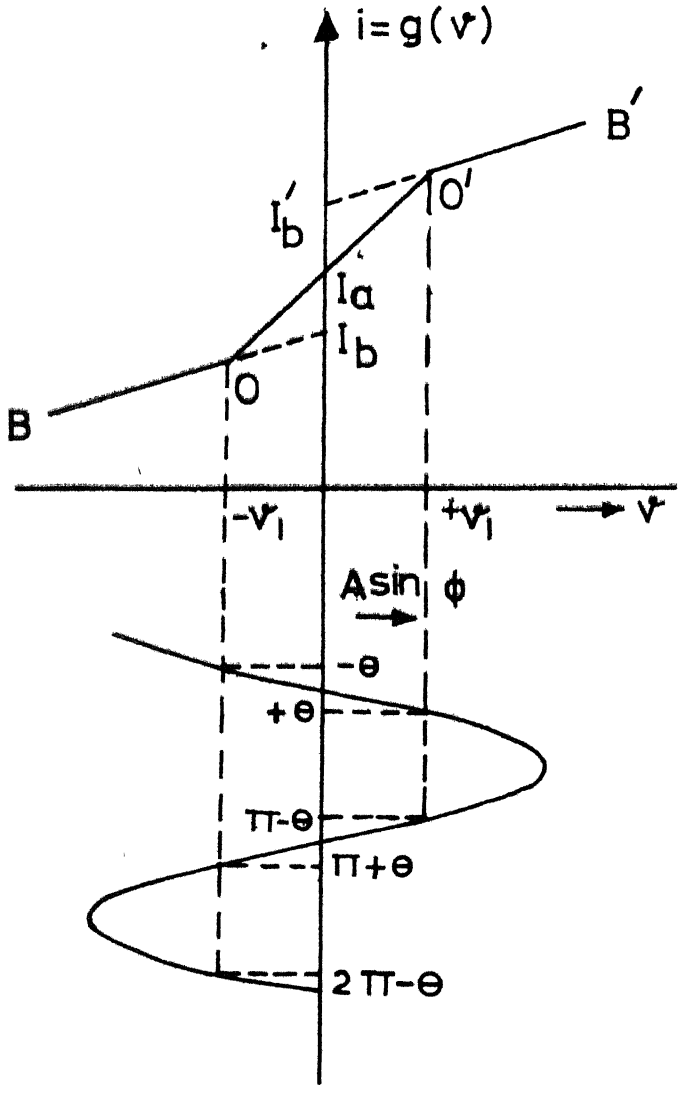

FIG.20 PIECEWISE LINEAR CHARACTERISTIC WITH THREE SEGMENTS.

follows

$$\frac{dA}{dt} = \frac{-L\omega_o^2 A}{2\pi}\left[\left(\frac{1}{R} - g_a\right)\int_{-\theta}^{+\theta}\cos^2\phi d\phi + \left(\frac{1}{R} - g_b\right)\int_{+\theta}^{\pi-\theta}\cos^2\phi d\phi\right.$$

$$\left. + \left(\frac{1}{R} - g_a\right)\int_{\pi-\theta}^{\pi+\theta}\cos^2\phi d\phi + \left(\frac{1}{R} - g_b\right)\int_{+\theta}^{2\pi-\theta}\cos^2\phi d\phi\right]$$

where $\theta = \sin^{-1}(v_1/A)$ (Figure 20, equation (3.7)). After carrying out the integration, we have

$$\frac{dA}{dt} = \frac{-L\omega_o^2 A}{4\pi}\left[\left(\frac{1}{R} - g_a\right)(\sin R\theta + 2\theta) + \left(\frac{1}{R} - g_b\right)(\pi - 2\theta - \sin 2\theta)\right] \quad (3.21)$$

By putting $dA/dt = 0$, we get the steady state solution for A. Thus we have

$$\sin 2\theta + 2\theta = \frac{\pi}{(g_a R - g_b R)}(1 - g_b R) \quad (3.22)$$

Equation (3.22) gives the values of θ for a given set of values of $g_a R$ and $g_b R$. Figure 21 gives the amplitude A normalised with respect to v_1 as a function of $g_a R$ and $g_b R$. Here again, the values of interest of θ lie between zero and $\pi/2$. Unlike the case of the two segment characteristic, here the upper limit of $g_a R$ is at infinity for any given value of $g_b R$.

The sensitivity S of A with respect to R is defined as before

$$\text{i.e.} \qquad S = \frac{\partial A/A}{\partial R/R}$$

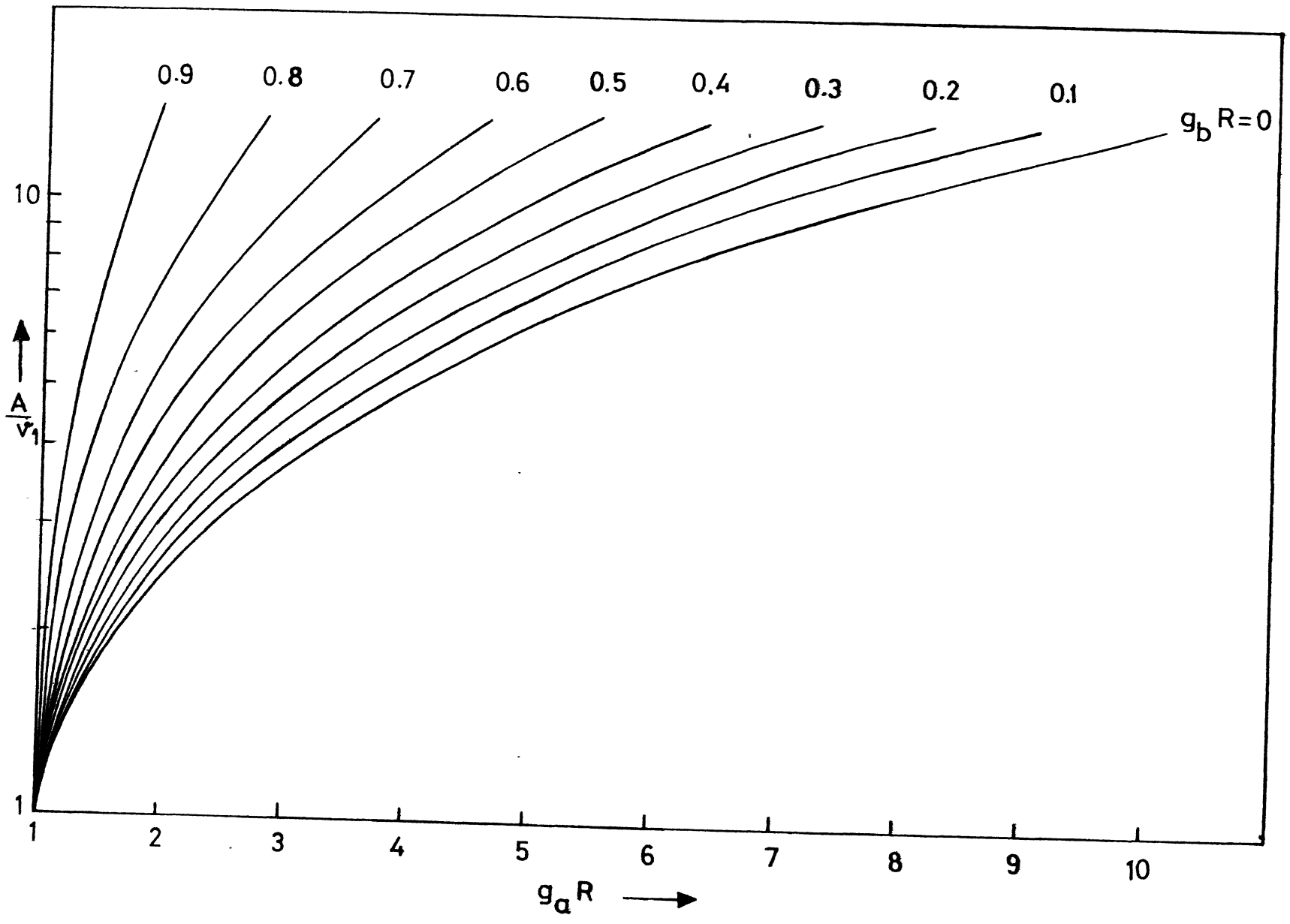

FIG. 21 AMPLITUDE OF OSCILLATION (NORMALISED WITH RESPECT TO v_1) AS A FUNCTION OF $g_a R$ AND $g_b R$ OF THE THREE SEGMENT PIECE WISE LINEAR CHARACTERISTIC.

S is easily evaluated in terms of g_a, g_b and R using equations (3.7) and (3.22). Thus we get

$$S = \frac{\pi}{2(g_aR - g_bR) \text{ Sin } 2\theta} \qquad (3.23)$$

Figure 22 shows variation of S with respect to variations of g_aR and g_bR. It is seen that the value of S for a given value of g_bR tends to a constant value as g_aR is increased. It tends to infinity as g_aR tends to unity. The limit of S as g_aR tends to infinity can be evaluated as follows. Using equation (3.22) we can substitute for $\pi/(g_aR - g_bR)$ in equation (3.23) and write

$$\underset{g_aR \to \infty}{\text{Lt}} S = \underset{\theta \to 0}{\text{Lt}} \frac{1}{2(1 - g_bR)} \frac{\text{Sin } 2\theta + 2\theta}{\text{Sin } 2\theta} = \frac{1}{1 - g_bR} \qquad (3.24)$$

From equation (3.24) we can see that the limiting value of S at high values of the loop gain g_aR is unity (which is the same as what was given by Robinson, when $g_bR = 0$).

3.5 EXPERIMENTAL CIRCUIT ARRANGEMENT

The circuit arrangement shown in Figure 23 was employed to experimentally study the behaviour of an oscillator employing a two segment PWL characteristic. The voltage v across the tuned circuit is sensed by the transistors T_2 and T_3 connected in a Darlington configuration. The resistance R_E linearises the relationship between the collector current i and the voltage v. The transistor T_1 acts as a current

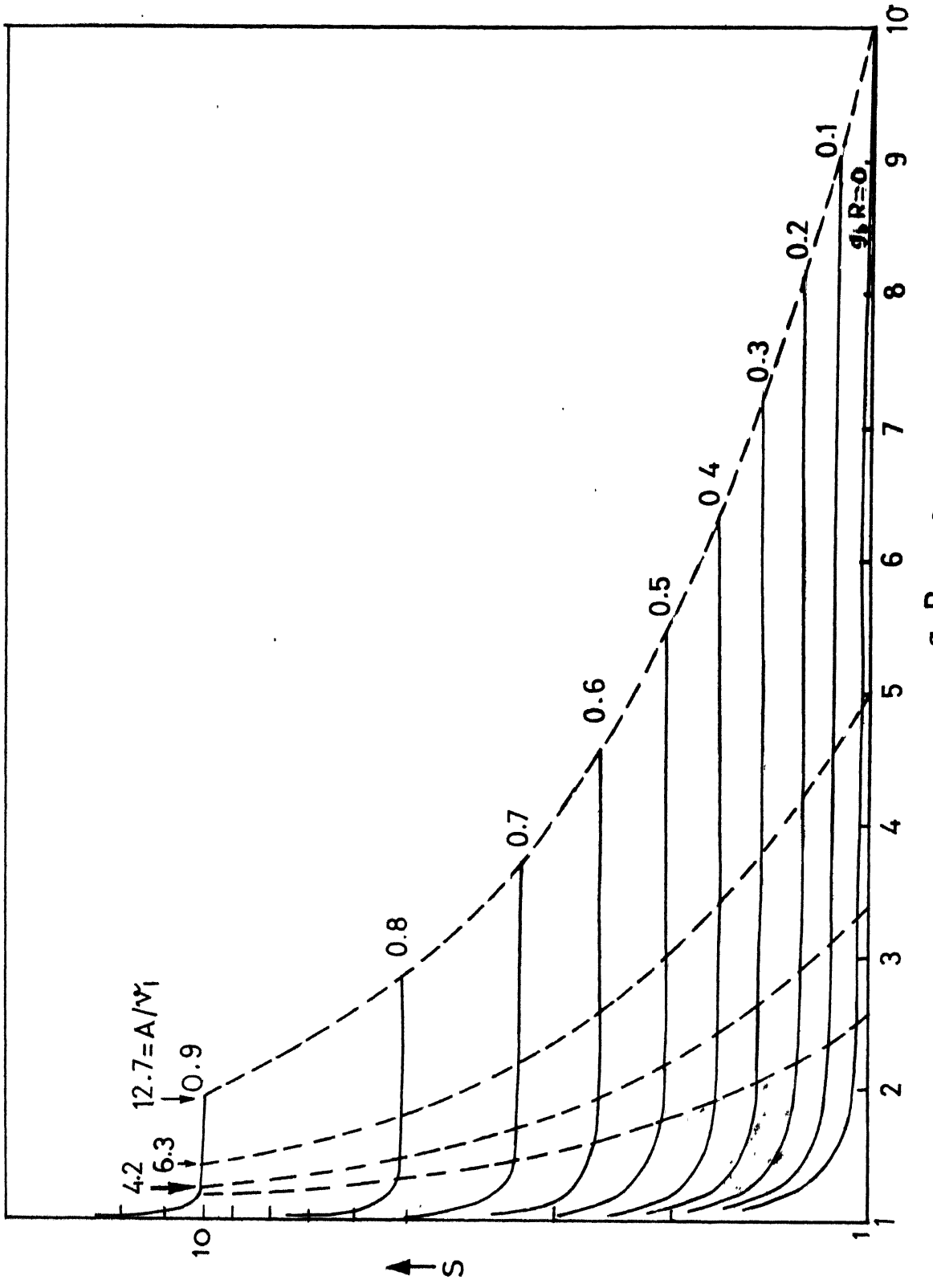

FIG. 2.2 SENSITIVITY S AS A FUNCTION OF g_aR AND g_bR (OF THE THREE SEGMENT PIECEWISE LINEAR CHARACTERISTIC).

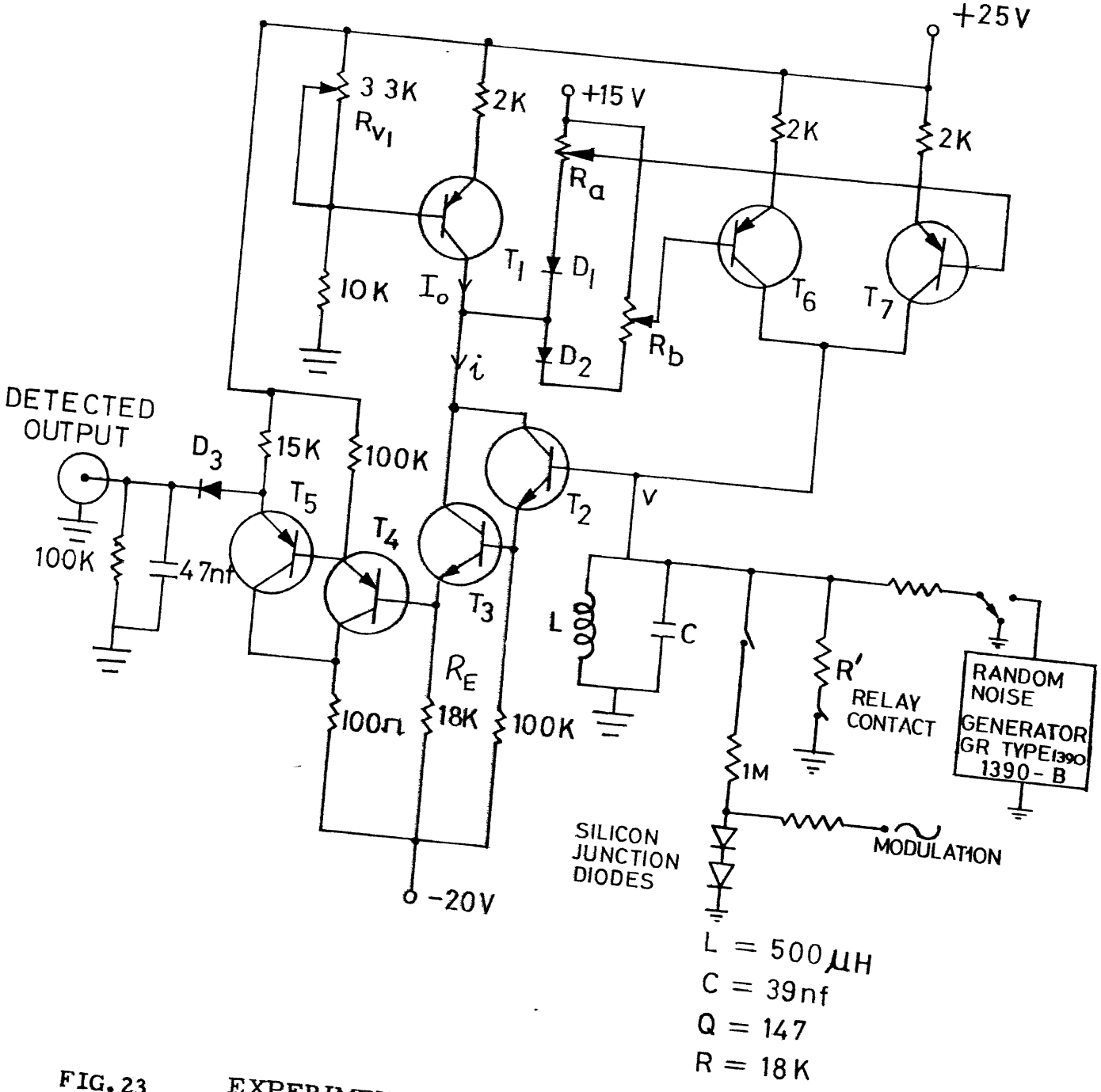

FIG. 23 EXPERIMENTAL CIRCUIT ARRANGEMENT

source I_o which can be adjusted with the help of the variable resistor R_{V_1}. The current I_o determines the corner point voltage v_1. At v equal to zero, i is set such that it is greater than I_o. The difference current flows through the diode D_1 which remains forward biased so long as i is greater than I_o. When the input voltage v is decreased, i decreases and it eventually becomes equal to I_o, when the input voltage assumes a negative value of magnitude v_1. For values of v less than v_1, i is less than I_o and the diode D_2 conducts. The slopes of the two segments in the characteristics are thus controlled by the potentiometers R_a and R_b. The sum of the collector currents of T_6 and T_7 is fed back to the tuned circuit. Diode D_3 in combination with the low pass RC combination form the envelope detector. The Darlington pair of transistors T_4 and T_5 act as a buffer feeding the detector.

The corner voltage v_1 was set at 1 volt. A vacuum tube voltmeter (HP type 400D) was used to measure the RMS value of the voltage across the tuned circuit. R_a and R_b were decade resistance boxes (Heathkit type IN-11). R_E was so chosen as to make g_a or g_b equal to unity corresponding to R_a or R_b value of two KΩ. For the power supply shown, the dynamic range of the oscillator was more than 3 volts RMS. Any required value of amplitude could be chosen by adjusting g_a and g_b according to equation (3.10).

Measurement of Sensitivity

A small perturbation of the resistance R was brought about with the help of a series combination of a relay contact and a high value resistor (1 MΩ) connected across the tuned circuit. The relay was turned on and off at a very low frequency (0.1 Hz) so that the oscillator was given enough time to attain the steady state amplitude at each value of R. The change in the amplitude was measured as a change of voltage level at the output of the detector. Thus the sensitivity was experimentally evaluated for different combinations of g_aR and g_bR. The results are given in Table 4a. The results were found to agree with the theoretical values within limits of experimental error (5%).

Measurement of the Effective Bandwidth

In the experimental arrangement, the tank circuit resistance was modulated sinusoidally by modulating the incremental conductance of the forward biased diodes connected in series with the one MΩ resistor (Figure 23). The modulation signal included a d.c. offset voltage to keep the diodes forward biased, throughout the modulation cycle. The detector bandwidth was kept much larger than the bandwidth of the tuned circuit. The output of the detector was measured for increasing frequencies starting from a low value like one Hertz until the output reduced by 3db below the low frequency value. This frequency is taken as the effective bandwidth of the oscillator.

TABLE 4

RESULTS OBTAINED USING THE EXPERIMENTAL CIRCUIT ARRANGEMENT

(a)

A	R_a	R_b	CALCULATED	MEASURED
r.m.s. volts	K. Ω	K Ω	ΔA (mv)	ΔA (mv)
2.0	2.63	0.53	238	240
2.0	2.31	1.39	535	530
1.5	2.6	0.00	114	110
1.5	2.46	0.492	148	145

(v_1 = 1 volt, R = 18K Ω, $(\Delta R/R) = 18 \times 10^{-3}$

R_a corresponding to starting condition = 2.04 K Ω)

(b)

Measured value of S	Measured value of Bandwidth (BW)	SxBW
3.75	40	150
4.75	30	143
5.8	26	151
10.7	13	139

(A = 2 volts r.m.s., v_1 = 1 volt)

Experimental results given in Table 4b agree with the theoretical predictions within the limits of experimental error and we conclude that the sensitivity bandwidth product remains constant.

3.6 SIGNAL TO NOISE RATIO

It is well known that the noise in the detector output tends to increase when the oscillator is adjusted for higher sensitivities. However, we have seen that the effective bandwidth also decreases simultaneously. Thus, it is of interest to study the variation of signal to noise ratio as a function of sensitivity. This has been done experimentally using the circuit arrangement of Figure 23.

Figure 23 shows a noise current source connected across the tuned circuit. The noise current was adjusted to obtain an observable deflection on the vacuum tube voltmeter connected across the output of the detector. Care was taken to see that the detector bandwidth was kept large so that the overall bandwidth was controlled by the oscillator itself. The output noise was measured for various values of g_b/g_a (0 to 0.8) keeping the amplitude of oscillation constant (along the curve x-y of Figure 18). The measured noise output increased approximately by a factor of 2. The corresponding increase in the sensitivity was from 3 to 22 (a factor of 7). Thus, the experiment shows that an overall improvement in signal to noise ratio should be expected at higher sensitivity conditions.

3.7 3 MHz OSCILLATOR-DETECTOR CIRCUIT

An oscillator-detector circuit which incorporates a smooth nonlinearity is shown in Figure 24. The FET T_1 senses the voltage across a part of the tuned circuit. The relationship between the input gate voltage and the drain current is linearised by the inclusion of a resistance R_{S1} in series with the source. Transistor T_2 controls and stabilises the bias current of T_1 which can be varied by the variable resistor R_{S2}. R_L forms the load resistance of T_1, voltage across which is sensed by the transistor T_3. Once again, the transfer characteristic of T_3 is linearised by R_{S4} and the bias current through it is stabilised by T_4. Further, transistor T_3 provides the necessary phase inversion for positive feedback as shown in Figure 24. T_5 forms the source follower feeding the detector.

It can be seen that the resistors R_{S1}, R_L and R_{S4} primarily control the overall transconductance of the circuit. The hot carrier diode D_1 in series with the resistor R forms a shunt path across R_{S4}, thus controlling the gain to a small extent. However, D_1 gets reverse biased when the voltage at the source of the transistor T_3 goes below the voltage set by the potentiometer R_{V2}. Thus, we get a break point and a slight reduction in loop gain resulting in a two segment smooth nonlinearity.

Since the bias conditions of the FETs have been stabilised with respect to power supply voltage variations, the most dominant factor contributing to instability in the overall

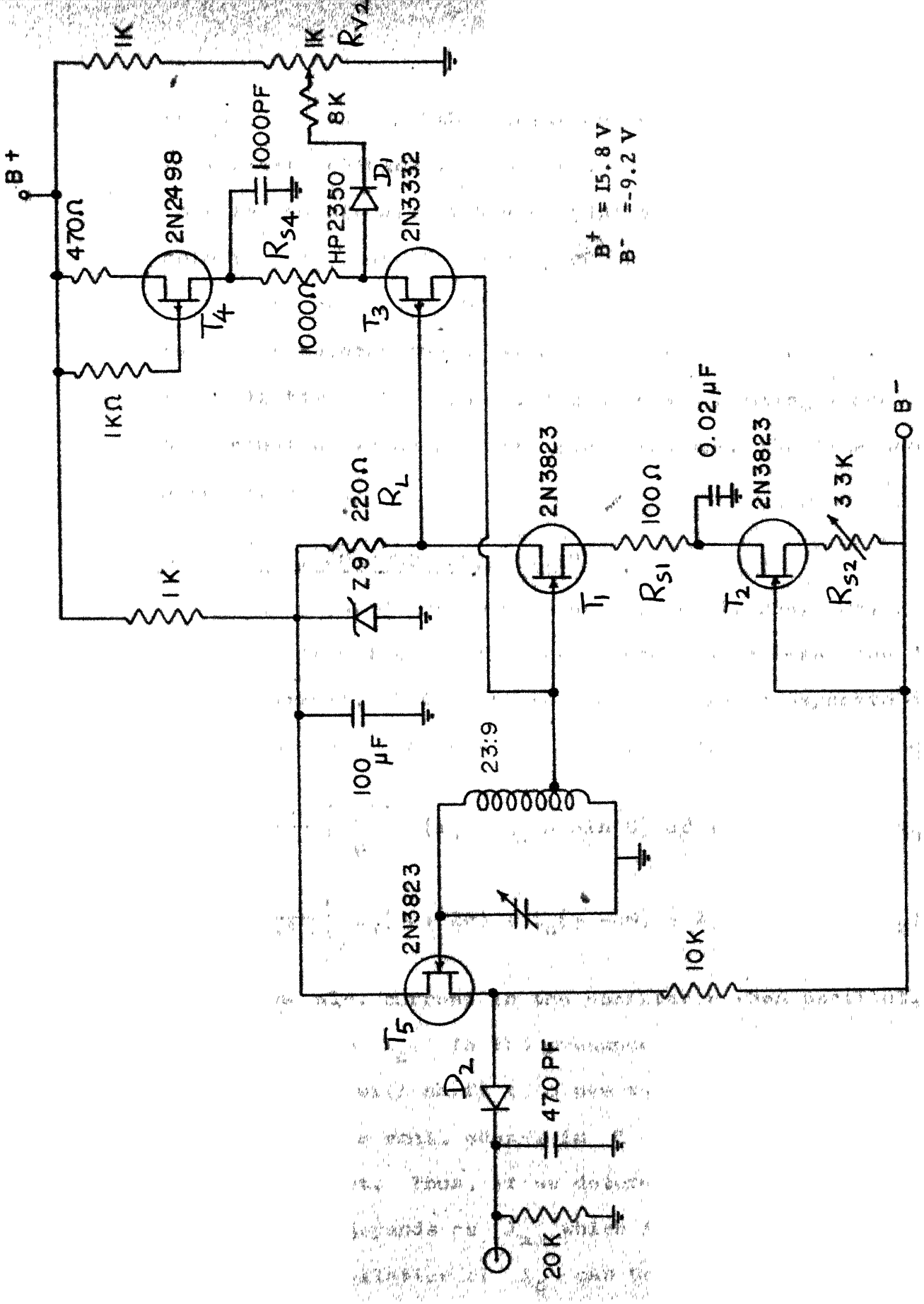

FIG. 24 OSCILLATOR-DETECTOR CIRCUIT BASED ON A PIECEWISE LINEAR CHARACTARISTIC

transconductance is the variation in the transistor characteristics with changes in ambient temperature. Thus, in order to operate the circuit at higher sensitivities, the oscillator-detector will have to be temperature controlled.

The derivative of the absorption line of a polycrystalline sample, Hexamethylene tetramine (35 cc), at room temperature, is shown in Figure 25. The plot was obtained using a one second time constant which was ten times less than the time constant used earlier.

3.8 D.C. CURRENT SENSITIVITY

As pointed out in Chapter II, an alternate way of obtaining an output from the oscillator-detector is to sense the d.c. current in the circuit. This obviates the need for a separate detector. With reference to Figure 16 the output d.c. current is given by

$$I_{dc} = \frac{1}{2\pi}\left[\int_{-\theta}^{\pi+\theta}(I_a + g_a A \sin\phi)\,d\phi + \int_{\pi+\theta}^{2\pi-\theta}(I_b + g_b A \sin\phi)\,d\phi\right]$$

$$= \frac{1}{2\pi}\left[I_a(\pi + 2\theta) + I_b(\pi - 2\theta) + 2\cot\theta\,(I_a - I_b)\right] \quad (3.25)$$

The d.c. current in the oscillator when oscillations are not present is I_a. In the presence of oscillations the d.c. current level will shift to a new value given by equation (3.25). When there is a small change in R there will be a minute change in this current. Thus, if we determine the percentage change in I_{dc}, it depends on I_a which is arbitrary. In an actual circuit, cancellation of I_a can be attempted. Thus, we define

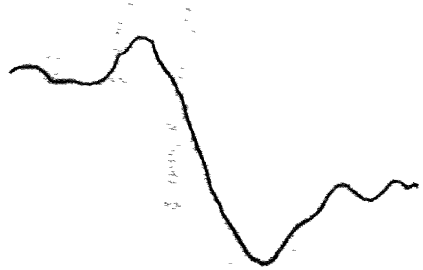

FIG. 25 DERIVATIVE OF THE ABSORPTION LINE OF HEXAMETHYLINE-TETRAMINE

an output current i_o given by

$$i_o = I_{dc} - I_a$$

i.e. $$i_o = \frac{1}{2\pi} (I_a - I_b) \left[2(\theta + \text{Cot}\, \theta) - \pi\right] \qquad (3.26)$$

The sensitivity of i_o with respect to R is defined as

$$S_I = \frac{\partial i_o / i_o}{\partial R / R}$$

Using equations (3.7), (3.10) and (3.26) we get

$$S_I = \frac{\pi}{(g_a R - g_b R) \sin^2 \theta \left[2(\theta + \text{Cot}\, \theta) - \pi\right]} \qquad (3.27)$$

Figure 26 shows the dependence of S_I on $g_a R$ and $g_b R$. We see that the behaviour of S_I is very similar to S.

In the case of a symmetrically biased three segment PWL, it is easily seen that the current i_o is always zero and this type of detection cannot be employed.

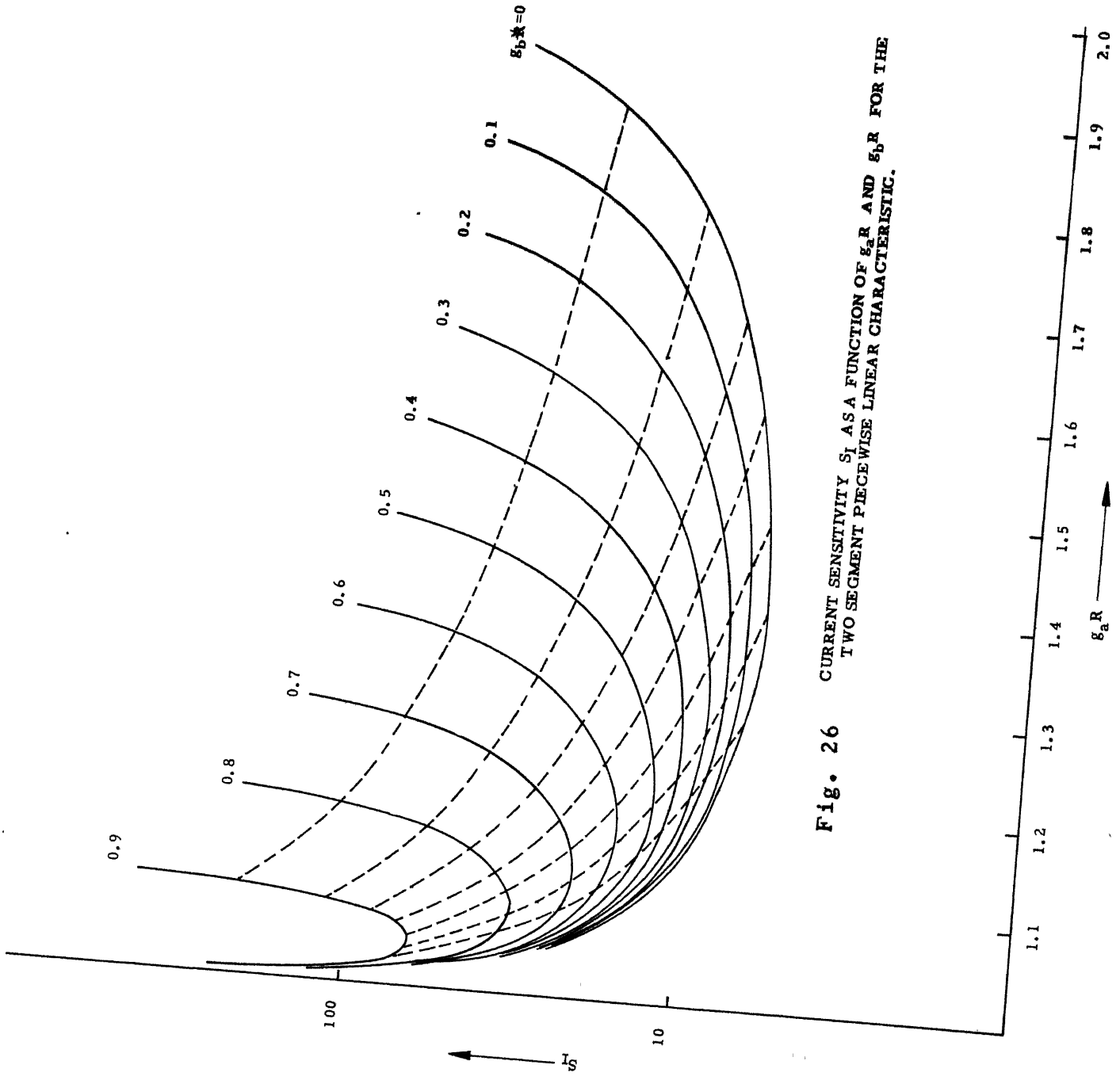

Fig. 26 CURRENT SENSITIVITY S_I AS A FUNCTION OF $g_a R$ AND $g_b R$ FOR THE TWO SEGMENT PIECEWISE LINEAR CHARACTERISTIC.

CHAPTER - IV

MODULATION

4.1 GENERAL CONSIDERATIONS

In an oscillator-detector the output is made periodic to enable its detection in presence of noise. Both frequency modulation and magnetic field modulation are widely used.

The application of an external magnetic field broadens the line, reducing its magnitude. It is possible to make the absorption line almost vanish by switching on a magnetic field of the order of a few hundred gauss. Thus, a small permanent magnet is often used to distinguish an absorption line from spurious signals. This phenomenon is used to make the output periodic by switching a magnetic field on and off at an audio frequency with the aid of a pair of Helmholtz coils. The frequency of the oscillation is now slowly swept through the absorption band and the output is phase sensitive detected. Thus, a plot of the absorption as a function of frequency can be obtained on a recorder (WATKINS AND POUND, 1952).

Although parallel plate tuning capacitors coupled to low r.p.m. motors have been used to sweep the frequency, the use of a varicap simplifies the system considerably, especially when different sweep rates have to be incorporated. The tuning range that can be obtained with varicaps is adequate to sweep the frequency over a few line widths. Any attempt to incorporate large frequency sweeps using the varicap will put stringent demands on the stability of the d.c. voltage used to reverse

bias the varicap diode, since the drift in the d.c. supply will impair the frequency stability of the oscillator. Thus, large frequency variations which are required for locating the line must be achieved through the use of mechanically controlled parallel plate capacitors.

The introduction of the varicap in the circuit simultaneously enables frequency modulation. This, in turn, makes the oscilloscope display and derivative plot possible. However, this modulation scheme has a disadvantage in that it also senses the slope of the 'amplitude vs. frequency characteristic' of the oscillator. Thus, even in the absence of absorption, a large unwanted output (incidental AM) mostly containing the modulation frequency (fundamental) component is generally obtained. In the oscilloscope display where a wide frequency deviation (a few line widths) is employed, this manifests itself in the form of an ellipse. A small ellipse does not interefere with the display of the line. When the amount of the unwanted output becomes excessive as compared to the signal level, oscilloscope display becomes impossible since it saturates the preamplifier whose gain is to be set at a large value to get a good picture of the line.

The incidental AM can be suppressed by adjusting the lower cutoff frequency of the bandpass filter or by using a twin-T network. Alternately, a first-order cancellation can be attempted by subtracting an in phase signal at the modulating frequency. A variable amplitude and phase shift

arrangement described in Appendix II is used for this cancellation.

From the point of view of line width measurement, the derivative plot is a more convenient form. Here again, the presence of the incidental AM results in a d.c. at the output of the phase sensitive detector leading to a shift in the base line of the recorder. Since the AM varies while the frequency of the oscillator is swept, the base line might show a large slope which can be avoided by performing the phase sensitive detection at the second harmonic of the modulating frequency.

When the oscillator frequency has to be changed over a wide range, the variations in the quality factor of the coil with frequency will result in a change in the loop gain in the circuit. Thus, the amplitude of oscillation will vary widely or the oscillations might cease altogether. This should be avoided by incorporating an automatic gain control (WATKINS, 1952) whose time constant is of the order of many seconds. This provides gain corrections as the frequency is varied slowly and does not provide any feedback at the modulating frequency.

The Shape of the Absorption Line

Since the line shape is generally assumed to be gaussian (DAS AND HAHN, 1958), the output $e_o(f)$ of the oscillator-detector is of the normalized form

$$e_o(f) = \exp\left[-\frac{1}{2}\left(\frac{f-f_o}{f_1}\right)^2\right] \qquad (4.1)$$

where f_o is the centre frequency of the line and f_1 the frequency deviation from the centre at which the derivative assumes the maximum and minimum values as shown in Figure 27. The frequency deviation f_1 and half power line width are related by a constant ($\Delta\upsilon = 0.83\ f_1$).

4.2 WIDE BAND MODULATION

The modulation frequency f_m must be chosen such that it is very much less than the effective bandwidth of the oscillator, so that the line shape is reproduced faithfully. The detected output must be amplified using a bandpass amplifier whose bandwidth is adjusted to pass the significant harmonics contained in the output waveform. This eliminates the noise from the unwanted regions of the spectrum and improves the signal to noise ratio. The amplifier bandwidth required will now be estimated.

Let f_m represent the modulating frequency and f_c, the oscillator frequency. The frequency modulated wave $A(t)$ can be represented as

$$A(t) = A \cos \left[\omega_c t + \frac{\Delta\omega}{\omega_m} \sin \omega_m t\right] \qquad (4.2)$$

where $\Delta\omega$ is the maximum frequency deviation from ω_c. The ratio $\Delta\omega/\omega_m$ is generally called the modulation index (m_f).

The frequency deviation $\Delta\omega$ to be employed is a few line widths. Assuming the line width to be 1 KHz, the use of modulating frequency of 100 Hz will correspond to a modulation

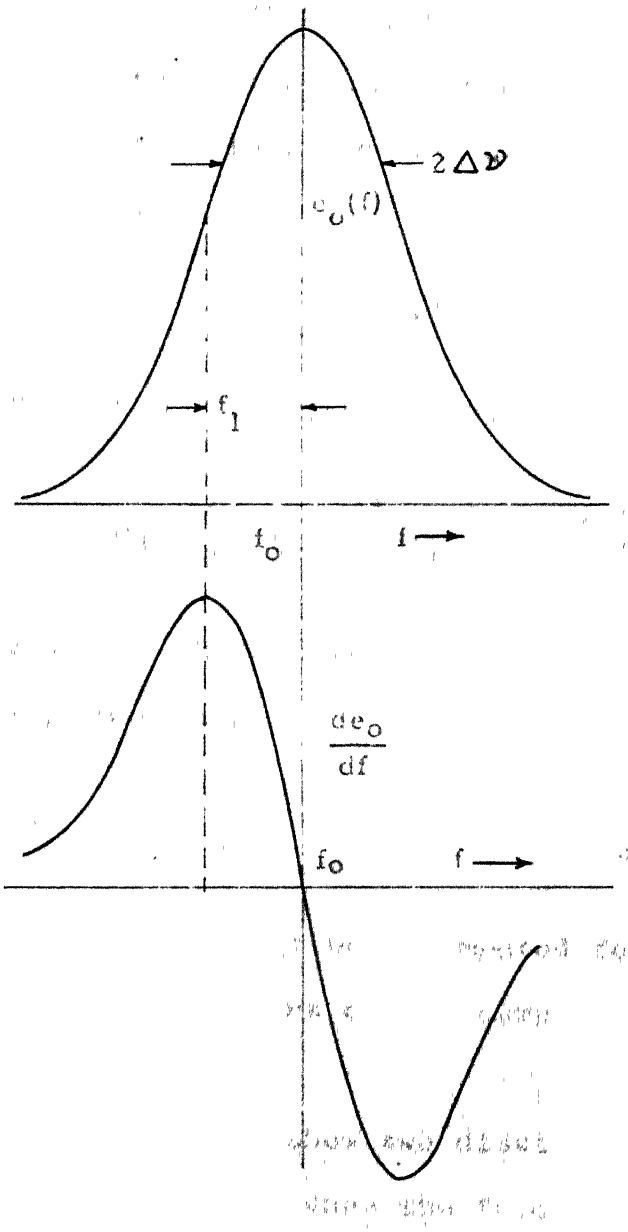

FIG.27 GAUSSIAN ABSORPTION LINE AND ITS DERIVATIVE

index greater than 10. Under these circumstances, a quasi-steady-state analysis (TERMAN, 1955) can be performed to determine the output spectrum of the detected signal. Thus, for wide band modulation, the frequency of the oscillator (f) can be written as

$$f = f_c + \Delta f \ \mathrm{Sin}\, \omega_m t \qquad (4.3)$$

Substituting for f in equation (4.1) we get

$$e_o(t) = \exp \left\{ -\frac{1}{2} \left[\frac{f_c - f_o}{f_1} + \frac{\Delta f}{f_1} \mathrm{Sin}\, \omega_m t \right]^2 \right\} \qquad (4.4)$$

in order to obtain the spectrum of the output, $e_o(t)$ is Fourier analysed giving

$$e_o(t) = \frac{C_o}{2} + \sum_{n=1}^{\infty} C_n \cos (n\omega_m t + \phi_n) \qquad (4.5)$$

The coefficients C_n have been computed for different situations. The flow chart of the computer program used is given in Appendix III

Figures 28 and 29 show two distinct situations and the corresponding waveforms. When the frequency of the oscillator f_c coincides with the centre frequency of the line f_o, the output is an even function and does not contain the fundamental component. In the asymmetric case, odd harmonics will also be present in the output.

The spectrum of the output and the significant frequencies to be retained depend upon the ratio of the frequency deviation

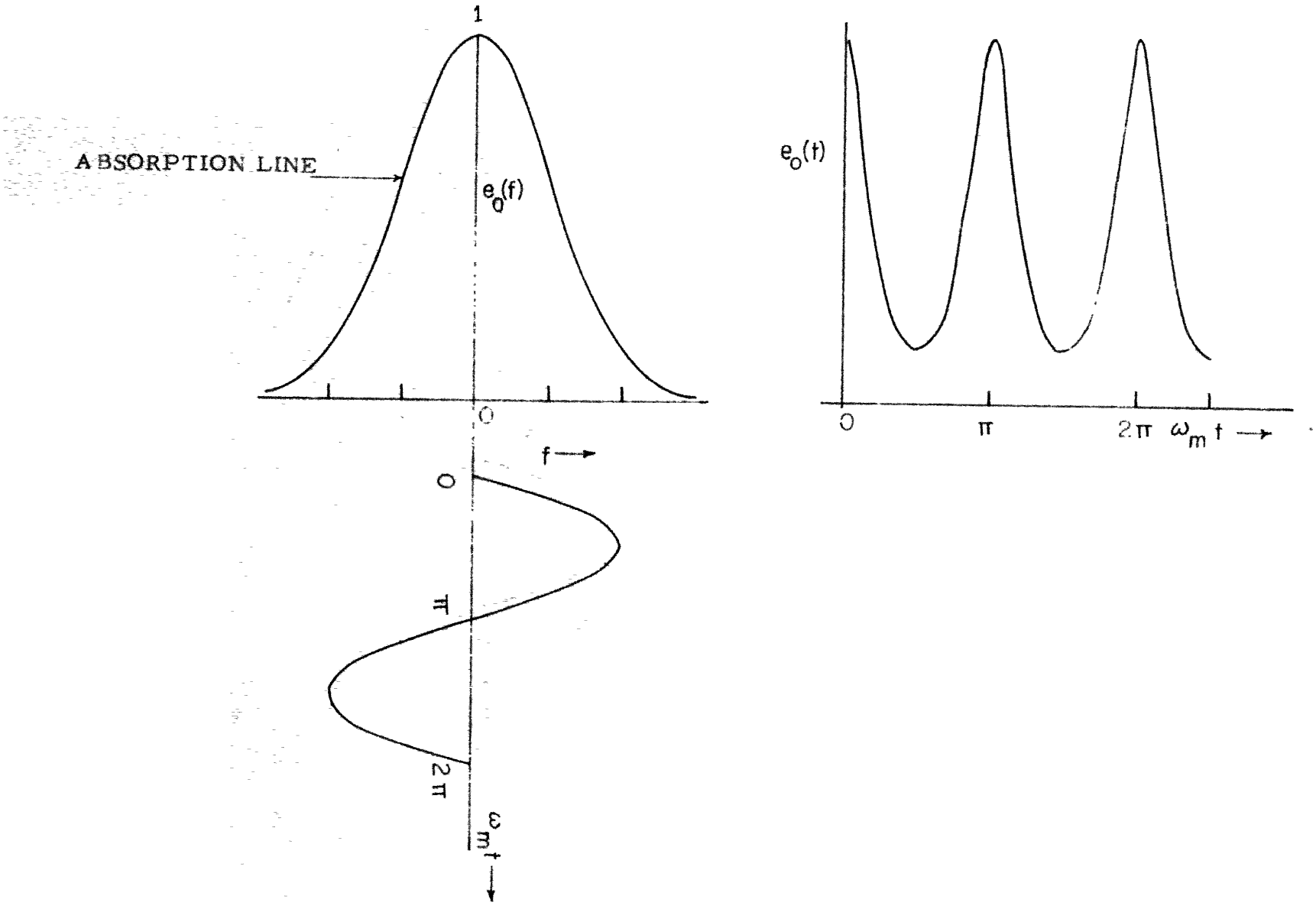

FIG. 28 WIDE BAND MODULATION (CENTRE OF THE SWEEP COINCIDING WITH THE CENTRE OF THE LINE)

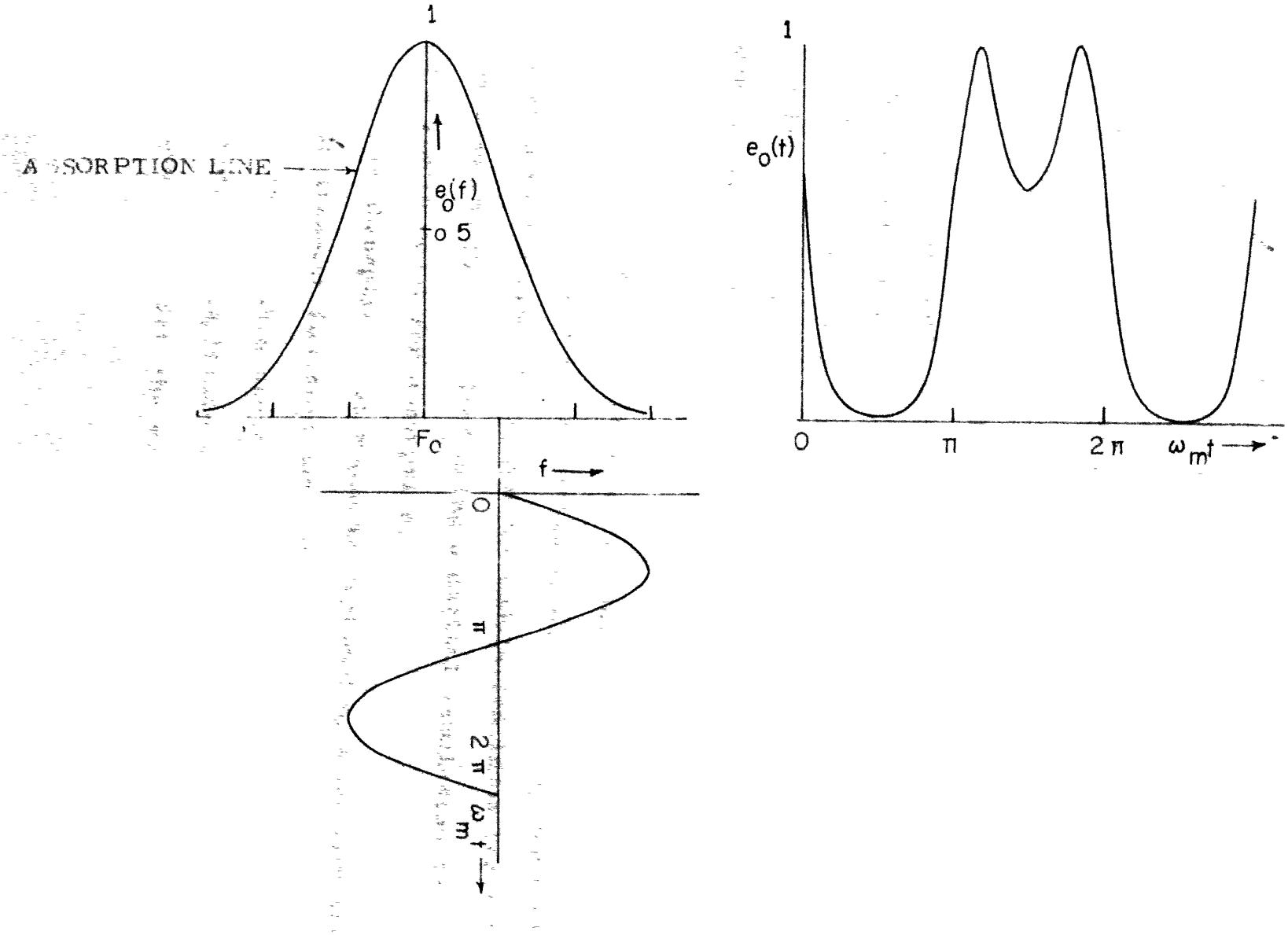

FIG. 29 WIDE-BAND MODULATION (OFF-CENTRE SWEEP)

to the line width, $\Delta f/f_1$. Examples of this are shown in Figure 30, where the harmonics whose amplitudes are below 1% of the peak absorption are neglected. As the ratio $\Delta f/f_1$ is made large, the spectrum tends to become flat and wide, which necessitates a higher bandwidth for the filter. This results in a reduced signal to noise ratio. For a choice of $\Delta f/f_1 = 4$, a bandwidth $10\ f_m$ is adequate.

4.3 DERIVATIVE OF THE ABSORPTION LINE

Figure 31 shows the experimental derivative plots of polycrystalline sodium chlorate at room temperature for different modulation frequencies keeping the frequency deviation constant at 400 Hz. All these plots are obtained using identical conditions of gain and bandwidth in the detection system. One can see that both the amplitude of the output as well as the indicated line width are dependent on the modulation frequency. The exact line width information is obtained for large modulation indices (i.e., quasi-steady-state situation). The apparent increase in the line width when the modulation index becomes less than unity, is studied using a digital simulation technique and a simple model for absorption.

The absorption phenomenon is replaced by a network whose amplitude transfer function has a gaussian shape. The output of such a network when excited by a frequency modulated input is computed. The amplitude modulation envelope of the output is obtained from which the component at modulation frequency

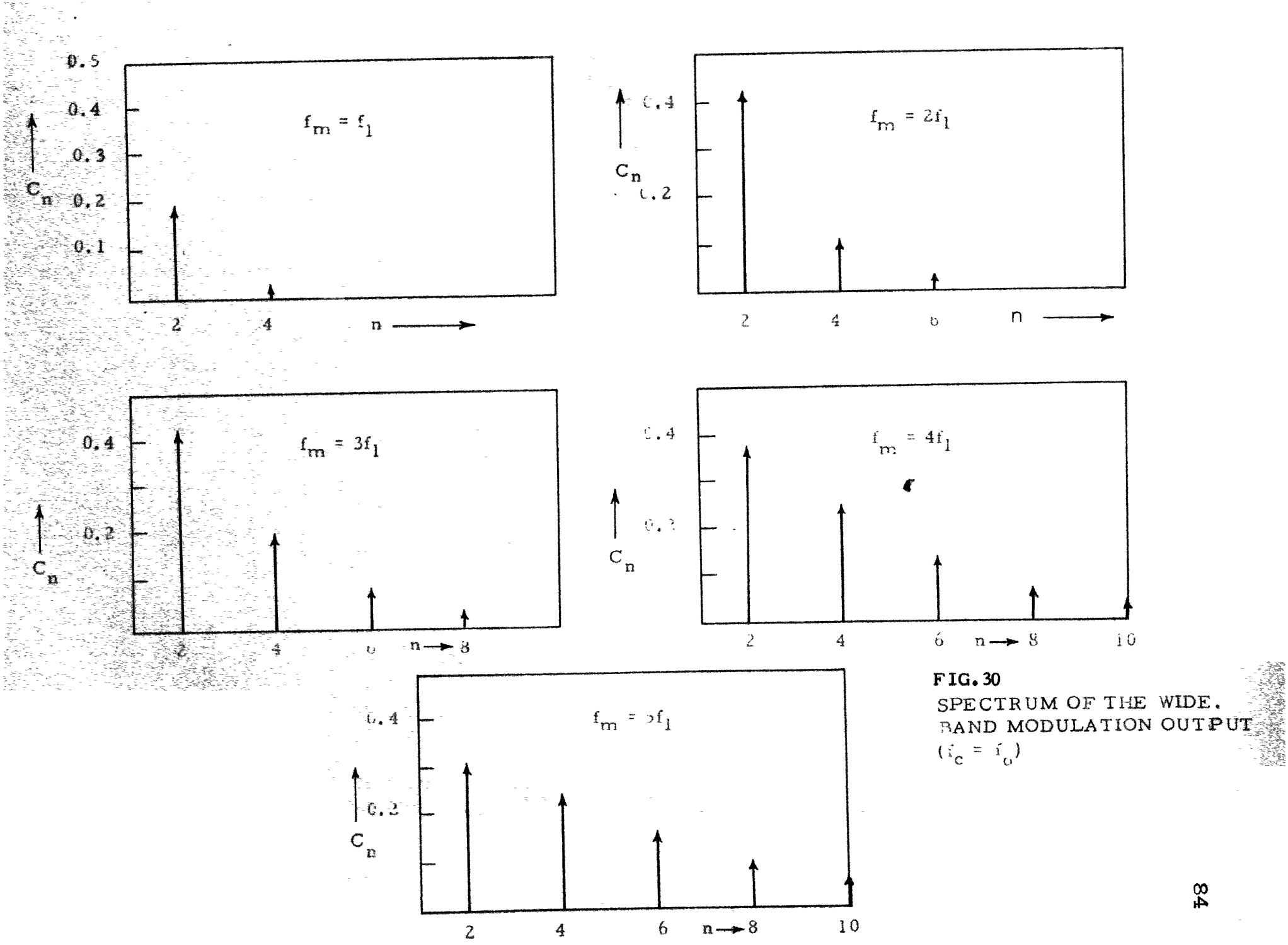

FIG. 30
SPECTRUM OF THE WIDE-BAND MODULATION OUTPUT ($f_c = f_0$)

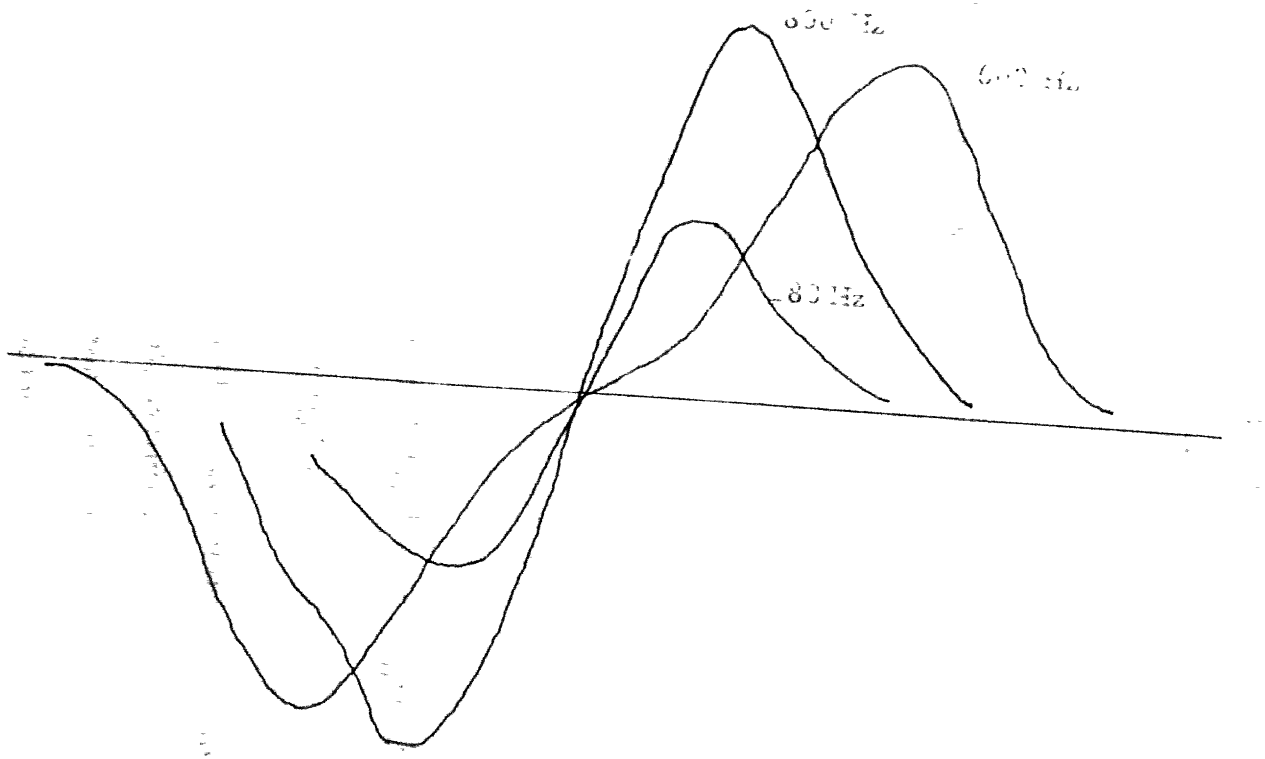

FIG31 EXPERIMENTAL PLOT OF THE DERIVATIVE AS A FUNCTION OF MODULATING FREQUENCY

is recovered. These computations are repeated for different values of oscillator frequency f_c so that it corresponds to a sweep through the absorption band.

Expressing the r.h.s. of equation (4.2) in a series form we get

$$\frac{A(t)}{A} = \cos\omega_c t \left[J_o(m_f) + 2\sum_{n=1}^{\infty} J_{2n}(m_f) \cos 2n\omega_m t\right] - \sin\omega_c t\left[2\sum_{n=1}^{\infty} J_{2n-1}(m_f) \sin(2n-1)\omega_m t\right] \quad (4.6)$$

where $J_n(m_f)$ are Bessel function of the first kind. Equation (4.6) is rewritten in terms of the sideband frequencies giving

$$\frac{A(t)}{A} = J_o(m_f)\cos\omega_c t + \sum_{n=1}^{\infty}\left[-J_{2n-1}(m_f)\left\{\cos(\omega_c - (2n-1)\omega_m)t - \cos(\omega_c + (2n-1)\omega_m)t\right\} + J_{2n}(m_f)\left\{\cos(\omega_c - 2n\omega_m)t + \cos(\omega_c + 2n\omega_m)t\right\}\right] \quad (4.7)$$

Now the amplitudes of the various sideband frequencies are multiplied by the magnitudes of the transfer function at the corresponding frequencies, giving the output amplitudes of the sideband frequencies. These when superposed yield the output waveform. The details of the computer program which is used for these calculations including the detection of the modulation envelope and the recovery of the fundamental component is given in Appendix III. Figure 32 shows the

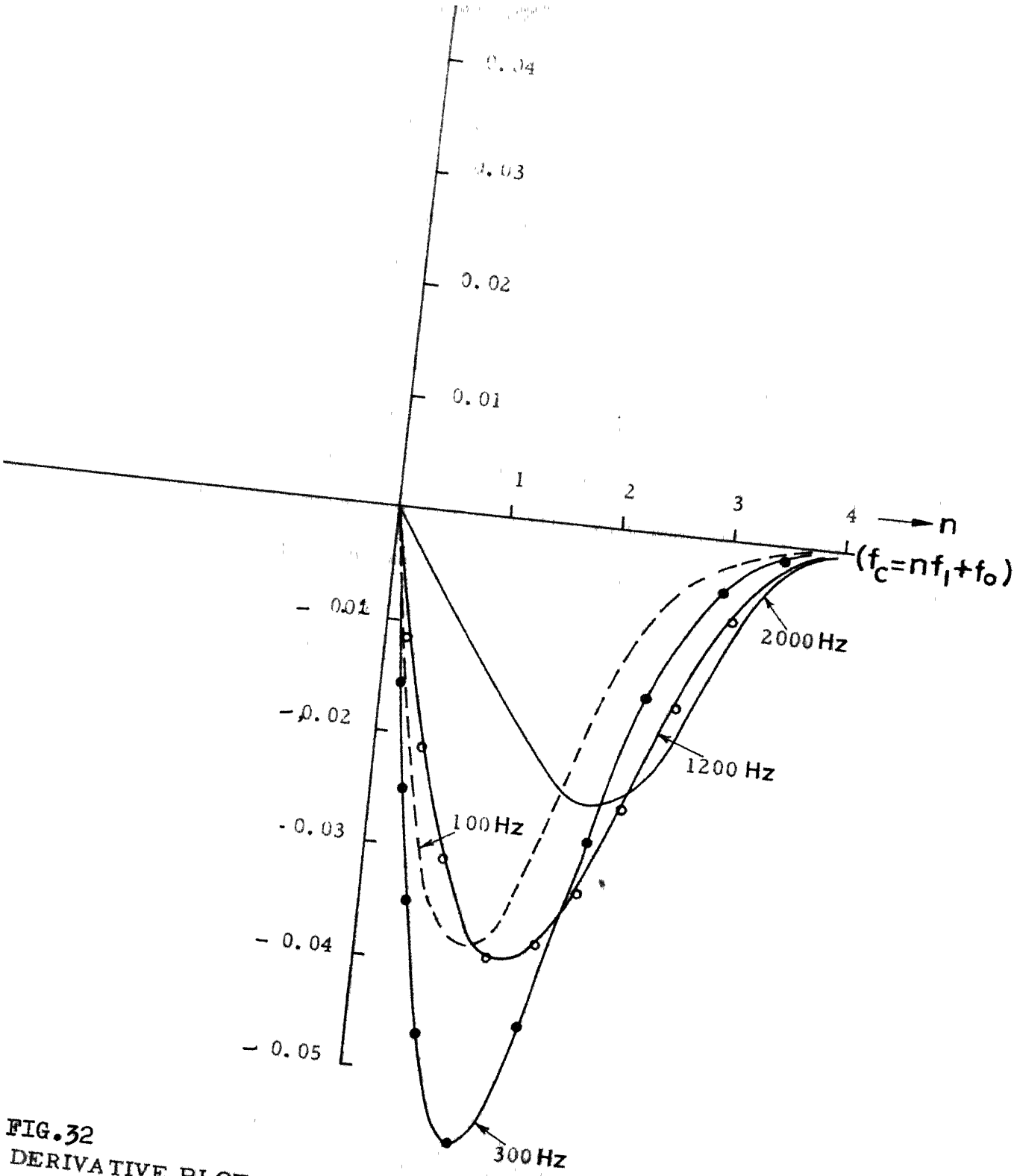

FIG. 32
DERIVATIVE PLOT AS A FUNCTION OF MODULATION FREQUENCY.

results of such a computation which qualitatively explain the experimentally observed results. We see that the best plot is obtained at an optimum modulation frequency. For higher values of f_m the line broadens and for lower values the output reduces.

An exhaustive study to evolve quantitative relationships was not undertaken since the computation time increases enormously for higher values of modulation indices. An experimental approach shows that the errors in line width information are negligible even if one employs a modulation index as low as unity. Further, using a deviation of about one quarter the line width gives a good plot of the derivative.

CHAPTER - V

CONCLUSIONS

The use of FETs in marginal oscillator circuits used for the detection of NQR, has several advantages. The low noise property of the FET helps to obtain a higher signal to noise ratio.

The low frequency analog simulation technique, described in Chapter II, enables one to determine the sensitivity of an oscillator-detector circuit. This is a simple and direct approach to the problem. Thus, it facilitates comparative evaluation of different oscillator-detector circuits. Such a study helped to design NQR spectrometers which have been successfully used to detect absorption signals in the 30 and 3 MHz regions.

Since the percentage change in the conductance of the tank coil due to absorption is proportional to the quality factor Q of the coil, the tank coil must be carefully designed. Extreme care should be exercised in mounting the coil on the tuning capacitor, so that the tank circuit Q is approximately that of the coil.

The results of the analysis of an oscillator which has the simplest nonlinearity with two linear segments show that the sensitivity of the circuit tends to increase as nonlinearity becomes soft. In order to operate an oscillator under high sensitivity conditions successfully, the loop gain in the circuit must be controlled to a high degree of precision. As

we go down in the frequency domain, below 3 MHz, looking for weaker NQR absorption signals, it will be necessary to achieve higher sensitivity conditions. This will necessitate the temperature control of the oscillator-detector circuit in order to maintain the required stability of loop gain.

Under high sensitivity conditions, the effective bandwidth of the oscillator decreases, keeping the sensitivity bandwidth product constant. Experimental results show that the signal to noise ratio available from the oscillator-detector increases at higher sensitivity conditions.

The frequency used for modulation will have to be chosen compatible with the effective bandwidth of the oscillator. Thus, at higher sensitivities lower modulation frequencies will have to be employed. Varicaps are conveniently used for frequency modulating the oscillator. However, they should not be used for producing large frequency variations since this will impair the frequency stability of the oscillator. Long range search is best achieved by slow rotation of a parallel plate tuning capacitor. The amplitude of the oscillations should be maintained constant through a long time constant a.g.c. applied to the oscillator.

The derivative plot is the most useful form for line width measurements. In order to preserve the line shape information, the modulation index employed must be preferably greater than one and the frequency deviation should be less than one half the line width.

LIST OF REFERENCES

1. ABRAGAM, A., The Principles of Nuclear Magnetism, The International Series of Monographs on Physics, Clarendon Press, 1961, Oxford.

2. BLOEMBERGEN, N., PURCELL, E.M., and POUND, R.V., "Relaxation Effects in Nuclear Magnetic Resonance Absorption", Physical Review, Vol. 73, No. 7, April 1, 1948, pp 679-

3. DAS, T.P., and HAHN, E.L., Nuclear Quadrupole Resonance Spectroscopy, Academic Press Inc., New York, London, 1958.

4. DEAN, C., and POLLAK, M., "Suppressing Side-band Interference Super-regenerative rf Spectrometers", Rev. Sci. Instr., Vol. 29, No. 7, July 1958, pp 630-632.

5. DEHMELT, H., and KRÜGER, H., "Kernquadrupolfrequenzen in ferten Dichloräthylen", Natürwissenschaften, Vol. 37, No. 5, 1950, pp 111-112 (German).

6. DEHMELT, H.G., "Nuclear Quadrupole Resonance", Am. Jr. Phys., Vol. 22, No. 3, March 1954, pp 110-120.

7. FEDIN, E.I., and SEMIN, G.K., "Use of Nuclear Quadrupole Resonance in Chemical Crystallography", Zhurnal Strukturnoi Khimii, Vol. 1, No. 2, July-August, 1960, (Russian); English Translation: "The Mössbauer effect and its applications in Chemistry", Consultants Bureau, New York, 1964.

8. FEDIN, E.I., and SEMIN, G.K., "Use of Nuclear Quadrupole Resonance in Chemical Crystallography", Zhurnal Strukturnoi Khimii, Vol. 1, No. 4, November-December, 1960, pp 464-499; (Russian); English Translation: "The Mössbauer effect and its applications in Chemistry", Consultants Bureau, New York, 1964.

9. KNIGHT, W.D., "High level oscillator for Nuclear Resonance", Rev. Sci. Instr., Vol. 32, No. 1, Jan. 1961, p 95.

10. KRYLOFF, N., and BOGOLIUBOFF, N., Introduction to Non-linear Mechanics, Annals of Mathematical Studies, Princeton, Princeton University Press, 1947.

11. KUMAR, U.V., "A Regenerative Nuclear Quadrupole Resonance Spectrometer", Technical Report No. 2/70, Department of Physics, Indian Institute of Technology, Kanpur, India.

12. MYERS, O.E., and PUTZER, E.J., "Measurement Broadening in Magnetic Resonance", Jr. App. Phys., Vol. 30, No. 12, December 1959, pp 1987-1991.

13. RAO, C.N.R., and FERRARO, J.R., Spectroscopy in Inorganic Chemistry, Academic Press, New York, London, 1970 - Chapter on NQR by H.D. Shultz.

14. ROBINSON, F.N.H., "Nuclear Resonance Absorption Circuit", Jr. Sci. Instr., Vol. 36, No. 12, December 1959, pp 481-487.

15. ROBINSON, F.N.H., and EDMONDS, D.T., "On matching a Nuclear Resonance Circuit to an amplifier with an application to Quadrupole Resonance", Jr. Sci. Instr., Vol. 44, 1967, pp 475-476.

16. TERMAN, F.E., Electronic and Radio Engineering, McGraw-Hill Book Company, Inc., New York, 1955.

17. VAN DER ZIEL, A., "Thermal Noise in Field Effect Transistors", Proc. I.R.E., Vol. 50, No. 8, August 1962, pp 1808-1812.

18. VAN DER ZIEL, A., and BRUNKE, W.C., "Thermal Noise in Junction-Gate Field Effect Transistors", I.E.E.E. Trans., Vol. ED-13, No. 3, March 1966, pp 323-329.

19. VERDIECK, J.F., and CORNWELL, C.D., "Radio-frequency spectrometer with bidirectional square wave frequency modulation", Rev. Sci. Instr., Vol. 32, No. 12, December 1961, pp 1383-1386.

20. VISWANATHAN, T.L., VISWANATHAN, T.R., and SANE, K.V., "NQR Spectrometer using Field Effect Transistors", Rev. Sci. Instr., Vol. 39, No. 4, April 1968, pp 472-475.

21. VISWANATHAN, T.L., VISWANATHAN, T.R., and SANE, K.V., "A 3 MHz NQR Spectrometer", Rev. Sci. Instr., Vol. 41, No. 3, March 1970, pp 477-478.

22. VOLPICELLI, R.J., NAGESWARA RAO, B.D., and BALDESCHWIELER, J.D., "Locked rf spectrometer for Nuclear Quadrupole Resonance", Rev. Sci. Instr., Vol. 36, No. 2, February 1965, pp 150-153.

23. WANG, T.C., "Pure Nuclear Quadrupole Spectra of Chlorine and Antimony Isotopes in Solids", Physical Review, Vol. 99, No. 1, July 15, 1955, pp 566-576.

24. WATKINS, G.D., Ph.D. Thesis, Harvard University, 1952.

25. WATKINS, G.D., and POUND, R.V., "The Pure Nuclear Electric Quadrupole Resonance of N^{14} in three molecular solids", Physical Review, Vol. 85, No. 6, March 15, 1952, p 1062.

APPENDIX I

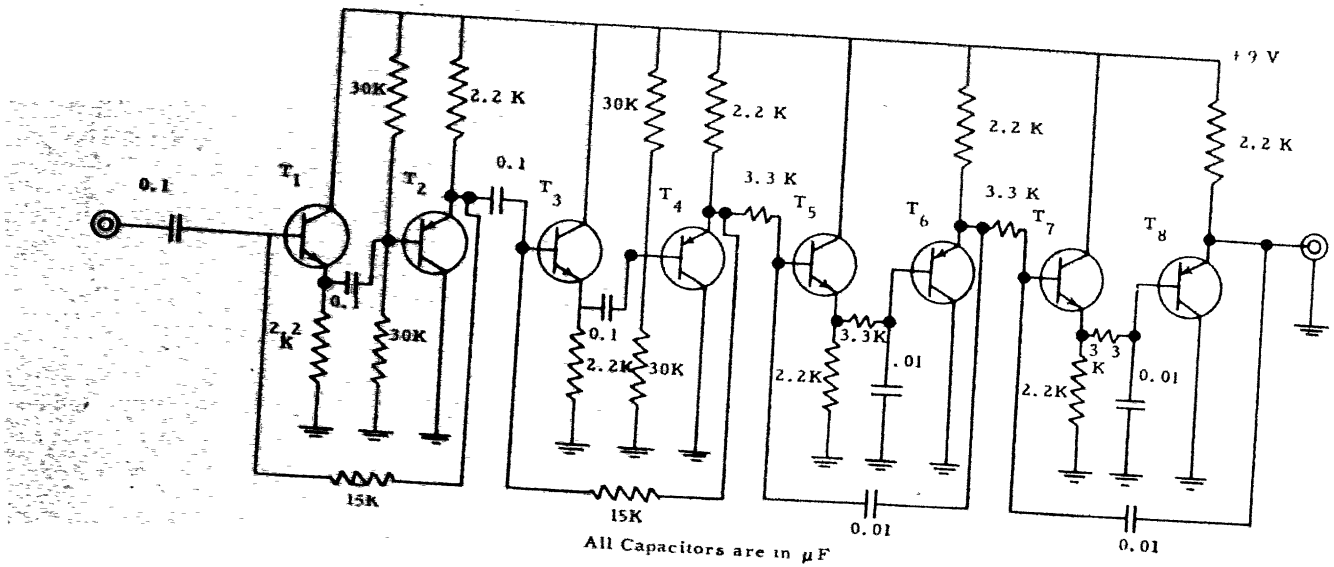

A1.1 CIRCUIT DIAGRAM OF THE ACTIVE FILTER

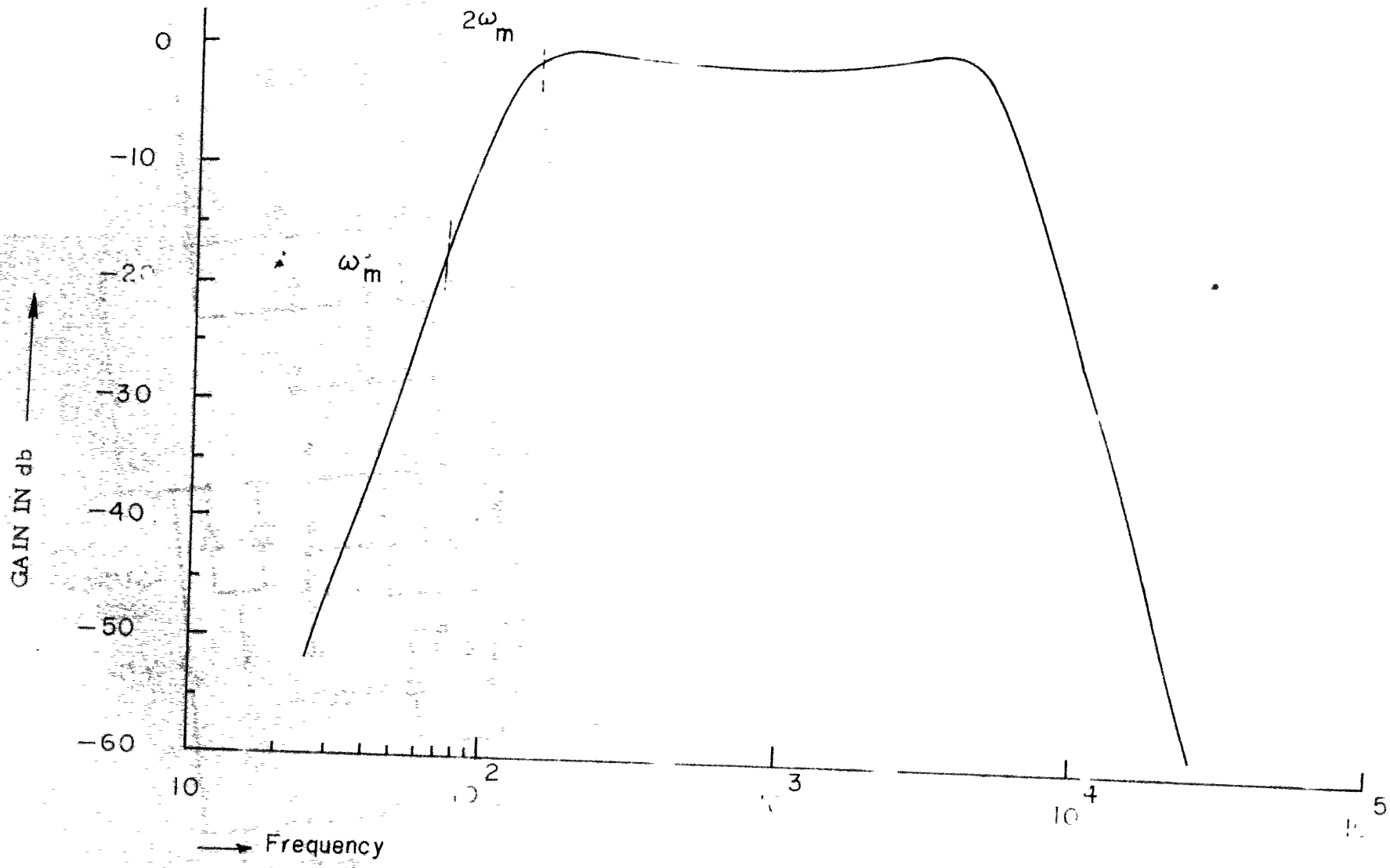

A1.2 FREQUENCY RESPONSE OF THE ACTIVE FILTER

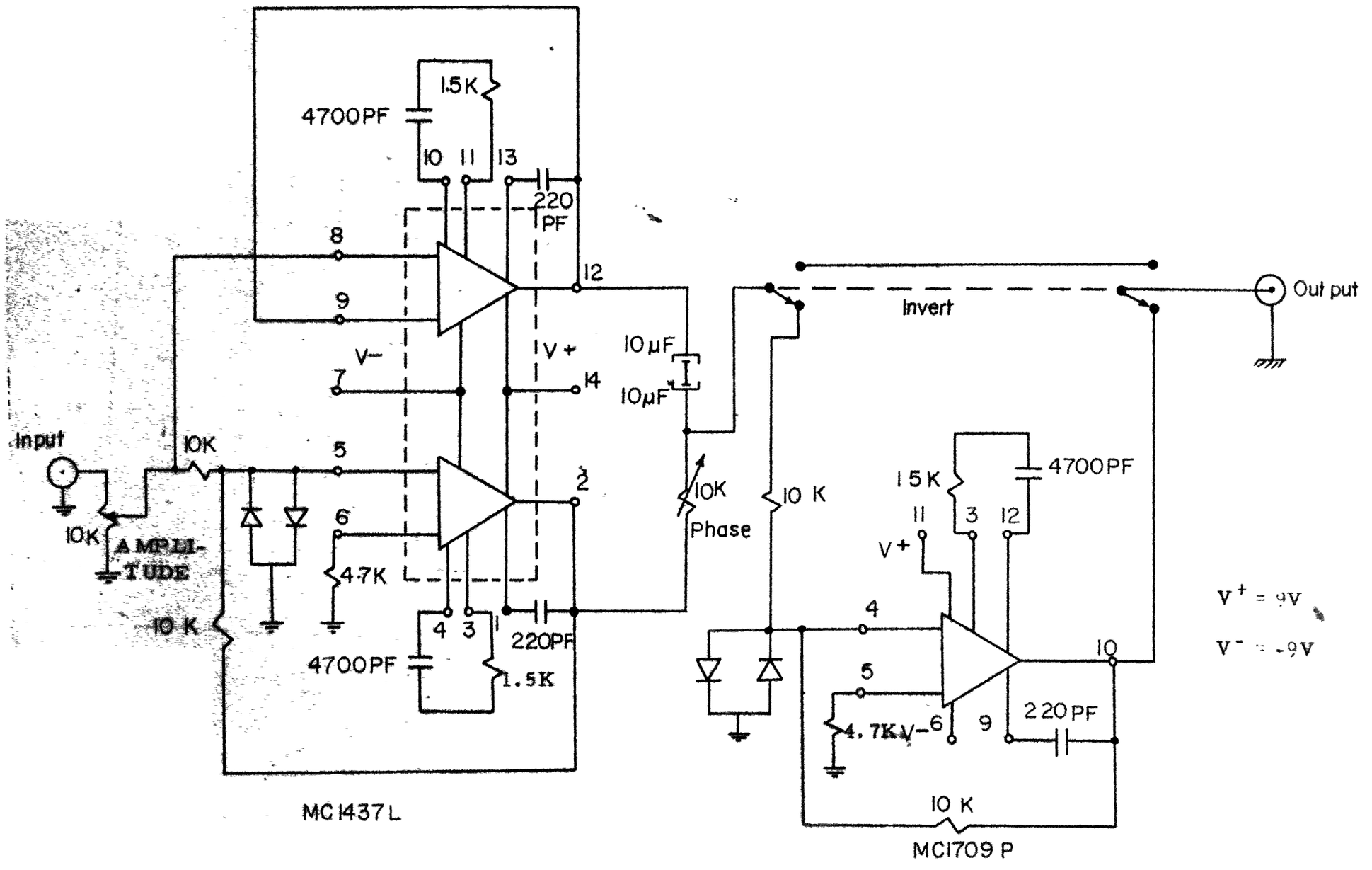

CIRCUIT DIAGRAM OF THE PHASE SHIFTER

APPENDIX III

A3.1 FLOW - CHART OF SUBROUTINE THEETA (Y)

$$Y = \frac{\pi}{g_a R - g_b R} \left(2 - (g_a R + g_b R)\right)$$

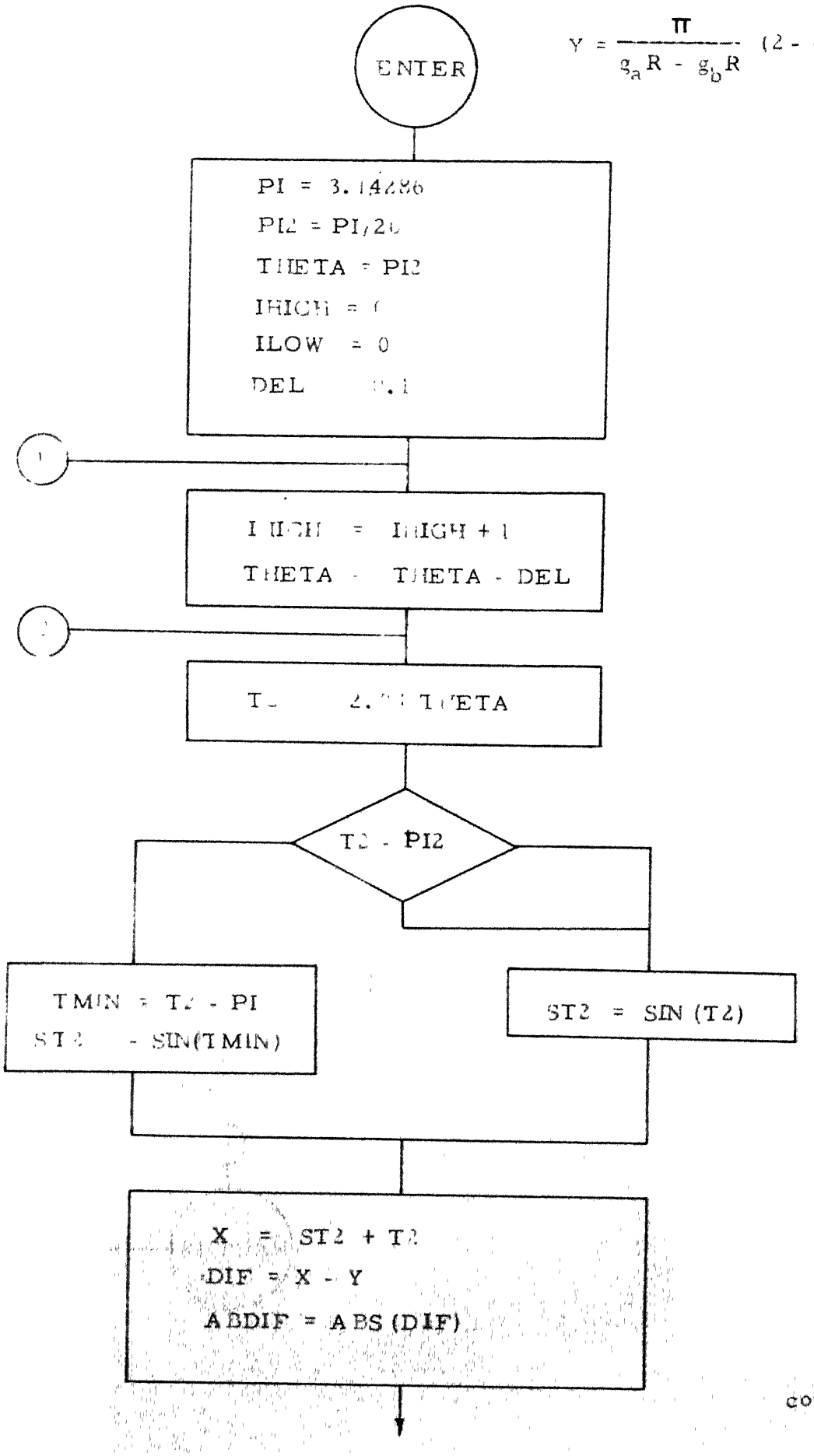

contd...

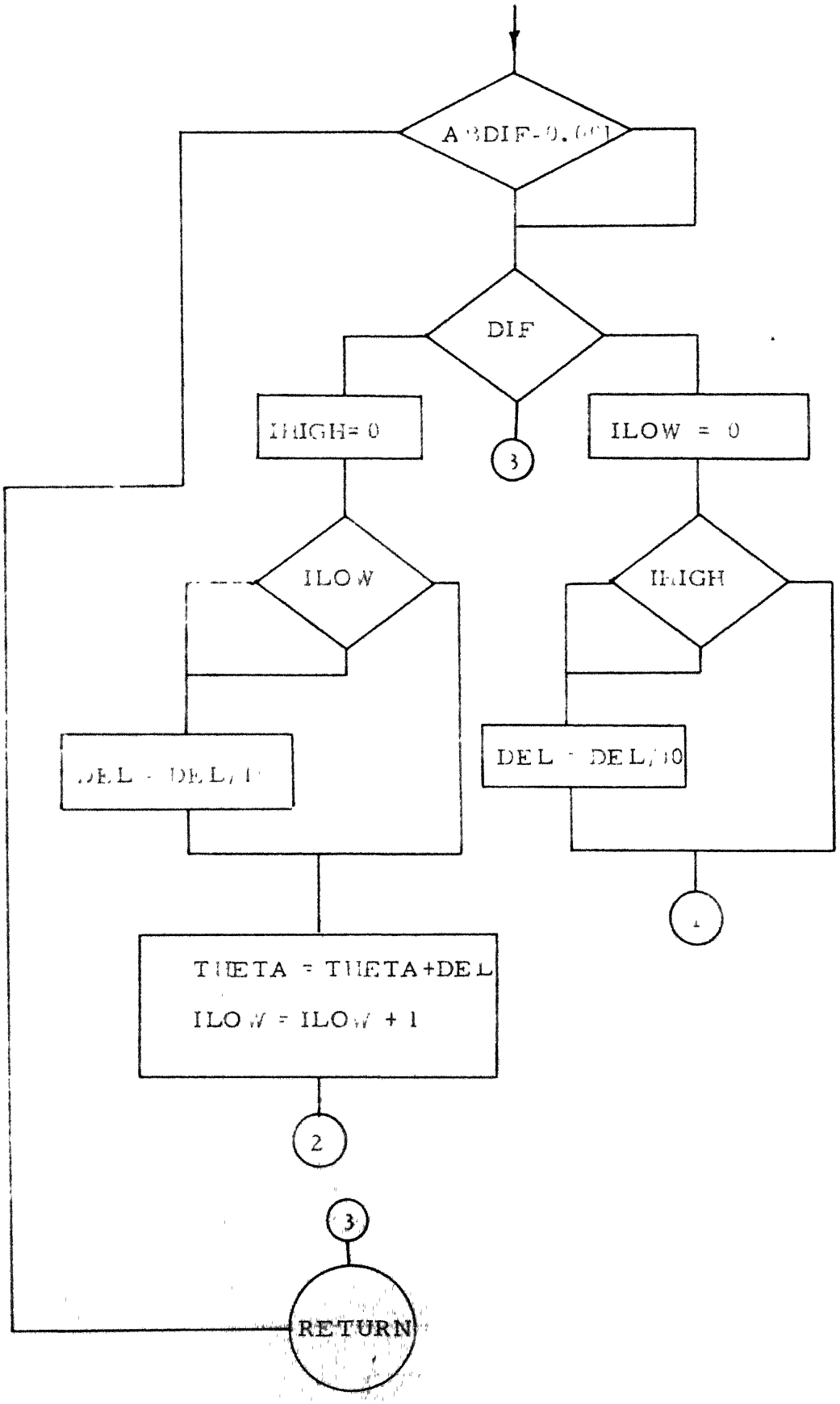
ABDIF-0.001
DIF
IHIGH= 0
3
ILOW = 0
ILOW
IHIGH
DEL = DEL/10
THETA = THETA+DEL
ILOW = ILOW + 1
2
3
RETURN

A3.2 FLOW-CHART OF THE OSCILLATOR RESPONSE CALCULATION

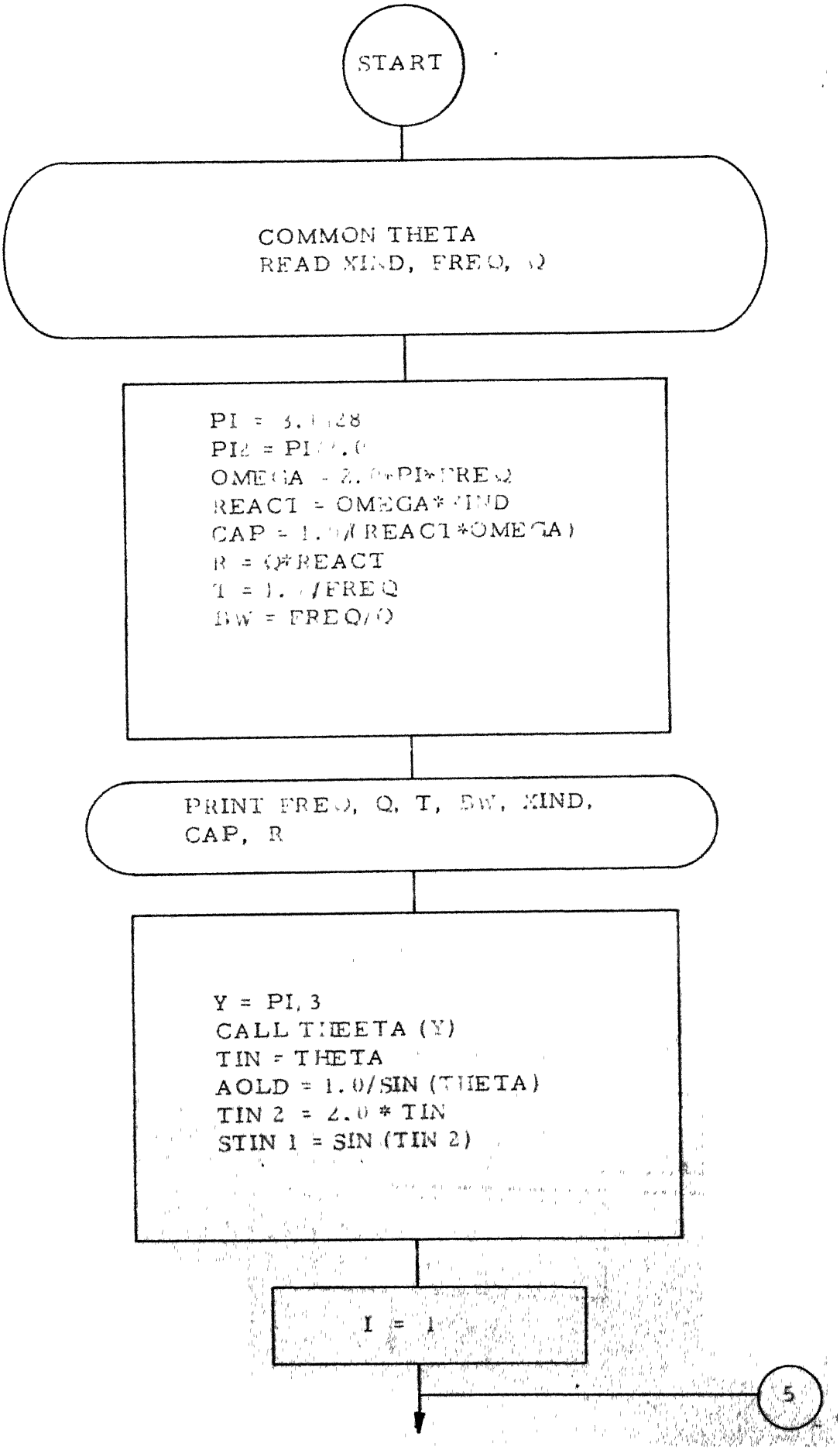

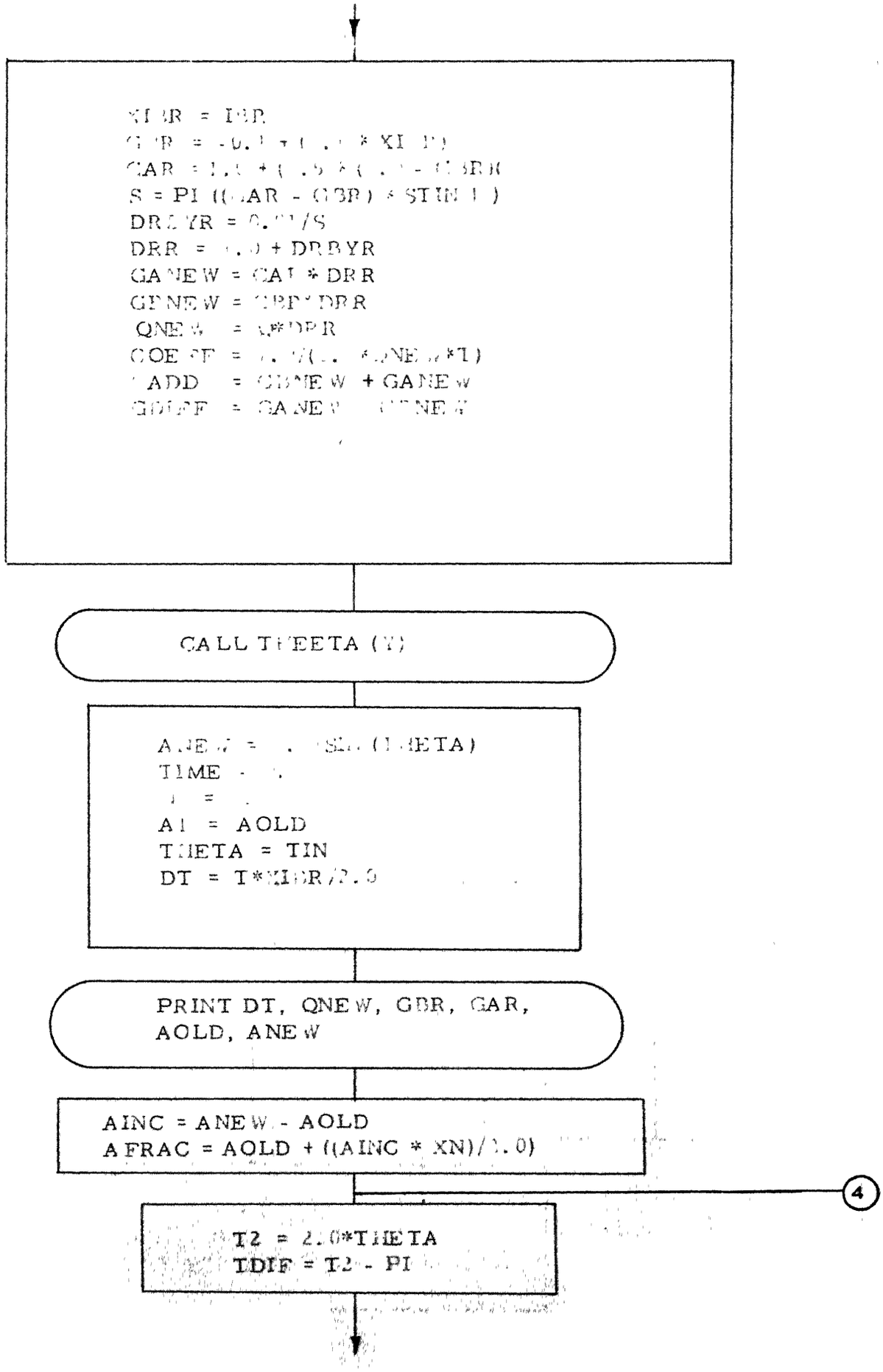
CALL THEETA (Y)
PRINT DT, QNEW, GBR, GAR,
AOLD, ANEW
AINC = ANEW - AOLD
AFRAC = AOLD + ((AINC * XN)/2.0)
T2 = 2.0*THETA
4

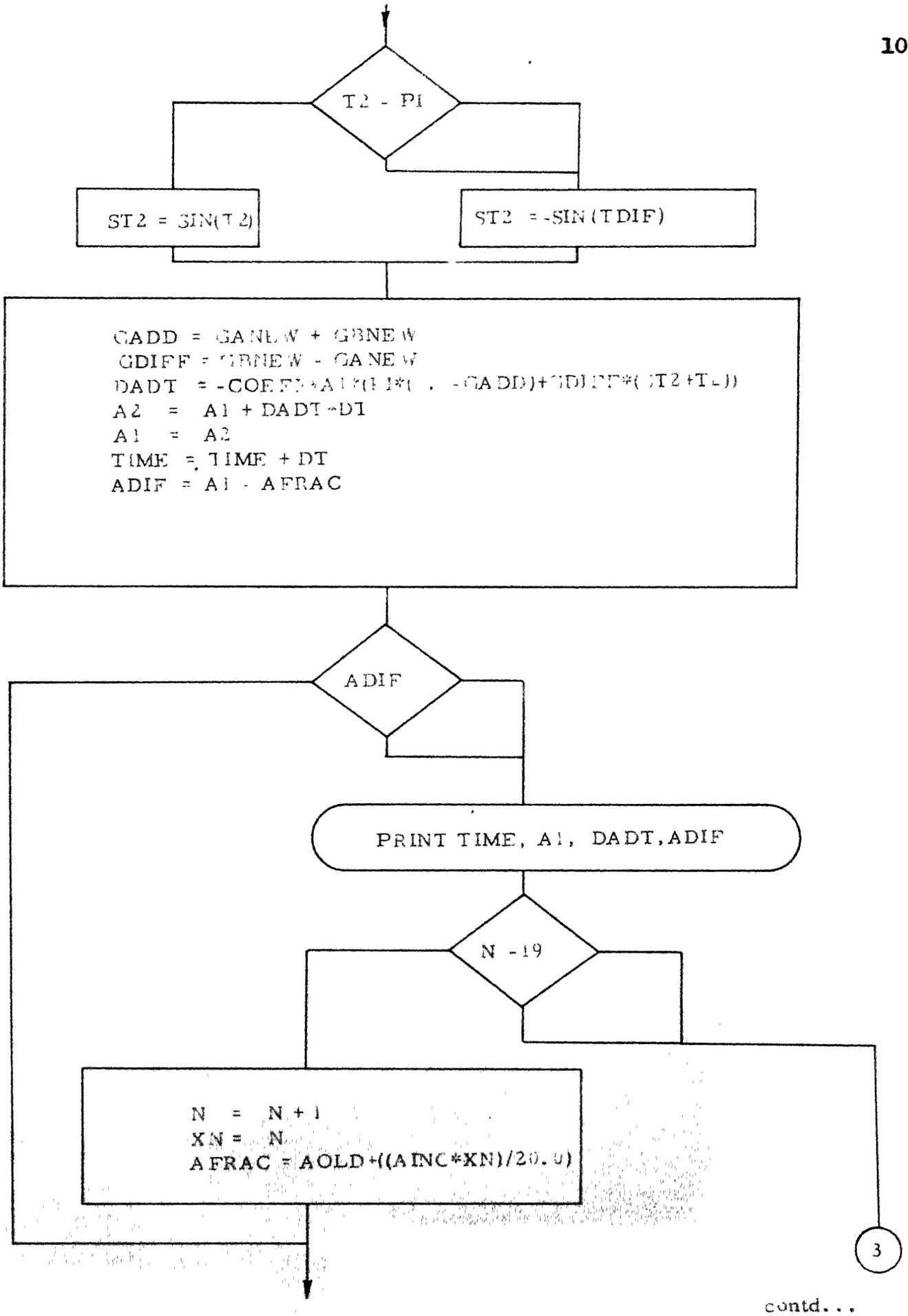
T2 - PI
ST2 = SIN(T2)
ST2 = -SIN(TDIF)
GADD = GANEW + GBNEW
GDIFF = GBNEW - GANEW
DADT = -COEFF*A1*(1.+COS(GDIFF)*COS(T2+T1))
A2 = A1 + DADT*DT
A1 = A2
TIME = TIME + DT
ADIF = A1 - AFRAC
ADIF
PRINT TIME, A1, DADT, ADIF
N - 19
N = N + 1
XN = N
AFRAC = AOLD+((AINC*XN)/20.0)
3

contd...

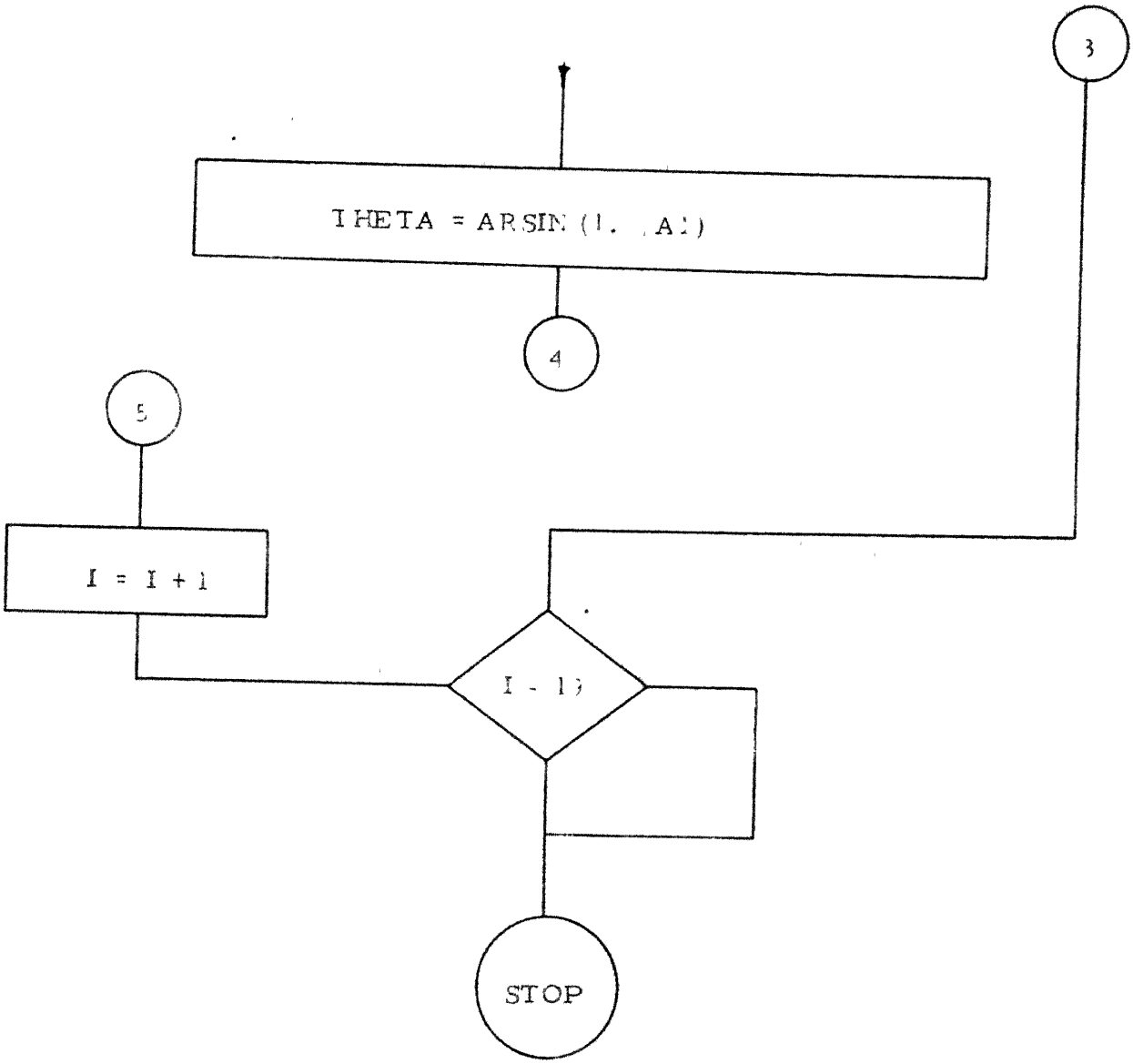
3
THETA = ARSIN (I. , A1)
4
5
I = I + 1
I - 1)
STOP

EQUIVALENT SYMBOLS

XIND	=	L
FREQ	=	$\omega_o/2\pi$
Q	=	Q
THETA	=	θ
AOLD	=	Initial Amplitude
ANEW	=	Final Amplitude
GAR	=	g_a
GBR	=	g_b
TIME	=	t (time)

A3.3 FLOW-CHART OF WIDE-BAND MODULATION ANALYSIS

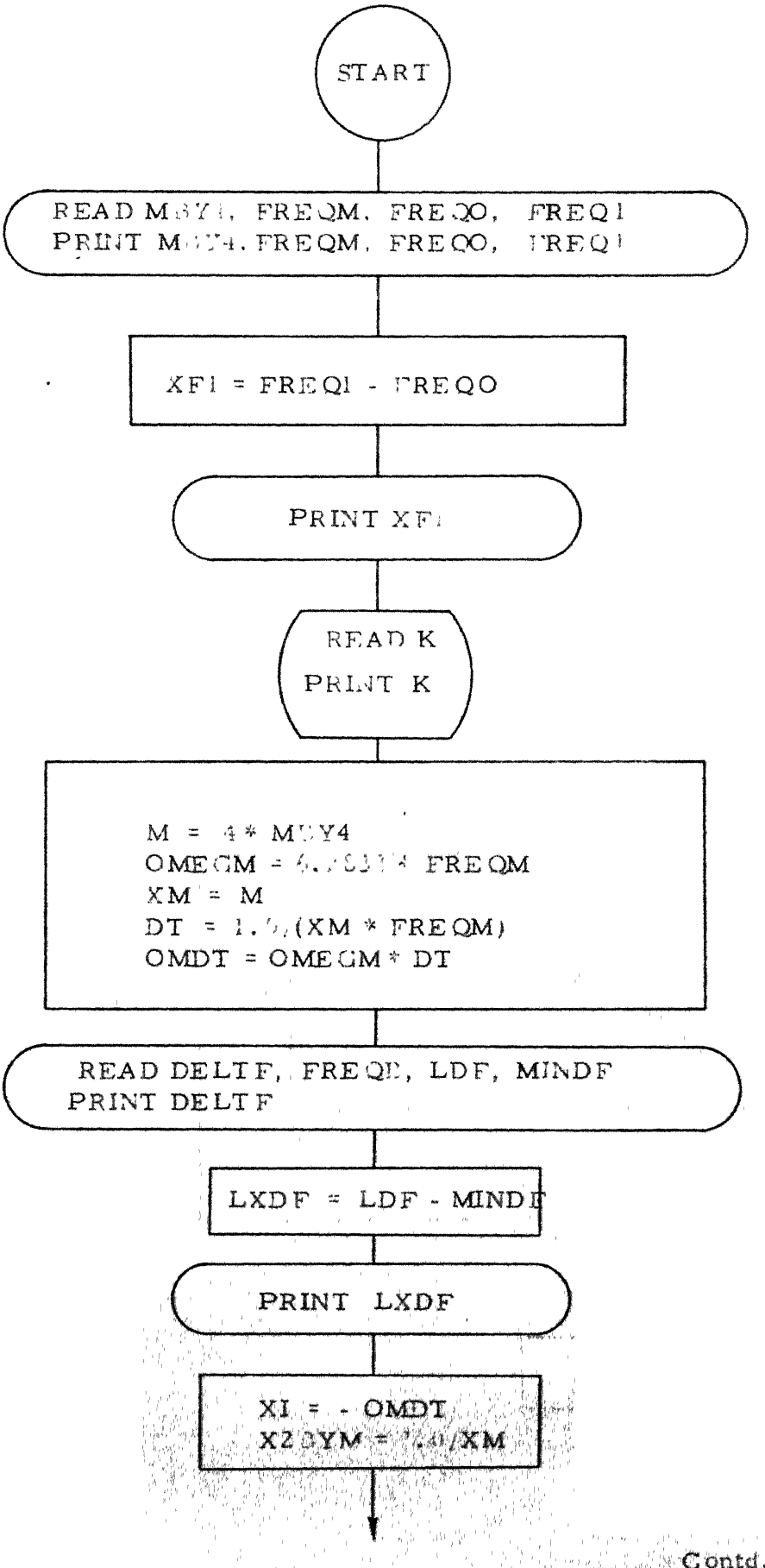

Contd...

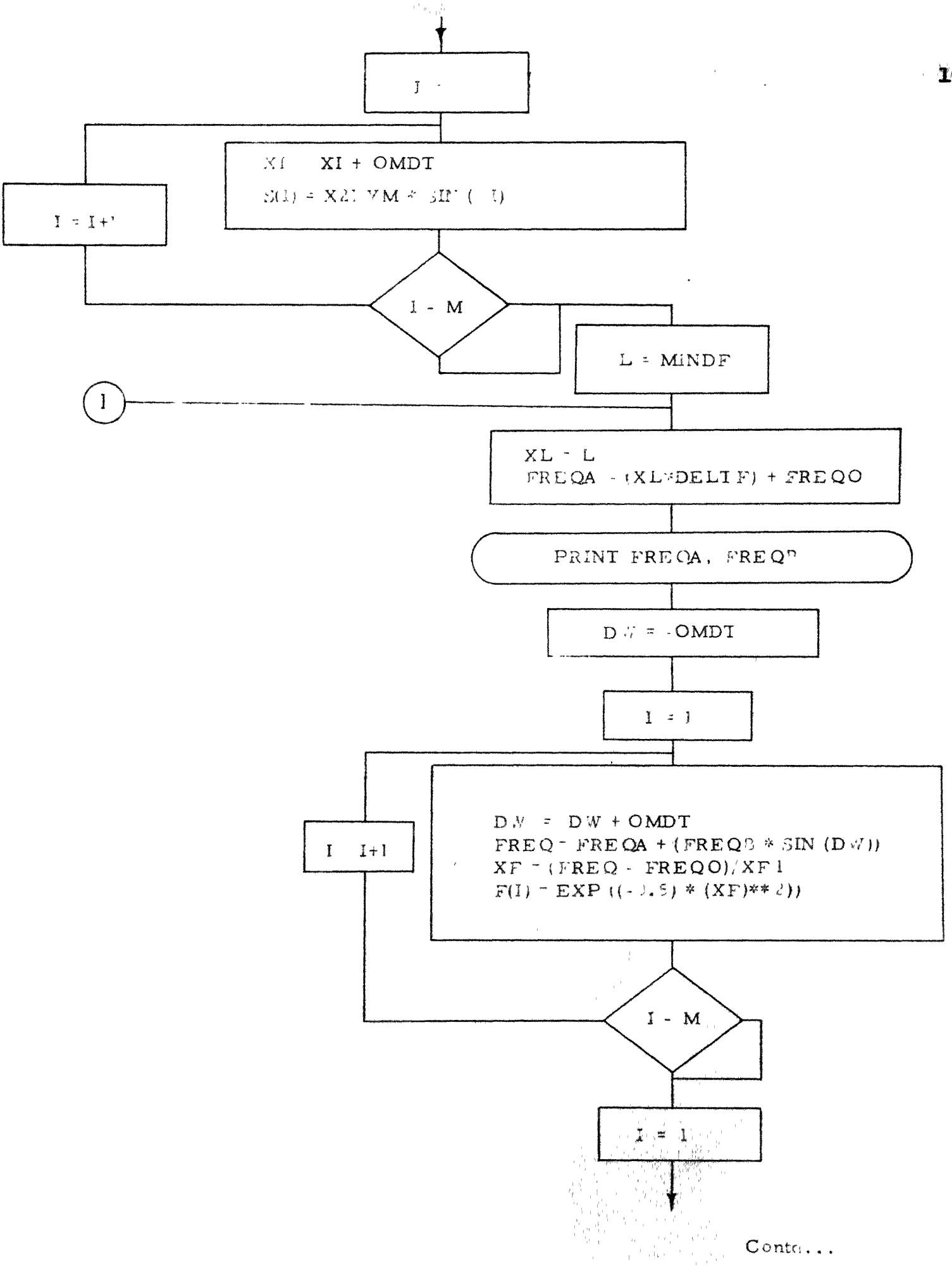
J -
XI XI + OMDT
S(I) = X2 VM * SIN (I)
I = I+'
I - M
L = MINDF
1
XL - L
FREQA - (XL*DELIF) + FREQO
PRINT FREQA, FREQ
DW = -OMDT
I = 1
I I+1
DW = DW + OMDT
FREQ - FREQA + (FREQ * SIN (DW))
XF - (FREQ - FREQO)/XF 1
F(I) - EXP ((-).5) * (XF)** 2))
I - M
I = 1

Conta...

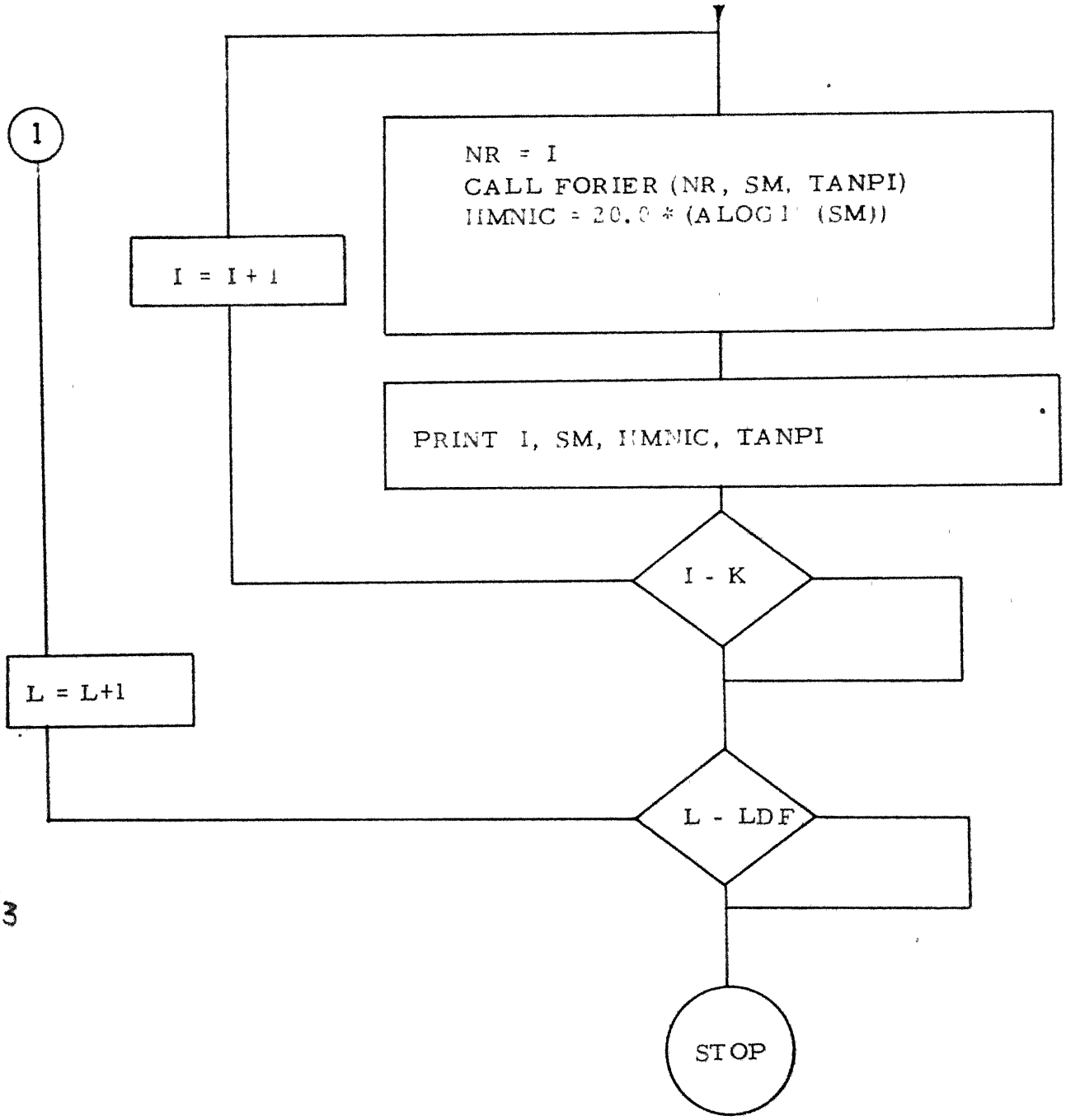
1
NR = I
CALL FORIER (NR, SM, TANPI)
I = I + 1
PRINT I, SM, HMNIC, TANPI
I - K
L = L+1
L - LDF
STOP

C3

EQUIVALENT SYMBOLS

FREQM	=	f_m
FREQO	=	f_o
FREQ1	=	$f_o + f_1$
DT	=	Sampling interval for Fourier analysis
DELTF	=	Increment for f_c
FREQB	=	$\triangle f$
LDF	=	Maximum value of f_c
MINDF	=	Minimum value of f_c

A3.4 FLOW-CHART FOR THE CALCULATION OF DERIVATIVE PLOT

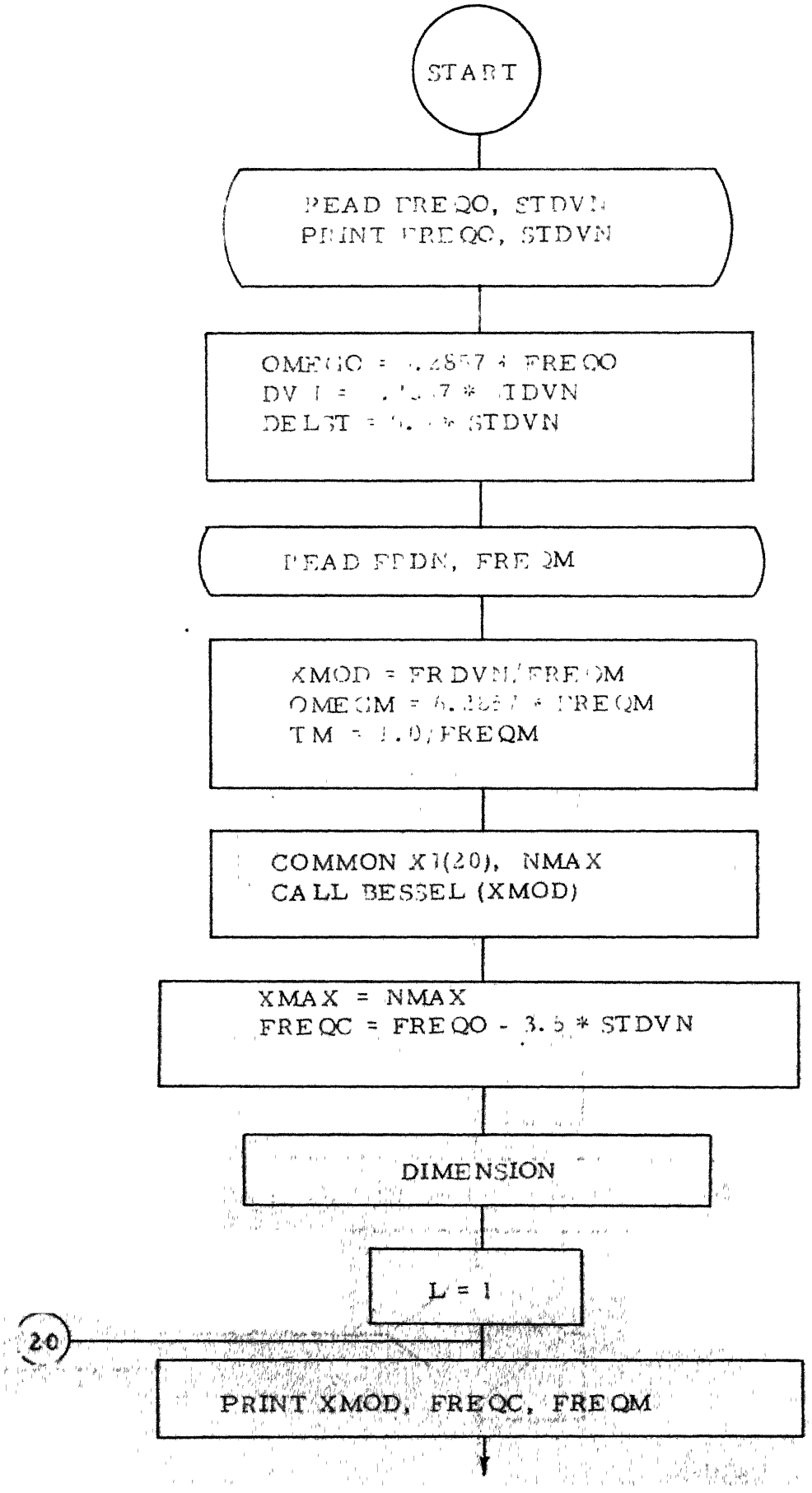

contd...

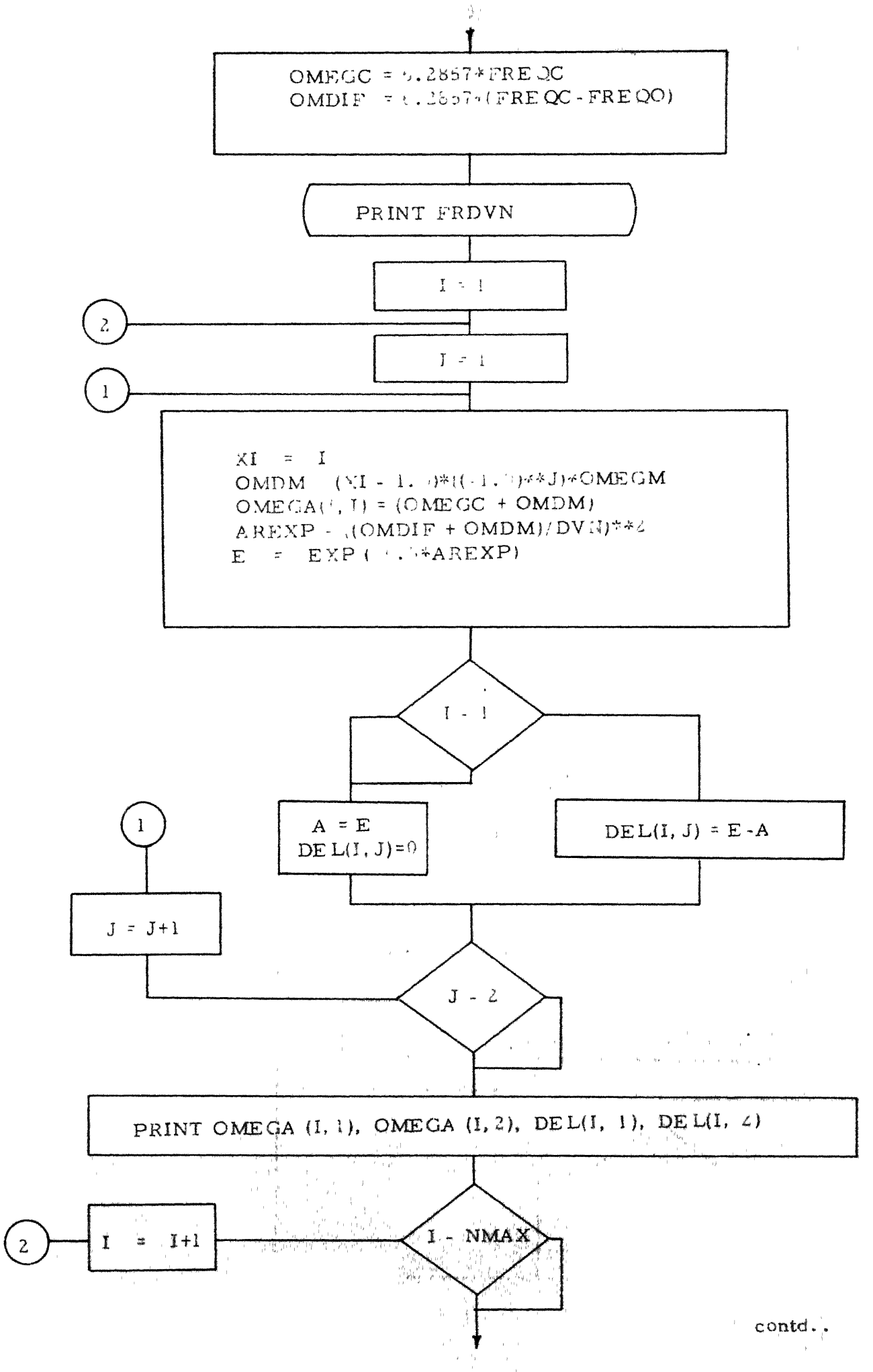
OMEGC = 6.2857*FREQC
OMDIF = 6.2857*(FREQC-FREQO)
PRINT FRDVN
I = 1
2
J = 1
1
XI = I
OMDM = (XI - 1.0)*((-1.0)**J)*OMEGM
OMEGA(I, J) = (OMEGC + OMDM)
AREXP = ((OMDIF + OMDM)/DVN)**2
E = EXP(-1.0*AREXP)
I - 1
A = E
DEL(I, J)=0
DEL(I, J) = E-A
1
J = J+1
J - 2
PRINT OMEGA (I, 1), OMEGA (I, 2), DEL(I, 1), DEL(I, 2)
2
I = I+1
I - NMAX

contd..

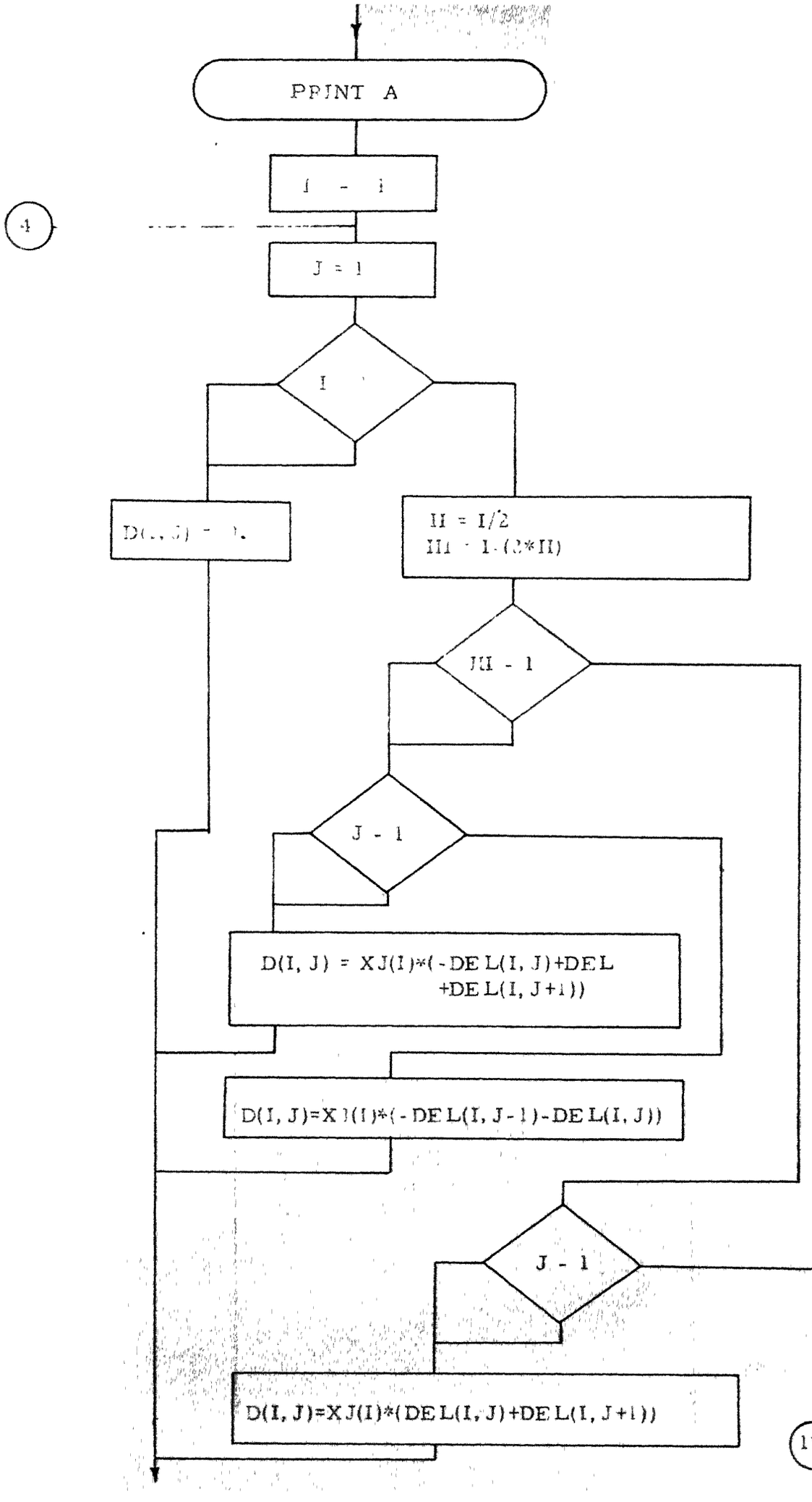
PRINT A
I = 1
4
J = 1
I
D(I, J) =
II = I/2
III = I-(2*II)
III = 1
J = 1
D(I, J) = XJ(I)*(-DEL(I, J)+DEL
+DEL(I, J+1))
D(I, J)=XJ(I)*(-DEL(I, J-1)-DEL(I, J))
J = 1
D(I, J)=XJ(I)*(DEL(I, J)+DEL(I, J+1))
contd.
19

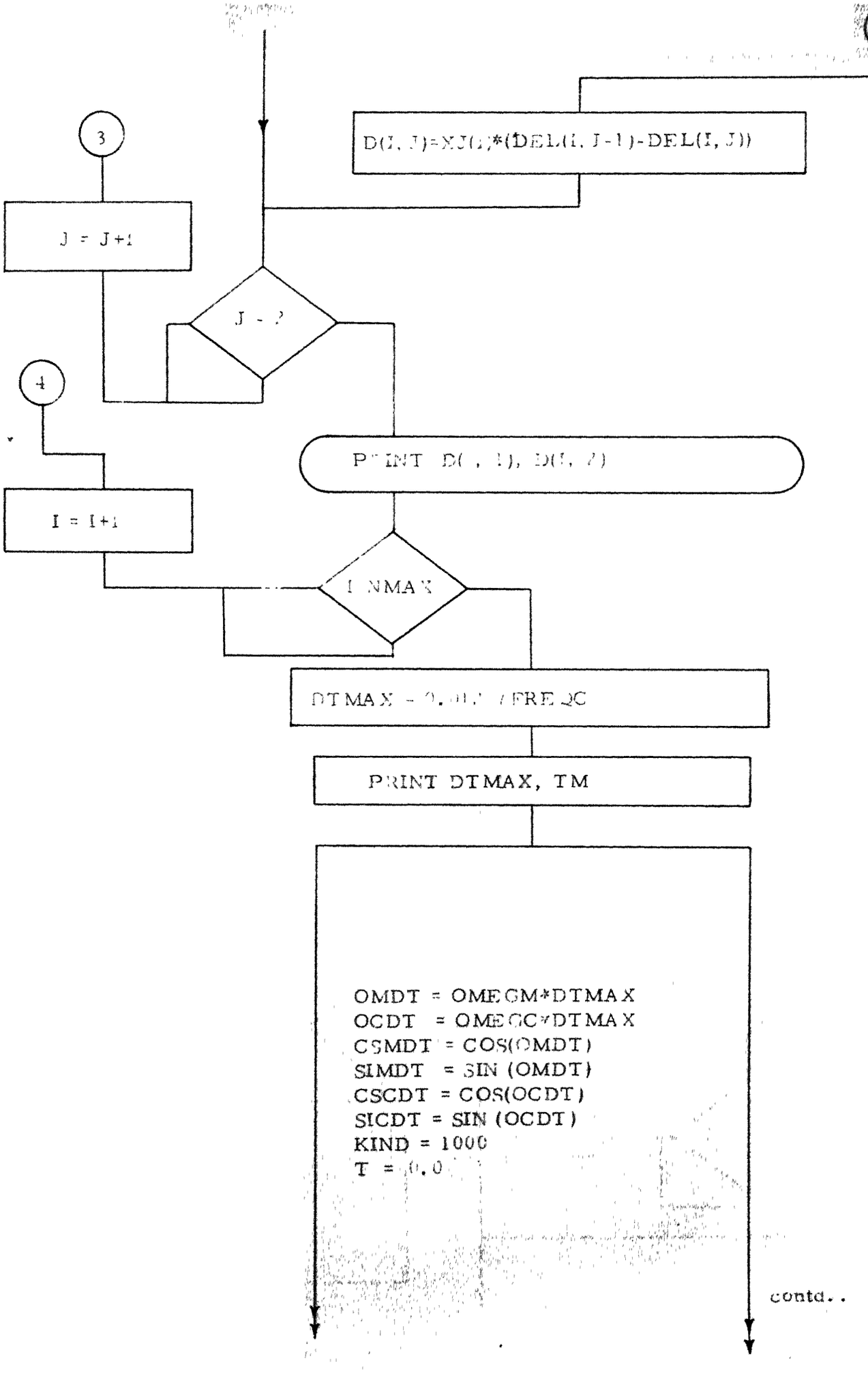
3
D(I, J)=XJ(J)*(DEL(I, J-1)-DEL(I, J))
J = J+1
J - 2
4
PRINT D(, 1), D(I, 2)
I = I+1
I NMAX
DTMAX = 0.01 / FREQC
PRINT DTMAX, TM
OMDT = OMEGM*DTMAX
OCDT = OMEGC*DTMAX
CSMDT = COS(OMDT)
SIMDT = SIN (OMDT)
CSCDT = COS(OCDT)
SICDT = SIN (OCDT)
KIND = 1000
T = 0.0
contd..

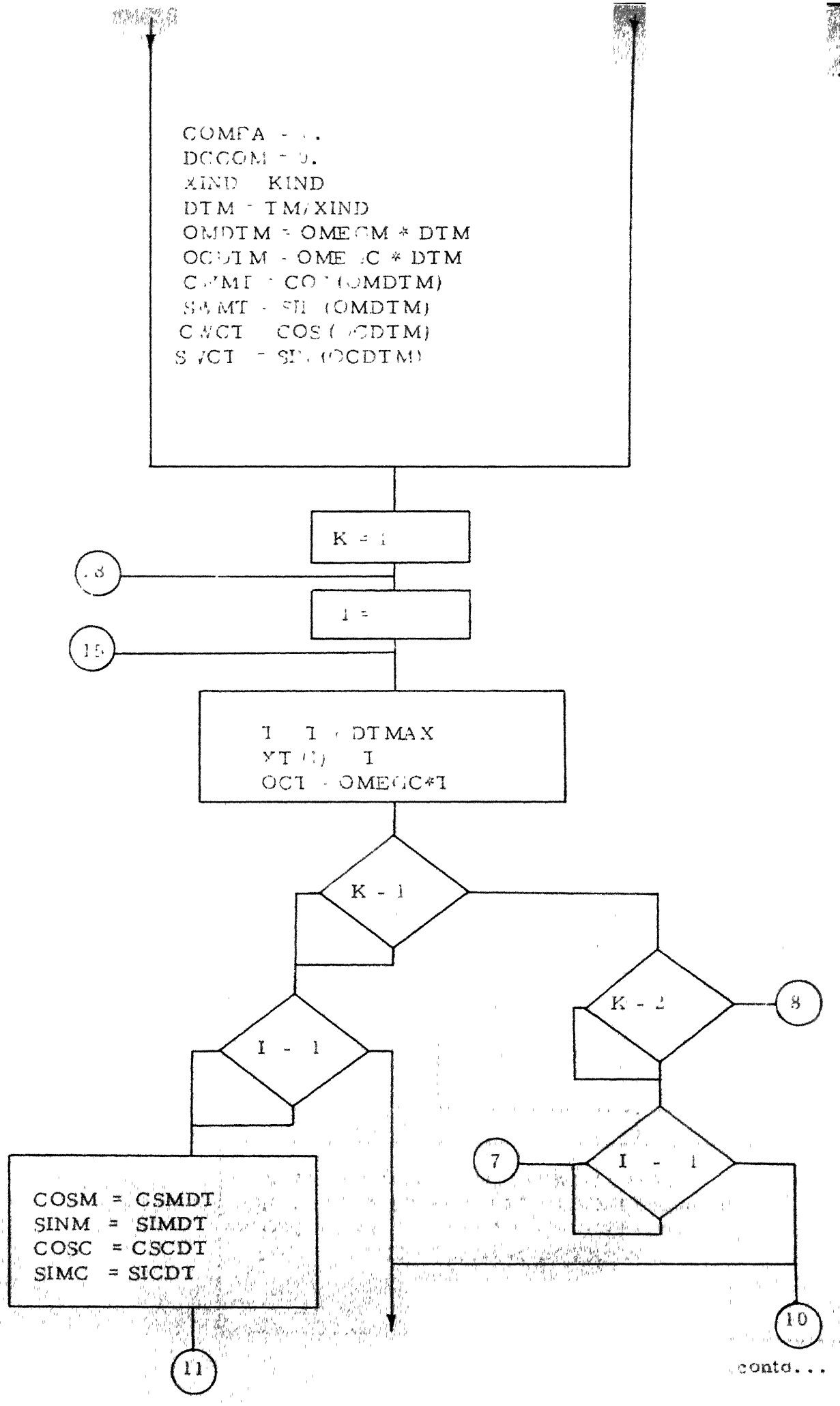
COMPA - .
DCCOM - 0.
XIND KIND
DTM - TM/XIND
OMDTM - OMEGM * DTM
OCDTM - OME C * DTM
C MT - CO (OMDTM)
SAMT - SI (OMDTM)
C CT COS (CDTM)
S CT - SI (OCDTM)
K = 1
8
I =
15
I I DTMAX
T ( ) I
OCT - OMEGC*T
K - 1
I - 1
K - 2
8
7
I - 1
COSM = CSMDT
SINM = SIMDT
COSC = CSCDT
SIMC = SICDT
11
10

conta...

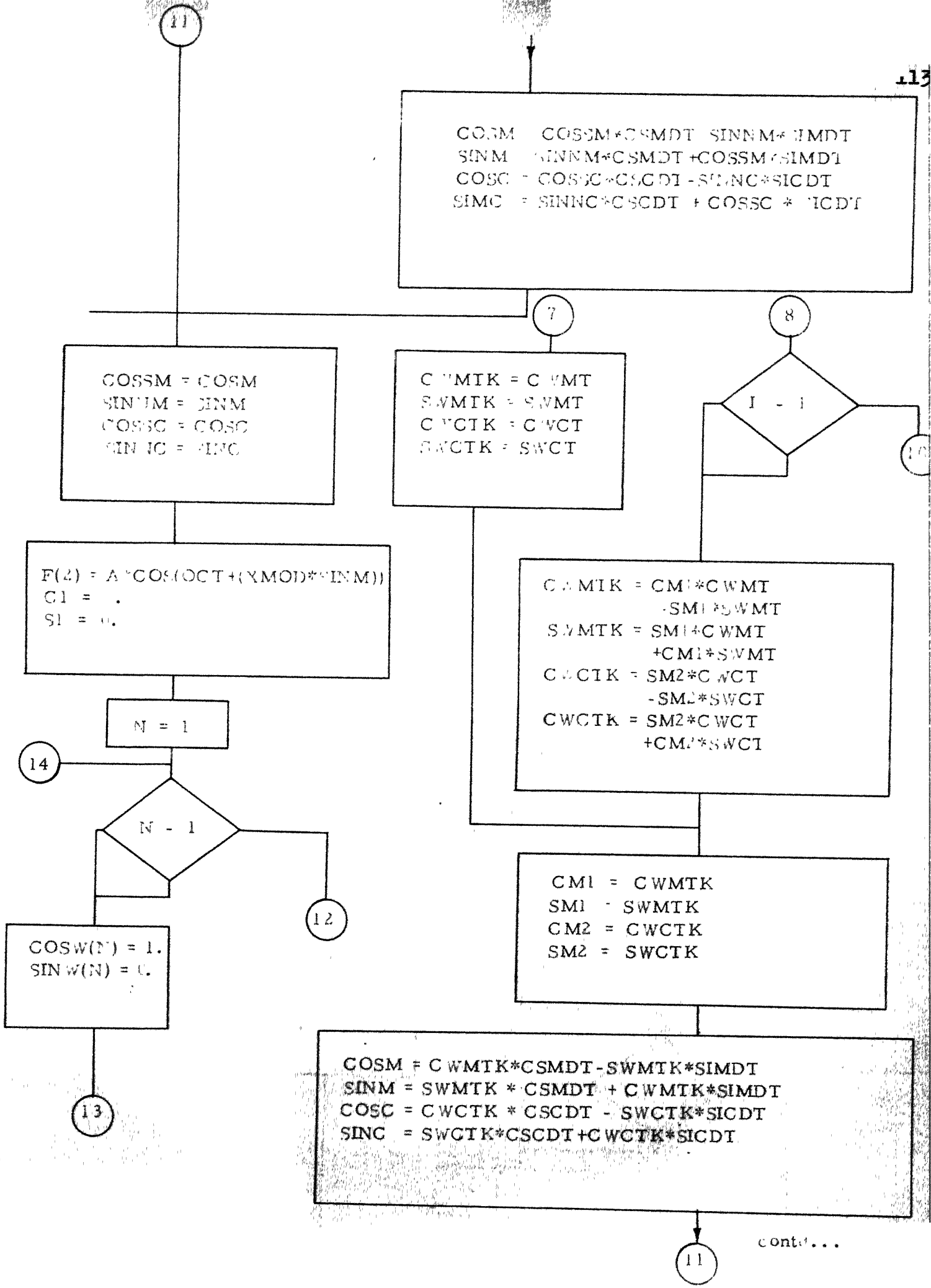
11
COSM = COSSM*CSMDT - SINNM*SIMDT
SINM = SINNM*CSMDT + COSSM*SIMDT
COSC = COSSC*CSCDT - SINNC*SICDT
SINC = SINNC*CSCDT + COSSC*SICDT
7
8
COSSM = COSM
SINNM = SINM
COSSC = COSC
SINNC = SINC
CWMTK = CWMT
SWMTK = SWMT
CWCTK = CWCT
SWCTK = SWCT
I = 1
F(Z) = ACOS(OCT+(XMOD)*SINM))
C1 = .
S1 = 0.
CWMTK = CM1*CWMT
-SM1*SWMT
SWMTK = SM1*CWMT
+CM1*SWMT
CWCTK = SM2*CWCT
-SM2*SWCT
CWCTK = SM2*CWCT
+CM2*SWCT
N = 1
14
N = 1
CM1 = CWMTK
SM1 = SWMTK
CM2 = CWCTK
SM2 = SWCTK
12
COSW(N) = 1.
SINW(N) = 0.
COSM = CWMTK*CSMDT-SWMTK*SIMDT
SINM = SWMTK*CSMDT + CWMTK*SIMDT
COSC = CWCTK*CSCDT - SWCTK*SICDT
SINC = SWCTK*CSCDT+CWCTK*SICDT
13
11
cont'...

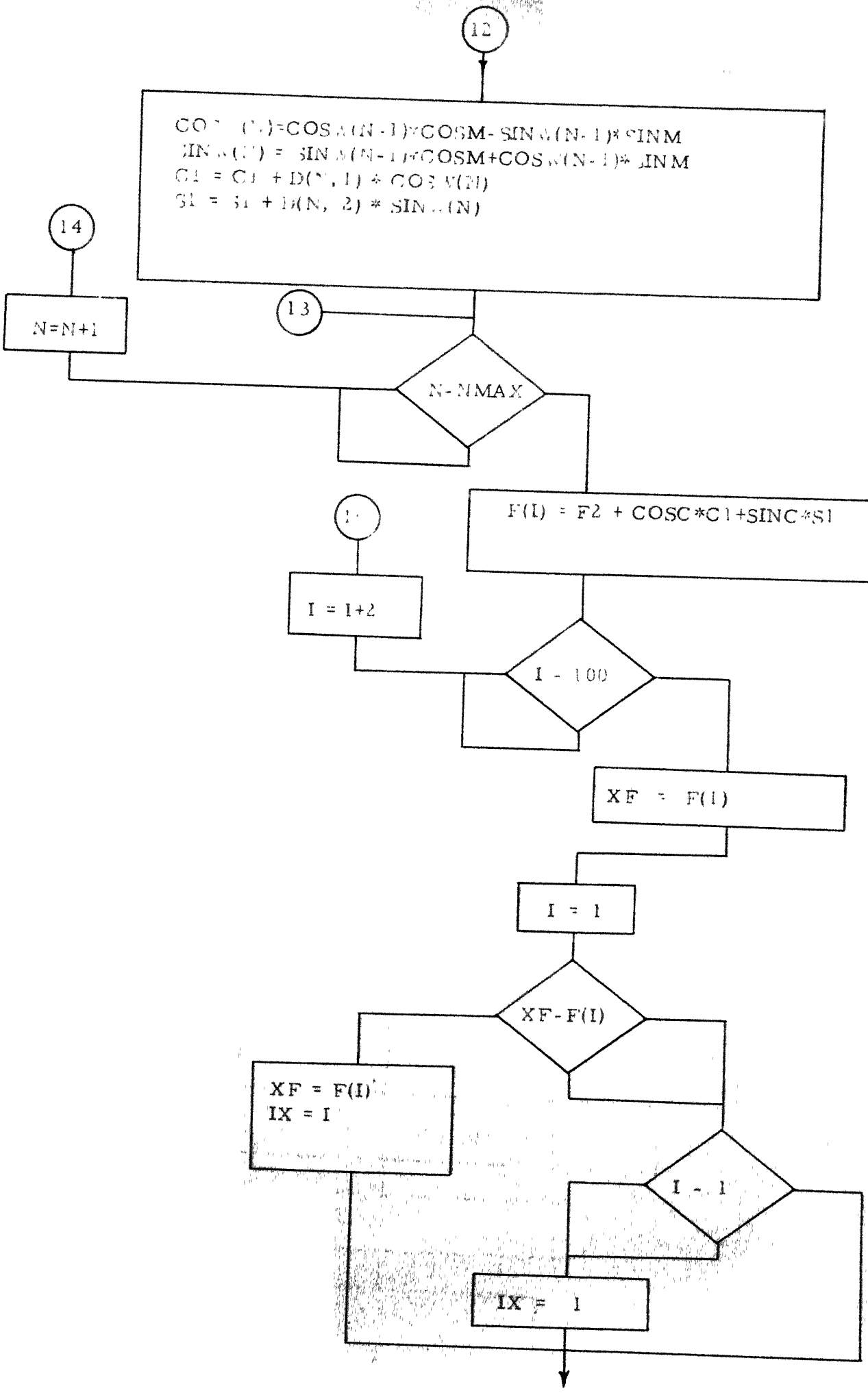
12
COS
SIN
C1 = C1 + D(N, 1) * COS
S1 = S1 + D(N, 2) * SIN
14
N=N+1
13
N-NMAX
F(I) = F2 + COSC*C1+SINC*S1
I = I+2
I - 100
XF = F(I)
I = 1
XF-F(I)
XF = F(I)
IX = I
I - 1
IX = 1

contd...

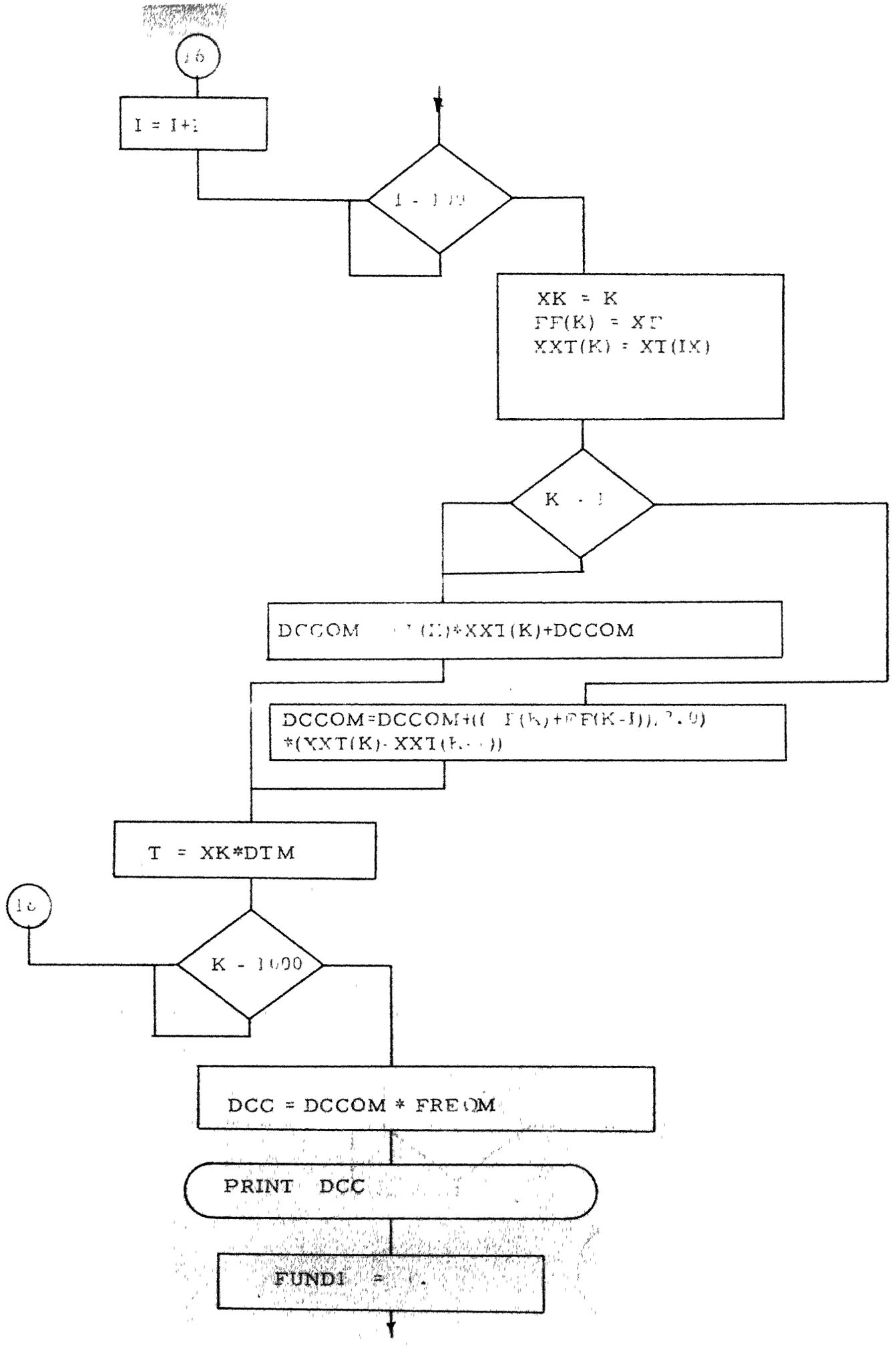
16
I = I+1
I - 179
XK = K
FF(K) = XT
XXT(K) = XT(IX)
K - 1
DCCOM = [illegible](K)*XXT(K)+DCCOM
DCCOM=DCCOM+(([illegible](K)+FF(K-1))/2.0)
*(XXT(K)-XXT(K-1))
T = XK*DTM
16
K - 1000
DCC = DCCOM * FREQM
PRINT DCC
FUNDI = 0.

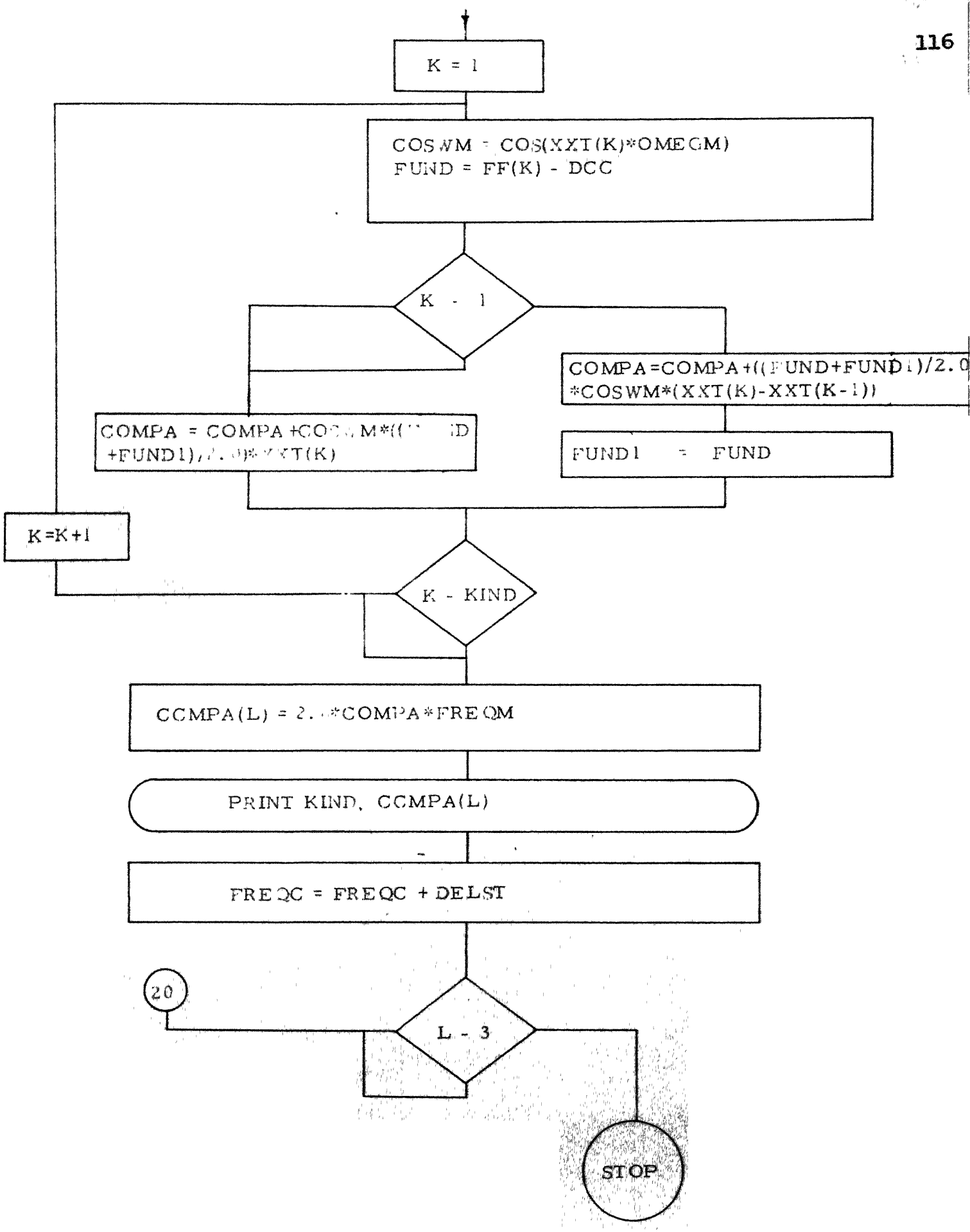
K = 1
COSWM = COS(XXT(K)*OMEGM)
FUND = FF(K) - DCC
K - 1
COMPA =COMPA+((FUND+FUND1)/2.0
COSWM(XXT(K)-XXT(K-1))
FUND1 = FUND
K=K+1
K - KIND
CCMPA(L) = 2.0*COMPA*FREQM
PRINT KIND, CCMPA(L)
FREQC = FREQC + DELST
20
L - 3
STOP

EQUIVALENT SYMBOLS

FREQO	=	f_o
STDVN	=	f_1
FRDVN	=	$\triangle f$
FREQM	=	f_m
CCMPA(L)	=	Output